uOttawa

Fabrication and Characterization of Novel Environmentally Friendly Thin Film Nanocomposite Membranes for Water Desalination

Farhad Asempour

A thesis submitted
in partial fulfillment of the requirements for the degree of

Master of Applied Science

in Chemical Engineering

Department of Chemical and Biological Engineering
Faculty of Engineering
University of Ottawa
September 2017

To My Parents

Abstract

Thin film Nanocomposite (TFN) membranes are a relatively new class of high-performance semipermeable membranes for Reverse Osmosis (RO) applications. Large scale applications of TFN membranes have not been achieved yet due to the high production cost of the nanoparticles, agglomeration of the nanoparticles in the thin polyamide matrix of the membrane, and leaching out of typically toxic inorganic nanoparticles into the downstream.

In this work, these challenges are addressed by incorporation of two different nanofillers: Cellulose NanoCrystals (CNC), and surface functionalized Halloysite NanoTubes (HNT). Amine groups, carboxylic acid groups, and the first generation of poly(amidoamine) (PAMAM) dendrimers were used for functionalization of the HNT. CNC and HNT are environmentally friendly, low/non-toxic, abundant, and inexpensive nanoparticles with a unique size, and chemical properties. TFN membranes were synthesized via in situ interfacial polymerization of m-phenylenediamine (MPD) with trimesoyl chloride (TMC) and the nanoparticles. The control Thin Film Composite (TFC) membranes, and CNC and HNT based TFN membranes were characterized by Scanning Electron Microscopy (SEM), Atomic Force Microscopy (AFM), X-Ray Diffraction (XRD), X-ray Photoelectron Spectroscopy (XPS), Fourier Transform Infrared spectroscopy (FTIR) and contact angle measurements. The antifouling capacity of CNC based membranes was investigated with a solution of Bovine Serum Albumin (BSA) as the fouling agent. Also, the leachability of the HNT from the membranes was examined by shaking the membranes in a batch incubator for 48 h, and then tracing the leached out HNT using Inductively Coupled Plasma Mass Spectrometry (ICP-MS).

Separation characteristics of the membranes were studied by desalination of synthetic brackish water with a cross flow RO filtration system. It was revealed that incorporation of functionalized HNT enhanced the permeate flux without sacrificing the salt rejection (99.1 % ± 0.1 %). Also, incorporation of 0.1% (w/v) CNC doubled the permeate flux (from 30 to 63 $L/m^2.h$ at 20 bar) without compromising the salt rejection (97.8%). At the same time, leaching out of HNT from the TFN membranes was decreased as a result of the HNT functionalization and formation of covalent bonds with the TMC. Also, antifouling properties of the CNC-TFN membranes were 11% improved in comparison with control TFC membrane.

Résumé

Les membranes nanocomposites d'osmose inverse (OI) à couche mince (TFN) constituent une nouvelle catégorie de membranes semi-perméables performantes dans les systèmes d'osmose inverse. Le traitement à grande échelle par osmose inverse à partir de cette catégorie de membranes est encore à l'état de recherche et de développement étant donné le coût élevé de production des nanoparticules, l'agglomération des nanoparticules contenues dans la matrice en polyamide de la membrane, et la séparation en aval des nanoparticules aux propriétés le plus souvent toxiques et inorganiques.

Mes travaux ont mobilisé deux types de nanocharges, chacun introduit dans la couche de polyamide positionnée sur le dessus de la membrane : les nanocrystaux de cellulose (CNC) ; les nanotubes d'halloysite (NHT) à surface fonctionnalisées. Les groupes aminés, d'acide carboxylique et première génération de dendriméres poly(amioamine) (PAMAM) sont utilisées pour la fonctionnalisation de NHT. Les CNC et NHT sont des nanoparticules de couleur verte, faiblement ou non-toxiques, abondantes, et accessibles en termes de coûts. Elles présentent en outre une taille unique et des propriétés chimiques qui leur sont propres.

La synthèse des membranes de type TFN est obtenue par polymérisation interfaciale *in situ* de la m-phénylènediamine (MPD) avec du *1,3,5-Benzenetricarboxylic chlorure d'acide* (TMC) et les nanocharges. Les membranes composites à couche mince de contrôle, et les nanocharges CNC et HNT ont été caractérisées par microscopie électronique à balayage (MEB-SEM), microscopie à force atomique (AFM), diffraction aux rayons X (DRX), spectroscopie électronique par rayons X (XPS), infrarouge à transformée de fourier (IRTF), et mesures d'angles de contact. Les propriétés antisalissure des nanocrystaux de cellulose (CNC) ont été vérifiées par le recours à de l'albumine de sérum bovin (ASB) qui joue le rôle d'agent salissant dans la solution d'alimentation. Aussi, les interactions/adhésions entre les HNT fonctionnels et la matrice en polyamide ont été étudiés par lixiviation au moyen d'agitation après 48 h et ils ont été analysés à l'aide de la technique de plasma par (ICP-MS)

La séparation caractéristique des membranes ont été étudiés par dessalement de l'eau saumâtre synthétique en tests de filtration à courants croisés ont permis de mettre en évidence que l'incorporation de NHT fonctionnels, avec un nombre optimal de groupes amine, améliore de façon significative le flux d'eau, sans réduire le taux de réjection des sels (99.1 % ± 0.1 %). Par ailleurs, l'ajout de 0,1 % (poids/ volume) de CNC a fait doubler le flux d'eau (de 30 à 63 $L/m^2.h$

pour une pression de 20 bars) sans abaisser le taux de réjection des sels (97,8 %). En outre, la lixiviation des nanoparticules NHT modifiées des membranes TFN a diminué en raison de leur fonctionnalisation. Enfin, les propriétés antisalissure des membranes CNC-TFN ont été améliorées de 11% en comparaison avec les membranes composites à couche mince de contrôle.

Acknowledgement

I would like to express my heartfelt appreciation to all those wonderful people who helped me through the course of my research and thesis; to explore, learn and enjoy!

First, I would like to express my gratitude to my thesis advisor Dr. Boguslaw Kruczek for his support, funding, guidance, and patience. The door of his office was always open to me whenever I needed help or had a question.

I would like to thank Dr. Takeshi Matsuura for providing me with his great insights and critically revising, and improving my articles. I would also like to thank Dr. Daryoush Emadzadeh for his mentorship. He introduced me to the amazing world of thin film nanocomposite membranes, and guided me through the membrane fabrication, and characterization. I like to thank Dr. Somaye Akbrai for introducing me to the dendritic polymers, surface modification of nanoparticles, and helping me with membrane characterization. Also, I would like to thank my friends and colleagues in Kruczek's and Matsuura's research groups: Du Bai, Andre Francois, and Haoyu Wu. I would like to thank to Margaux Armand, and my mother for translating the abstract of my thesis to French, and Dr. Sara Dastjerdi and Dr. Marc Dubé for providing the TEM images of cellulose nanocrystals.

I would like to acknowledge Dr. Siamak Lashkari and Qingdao Wosai Seawater Desalination Technology Ltd. for supporting and funding my work.

Finally and most importantly, I would like to thank my beloved parents, Mostafa Assempour and Fatemeh Tehrani, and my lovely sister Ladan Asempour for their unconditional support, endless love, motivation, and encouragement.

Table of contents

List of Figures

List of Tables

Nomenclature

AFM	Atomic Force Microscopy	NP	nanoparticles
APTES	Aminopropyltriethoxysilane	PA	Polyamide
ATR-FTIR	Attenuated total reflectance Fourier transform infrared spectroscopy	PAMAM	poly(amidoamine) dendrimer
CNC	Cellulose NanoCrystals	PS	Polysulfone
C_f	Salt concentrations in feed (mg/L)	R	Salt rejection (%)
C_p	Salt concentrations in permeate (mg/L)	RO	Reverse osmosis
DLS	Dynamic light scattering	SEM	Scanning electron microscopy
HNT	Halloysite Nanotubes	TEM	Transmission electron microscopy
HNT-COOH	Carboxylic acid functionalized HNT	TDS	Total Dissolved Solids
HNT-G1	First generation PAMAM functionalized HNT	TFC	Thin film composite
HNT-NH_2	Amin functionalized HNT	TFN	Thin film nanocomposite
HNT-x	HNT functionalized by x group	TFN-HNT-x	Thin film nanocomposite membrane embedded with HNT-x
HNT-x-MPD	HNT-x reacted by MPD monomer	TMC	trimesoyl chloride
HNT-x-TMC	HNT-x reacted by TMC monomer	WHO	World Health Organization
ICP-MS	Inductively Coupled Plasma Mass Spectrometry	x-CNC-TFN	Thin film nanocomposite membrane embedded with x % (w/v) CNC
NOM	Natural Organic Matter	XPS	X-ray Photoelectron Spectroscopy

Contributions

Chapters 1 and 2: Motivation, Background and the literature review

The Literature review was written thoroughly by Farhad Asempour, and revised by Dr. Boguslaw Kruczek.

Chapter 3: Synthesis and characterization of novel cellulose nanocrystals (CNC)-based thin film nanocomposite (TFN) membranes for reverse osmosis applications

Fabrication of all membranes, testing them with an RO system, and physicochemical characterizations of membranes were carried out by Farhad Asempour. The RO setup was initially built by Mr. David Carter and modified by Farhad Asempour. The idea of incorporating CNC in TFN membranes for RO applications was first proposed by Dr. D. Emadzadeh, and developed by Farhad Asempour. Commercial ultrafiltration membrane, nanostone PS35, used as the substrate layer for fabrication of RO membranes was first suggested by Dr. D. Emadzadeh. 24 h RO tests to investigate the antifouling properties of membranes were conducted with the help of Mr. Du Bai. TEM images of CNC were provided by Dr. Sara Dastjerdi and Dr. Marc Dubé. Writing the article was entirely done by Farhad Asempour, and Dr. Takeshi Matsuura and Dr. B. Kruczek critically revised and edited the article.

Chapter 4: Synthesis and characterization of various functionalized Halloysite NanoTubes (HNT) based Thin Film Nanocomposite (TFN) reverse osmosis membranes

Fabrication of TFC and HNT embedded TFN membranes, characterizing them, and testing them for saline water desalination via RO process was carried out by Farhad Asempour. Initially, incorporation of pristine HNT in TFN membranes was done as a research and development project for the Qingdao Wosai Seawater Desalination Technology Ltd. Surface functionalized HNT were synthesized and provided by Dr. Somaye Akbari. Some RO tests were carried out with the help of Mr. Andrea Francois and Mr. Du Bai. SEM and TEM images of the HNT as well as zeta potentials of the HNT were provided by Dr. S. Akbari. FTIR characterizations were conducted with the help of Dr. S. Akbari. The article was written by Farhad Asempour. Finally, Dr. T. Matsuura, Dr. S. Akbrai, and Dr. B. Kruczek critically revised and reviewed the article.

Chapter 1

Introduction

Chapter 1-Introduction

1.1. Motivation

Water shortages and stress are among of the most severe challenges of our time. According to world's health organization (WHO), more than one-third of the world's population does not have enough access to reliable fresh water supplies. Due to the climate change, industrialization, population growth, and contamination, the burden on the shrinking resources of fresh water is increasing [1,2]. These issues have sparked many investigations for finding unlimited water resources beyond the current hydrological cycle. Production of potable water by desalination of sea and brackish water is a measure to augment the water supplies [3]. In Canada, even though the water scarcity is not a significant current issue, water reclamation, and process water treatment has become a critical concern for the oil sands industry. Oil sand mines consume large amounts of fresh water with an approximation of 3 barrels of fresh water for each barrel of produced oil. As a consequence large amount of waste and process water which is brackish, alkaline and toxic to the environment is produced. Efficient treatment and desalination of process water are vital for sustainable growth and continuation of Canadian bitumen industry [4,5].

Desalination methods can be categorized into two groups: 1- desalination by phase change (thermal processes), such as multi-effect distillation, multistage flash and vapor compression, and 2- single phase methods (membrane processes) such as reverse osmosis and forward osmosis [6]. Reverse osmosis (RO) is the most widely used desalination method in the world [6,7]. In this process using an external hydrostatic pressure, water is passed through a semi-permeable membrane while salt is rejected by the membrane. The RO membrane is the most integral part of this process which greatly controls the rate of water production and efficiency of the process. Currently, thin film composite (TFC) membranes are the dominant type of membranes in RO industry [8]. TFC membranes are typically composed of three layers. The top layer is a thin film of polyamide (PA), made by interfacial polymerization technique, and is responsible for the rejection of salts. The PA layer is formed onto a porous ultrafiltration membrane which is deposited on a non-woven support fabric [9]. Although TFC membranes have gone through several improvements in the past few decades, there are still challenges for further development of the TFC membranes, thus desalination plants. Trade-off relationship between membrane permeability and selectivity,

membrane fouling and scaling as well as membrane degradation due to chlorination are the current major constraints of TFC membranes [7,10].

Researchers have proposed several approaches to overcome the challenges associated with the TFC membranes. Incorporation of nanoparticles (NP) into the matrix of the PA layer is a relatively new method which was first introduced by Hoek and coworkers at the University of California at Los Angeles in 2005 [7,11]. This new class of membranes is called "Thin Film Nanocomposites" (TFN) membranes. In recent years, fabrication of TFN membranes with various NP and techniques, and studying the membrane separation performance have been the focus of many investigations. So far, several types of zeolites, metal and metal oxide nanoparticles, carbon nanotubes, graphene oxides, etc. with various functionalities and properties have been employed in TFN membranes. It is reported that embedding NP provides TFN membranes with enhanced properties and separation characteristics, such as higher hydrophilicity and water permeability without sacrificing the salt selectivity, increased resistance to fouling, scaling and in some cases chlorination [11,12]. Currently, the application of TFN membranes in large scale is quite limited despite their advantages. One of the most important issues with TFN membranes is leaching out of the typically toxic inorganic NP from the membrane into the downstream. Another challenge for fabrication of TFN membranes is the agglomeration of the NP in the PA layer. These problems result in rising water safety and environmental concerns, membrane degradation and loss of properties over time, and the formation of defects in the structure of the membrane [12]. These problems have motivated many researchers to investigate for new methodologies to address these challenges, which is also the general objective of this thesis.

1.2. Objectives and structure of the thesis

This thesis is focused on fabrication of novel TFN membranes with enhanced properties and separation performance for brackish water desalination via RO process. Therefore, cellulose nanocrystals (CNC) and halloysite nanotubes (HNT) were chosen as the candidate nano-scale additive material in the TFN membrane. These NP are naturally occurring, green, abundant, low-cost, and considered as no/low toxicity [13,14]. In order to address the problem of NP leaching, surface modification and functionalization of HNT with amine groups, carboxylic acid groups, and poly(amidoamine) (PAMAM) dendritic structures are also selected to be studied.

Therefore, the objectives of this work are:

- Fabrication and characterization of RO TFN membranes with improved water flux without sacrificing the salt rejection.
- Incorporation of CNC into the TFN membranes, and finding the optimum range of CNC loading in the TFN membrane for desalination; there are no previous reports of using CNC in RO TFN membranes.
- Embedding HNT into RO TFN membranes, and investigating the effects of surface modification of HNT on the separation characteristics of the TFN membranes. Also, studying the interactions between the nanoparticles and the membrane using different functional groups and PAMAM dendrimer technology.

This thesis is divided into five chapters. The first chapter (current) is a review of the motivation and objectives of this thesis. Chapter 2 provides background information and literature review on RO membrane technology, challenges, and current trends for overcoming them. The 3rd and 4th chapters are written in article format. Chapter 3 focuses on the fabrication, characterization, and optimization of CNC based TFN membranes for RO application. Chapter 4 is focused on the synthesis and characterization of TFN membranes with embedded functionalized HNT. The final chapter provides general conclusions of this research and highlights some recommendations for future studies.

1.3. References

[1] WHO Drinking-water, WHO (2017) http://www.who.int/mediacentre/factsheets/fs391/en/ (accessed June 29, 2017).

[2] R.F. Service, Desalination Freshens Up, Science. 313 (2006) 1088–1090. doi:10.1126/science.313.5790.1088.

[3] M. Elimelech, W.A. Phillip, The Future of Seawater Desalination: Energy, Technology, and the Environment, Science. 333 (2011) 712–717. doi:10.1126/science.1200488.

[4] E.W. Allen, Process water treatment in Canada's oil sands industry: I. Target pollutants and treatment objectives, J. Environ. Eng. Sci. 7 (2008) 123–138. doi:10.1139/S07-038.

[5] E.W. Allen, Process water treatment in Canada's oil sands industry: II. A review of emerging technologies, J. Environ. Eng. Sci. 7 (2008) 499–524. doi:10.1139/S08-020.

[6] A. Pérez-González, A.M. Urtiaga, R. Ibáñez, I. Ortiz, State of the art and review on the treatment technologies of water reverse osmosis concentrates, Water Res. 46 (2012) 267–283. doi:10.1016/j.watres.2011.10.046.

[7] W.J. Lau, A.F. Ismail, N. Misdan, M.A. Kassim, A recent progress in thin film composite membrane: A review, Desalination. 287 (2012) 190–199. doi:10.1016/j.desal.2011.04.004.

[8] J.C. Crittenden, R.R. Trussell, D.W. Hand, K.J. Howe, G. Tchobanoglous, Reverse Osmosis, in: MWHs Water Treat. Princ. Des. Third Ed., John Wiley & Sons, Inc., 2012: pp. 1335–1414.

[9] J. Mulder, Basic Principles of Membrane Technology, Springer Science & Business Media, n.d.

[10] G.-R. Xu, J.-N. Wang, C.-J. Li, Strategies for improving the performance of the polyamide thin film composite (PA-TFC) reverse osmosis (RO) membranes: Surface modifications and nanoparticles incorporations, Desalination. 328 (2013) 83–100.

[11] B.-H. Jeong, E.M.V. Hoek, Y. Yan, A. Subramani, X. Huang, G. Hurwitz, A.K. Ghosh, A. Jawor, Interfacial polymerization of thin film nanocomposites: A new concept for reverse osmosis membranes, J. Membr. Sci. 294 (2007) 1–7. doi:10.1016/j.memsci.2007.02.025.

[12] W.J. Lau, S. Gray, T. Matsuura, D. Emadzadeh, J. Paul Chen, A.F. Ismail, A review on polyamide thin film nanocomposite (TFN) membranes: History, applications, challenges and approaches, Water Res. 80 (2015) 306–324. doi:10.1016/j.watres.2015.04.037.

[13] Y. Habibi, L.A. Lucia, O.J. Rojas, Cellulose Nanocrystals: Chemistry, Self-Assembly, and Applications, Chem. Rev. 110 (2010) 3479–3500. doi:10.1021/cr900339w.

[14] M. Liu, Z. Jia, D. Jia, C. Zhou, Recent advance in research on halloysite nanotubes-polymer nanocomposite, Prog. Polym. Sci. 39 (2014) 1498–1525.

Chapter 2

Background and literature review

Chapter 2- Background and literature review

2.1. Overview of membrane separation processes

Membrane separation processes can be used in a wide range of industries such as chemical, mineral, petrochemical, pharmaceutical, electronics, biotechnology, food, textile, paper and water purification and treatment [1]. A membrane is often referred to a permeable or semi-permeable thin barrier which allows the transport of certain molecules/particles while restricting the others. Depending on the type of membranes and the applied driving force for transport and separation of selected species, membrane processes are classified in various groups. Figure 2.1 illustrates the classification of membrane separation processes. Particularly for water purification the common pressure-driven membrane processes are categorized as microfiltration (MF), ultrafiltration (UF), nanofiltration (NF), and reverse osmosis (RO) [2]. The focus of this report is on the RO process and development of novel and environmentally friendly thin film nanocomposite membranes (TFC), with enhanced properties and performance for brackish water desalination.

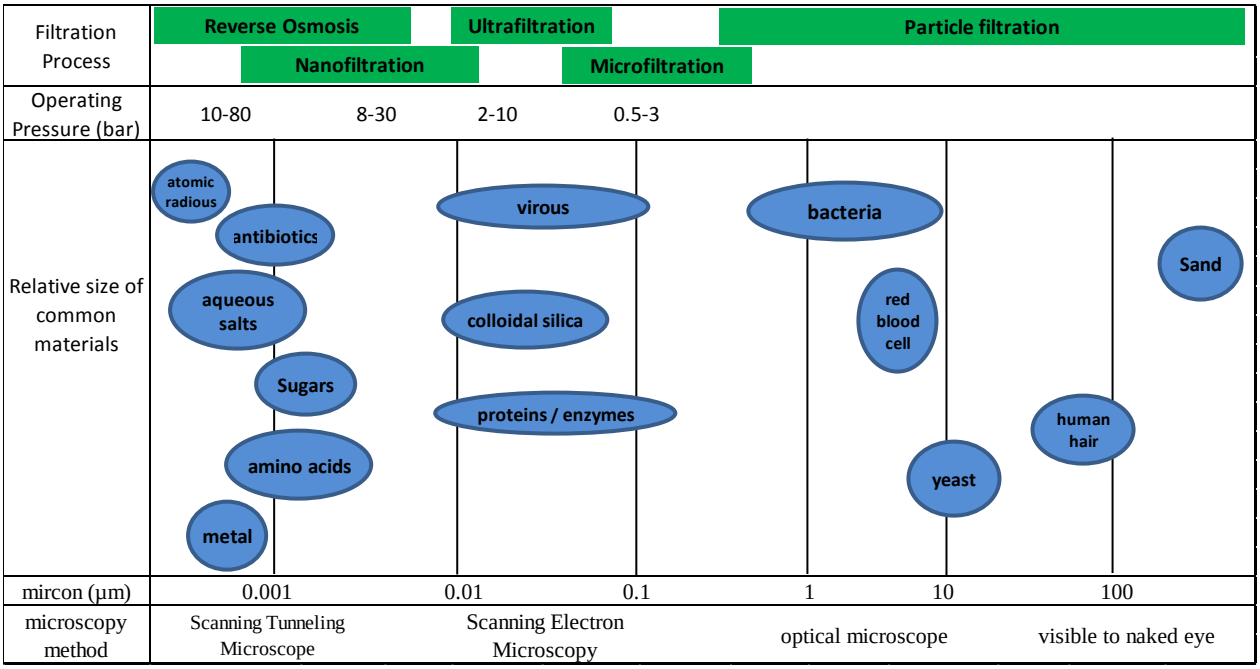

Figure 2.1 Relative size of material and their filtration process; adapted from [2,3].

2.2. Reverse osmosis

2.2.1. Principles and applications of reverse osmosis

If two solutions with different solute concentrations are divided by a semipermeable membrane, which restricts permeation of solute, molecules of the solvent tend to move from the less concentrated side into the region with higher solute concentration. The transfer of solvent molecules continues until reaching the chemical potential equilibrium, which here is the osmotic pressure. In the RO process, the direction of the solvent transport is reversed by applying an external hydrostatic pressure (ΔP) to exceed osmotic pressure difference ($\Delta\pi$) [1,2]. Directions of the transport in osmosis and reverse osmosis are illustrated in Figure 2.2.

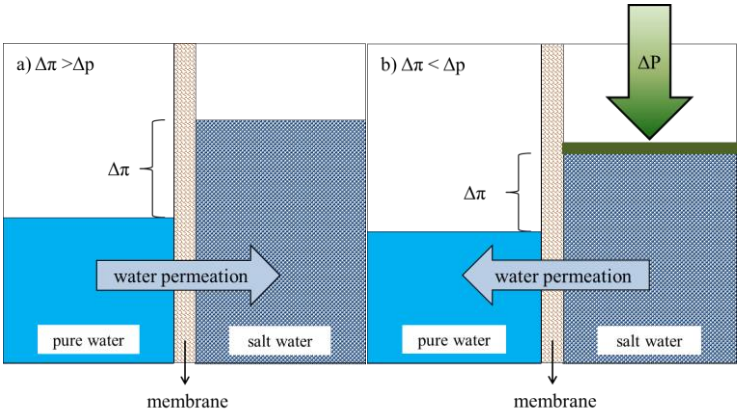

Figure 2.2 Direction of water permeation in: a) osmosis, and b) reverse osmosis [2].

Equation 2.1, which is referred to as Van't Hoff equation for the estimation of the osmotic pressure, can be thermodynamically derived for an ideal, incompressible solution [2,4]:

$$\pi = \frac{-RT}{V_b} \ln x_w \qquad (2.1)$$

Where π [bar] is the osmotic pressure, V_b [L/mol] molar volume of pure water (solvent), x_w [-] is the mole fraction of water in the solution, T [K] is the absolute temperature, and R, which is equal to 0.083145 [L.bar/(mol.K)], is the universal gas constant. For dilute solutions, $x_w \approx 1$, equation 2.1 can be approximated as equation 2.2. To account for compressibility of the liquid at high pressures, and non-ideality of the solution, the osmotic coefficient is added to the equation, equation 2.2.

$$\pi = i\phi CRT \qquad (2.2)$$

where i is the dissociation factor of solutes in the solution, C [mol/L] is the total molar concentration of all solutes in the solution, and ϕ [-] is the osmotic coefficient, which for seawater ranges from 0.93 to 1.03 [4]. The selective layer of RO membranes is typically a dense polymer film, which is considered nonporous. The transport in this nonporous selective layer w of the membrane is commonly described a solution-diffusion model. According to this model, solvent and solutes first dissolve in the membrane at the feed side, then diffuse through the membrane, and finally liquefy again at the permeate side [1,2]. Separation of the water and solutes occurs when their respective permeance coefficients in the membrane are different. Other models such as pore flow and preferential sorption-capillary flow or combination of them with the solution-diffusion model are also used for transport of molecules through the RO membranes [1,2]. The water and solute fluxes can be described as the product of the respective permeance coefficients and the driving forces. For water we have:

$$J_w = P_w(\Delta p - \Delta\pi) \qquad (2.3)$$

where J_w [L/m^2.h] is volumetric water flux, P_w [L/(m^2.h.bar)] is water permeance, Δp [bar] is transmembrane hydrostatic pressure difference, and $\Delta\pi$ [bar] is transmembrane osmotic pressure difference. For the solute flux, the equation 2.4 is used.

$$J_s = P_s(\Delta C) \qquad (2.4)$$

where J_s [g/(m^2 .h)] is the flux of the solute, P_s [L/(m^2 .h)] is solute permeance, and ΔC [g/L] is the concentration difference across the membrane [1,2] .

Reverse osmosis is a promising process for separation of monovalent, bivalent salts and natural organic material (NOM) from water. In fact, the most common application of RO membranes is for desalination of ground and brackish water, with 2,000 to 10,000 mg/L of Total Dissolved Solids (TDS), and sea water, with 34,000 to 38,000 mg/L of TDS. It should be noted that according to the World Health Organization (WHO), the maximum concentration of TDS in potable water is 500 mg/L. It is estimated that almost 65% of the world's desalination plants are based on the RO process. Depending on the concentration of the salts in the feed, the water applications of RO can be categorized in three groups: brackish water desalination, seawater desalination, and ultrapure water production and waste water treatment. This thesis is concerned

with desalination of brackish water. Due to a relatively low TDS in brackish water, 90% salt rejection is enough for the production of potable water. Also, the brackish water reverse osmosis (BWRO) is sometimes referred to as a low-pressure RO since the processing pressure is in the range of 10 to 30 bars compared to 50 – 60 bars for seawater desalination [2,4,5].

2.2.2. Conventional RO polymeric membrane materials

The membrane is the most important part of the RO process, and the gain in efficiency is greatly associated with improvements of the membrane material [6]. Over the past few decades RO membranes have gone through significant improvements in their performance (i.e. water flux) and selectivity, i.e. salt and boron rejection, as well as physical, chemical and biological durability [7].
In general, commercial RO membranes are classified in two groups: anisotropic (asymmetric) cellulosic membranes and thin film composite (TFC) polyamide (PA) membranes [2]. The commercial use of RO membranes for saline water desalination initially started with the development of anisotropic cellulose acetate (CA) membranes by Loeb and Sourirajan in the 1960s [8,9]. Loeb-Sourirajanian membranes are made of a single material with the phase inversion technique. In this method, a controlled interaction between solvent and non-solvent solutions induces a phase separation in which polymer dispersion is transformed into a solid polymer-rich phase (membrane), and a liquid polymer-lean phase which shapes the pores [1,4]. To synthesize CA RO membranes by Loeb-Sourirajan technique, a polymer solution comprising 20 to 25% CA and a water miscible solvent is cast on a glass or a nonwoven support fabric. Then, the cast is immersed in a non-solvent bath (typically water) where the absorption of water and loss of solvent cause the film to rapidly precipitate from the top surface down [1]. Although CA membranes are still commercially available, due to higher water flux and salt rejection, TFC membranes are dominantly used in the RO industry.

The idea of fabricating composite membranes via interfacial polycondensation on top of a sub layer was first proposed by Morgan [10]. However, high-performance TFC membranes were introduced by Cadotte and his coworkers in 1970s [6,11]. For RO applications, TFC membranes are generally comprised of three layers: a selective aromatic PA layer, a porous phase inverted polysulfone (PS) or polyethersulfone (PES) ultrafiltration (UF) membrane, and a polyester (PET) nonwoven fabric to provide mechanical strength (Figure 2.3). TFC membranes have a higher physical and chemical stability in a wider range of temperatures than CA membranes, and are

stable in the pH range of 4 to 6. However, TFC PA membranes do not tolerate free chlorine or any other oxidizer, i.e. chlorine tolerance < 0.02 ppm. TFC PA membranes are less hydrophilic than CA membranes, and have a rough surface morphology which makes them more prone to fouling [1,2,4]. Because of higher permeance, salt rejection, and dominance of TFC membranes in the RO industry, this thesis is focused on TFC membranes. The next few sections are allocated to the structure, chemistry, and strategies for enhancing the properties and performance of TFC PA membranes.

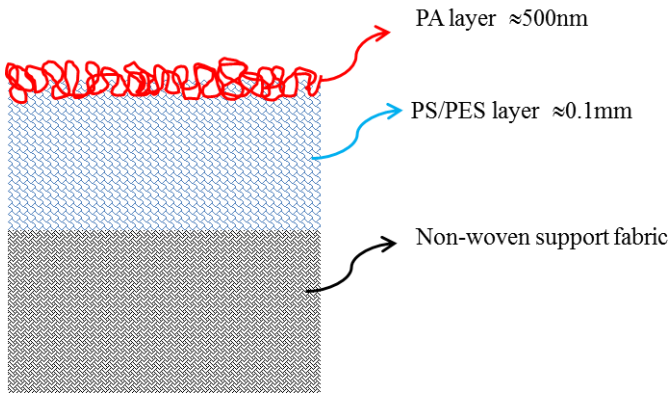

Figure 2.3 Schematic structure of a PA TFC membrane [2,12].

2.2.3. Fabrication, chemistry and structure of the polyamide layer in TFC membranes

Polyamide TFC membranes are fabricated by in-situ interfacial polymerization (IP). In this process, first the UF substrate is immersed in an aqueous amine rich solution, so the pores of the membrane are filled with the first monomer. Then, the amine loaded membrane is contacted with a water-immiscible solution, which consists of the second monomer. Therefore, at the interface of the two phases, a polycondensation reaction takes place, which forms a thin and cross-linked polyamide film [1,11,13]. Today, most of commercially available RO TFC membranes have a fully aromatic chemical structure, which is formed by the reaction of m-phenylenediamine (MPD) with trimesoyl chloride (TMC); this combination of monomers was proposed by Cadotte and FilmTec (Dow chemical) [11,14]. Morgan and Kowlek in their pioneering work suggested the mechanism of IP of polyamide [10]. According to them, when organic solution meets the aqueous solution, due to the very low aqueous solubility of the acid chlorides, IP occurs at the organic side of the interface. The imbalance in the solubility of the monomers forces diamines to diffuse to the

organic solution in order to form the polyamide layer [10]. This means that the polymer thin film grows perpendicular to the interface, and has an asymmetric morphology. Also, since the IP is controlled by the diffusion of diamine groups, the polymerization reaction continues until the formed thin film becomes a barrier for the diamine to diffuse. This morphology, a smooth layer at the interface and a rough and nodular with "ridges and valleys" top surface, is confirmed by SEM and TEM images of the dense layer in the MPD-TMC polyamide membranes.

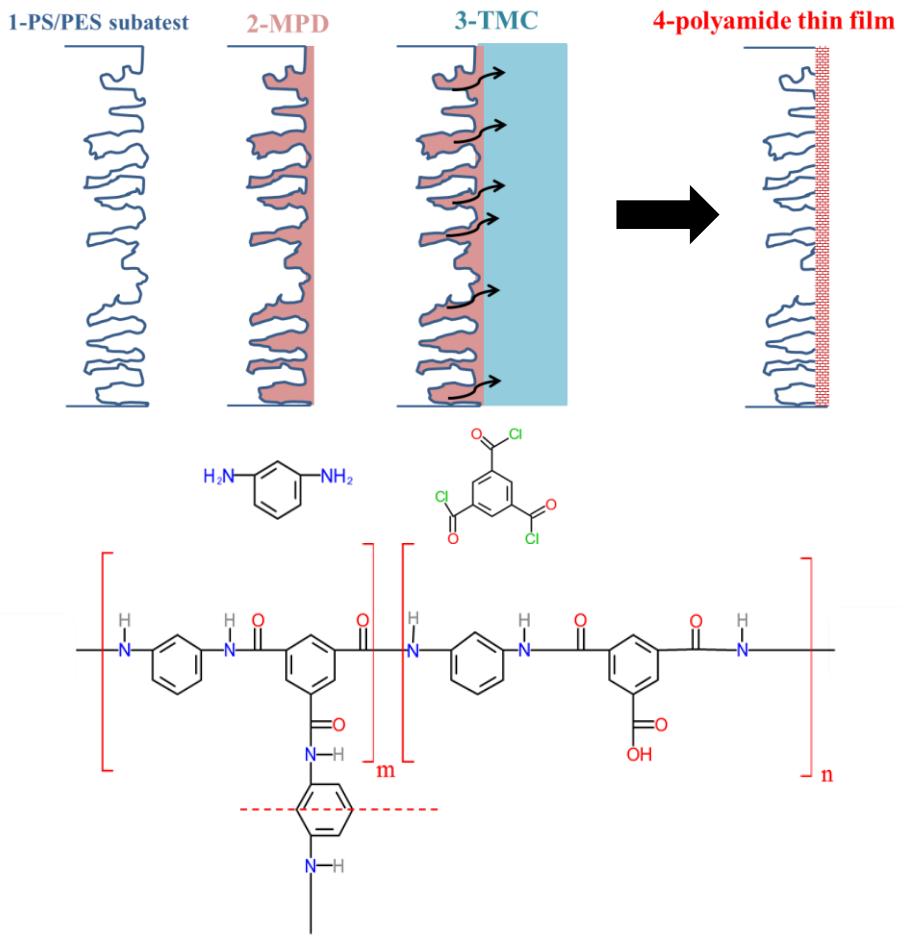

Figure 2.4 Schematic of formation of PA TFC membrane. 1- PSF or PES porous substrate 2- immersing substrate with aqueous amine rich solution (MPD) 3- contacting substrate with organic acid solution (TMC) in this step interfacial polymerization occurs i.e. molecules of MPD diffuse in to the organic phase and react with it 4-formation of dense polyamide matrix, m and n represent crosslinked and linear sections respectively; addapted from [13].

As it is illustrated in Figure 2.5, the top selective polyamide layer has a nodular and rough structure. It was commonly accepted that this layer is dense without any pores [4,15]. However,

recently using the modern imaging technologies, some reports have suggested that the globular and protuberance structures are in fact water filled nanopores. Pacheco et al. studied the polyamide RO membrane by TEM tomography and created a 3D visualization of any section of the thin film volume [16]. Based on the images they confirmed existence of the 20-60 nm voids, and suggested that some the voids are fully encapsulated by the polyamide while others are open to the lower surface of the thin film. They also suggested that density of the voids is greater in the lower parts of the polyamide layer. In another study, Lin et al. reported that the voids comprise between 15 to 32% of the polyamide layer, but they do not provide continuous passages across the polyamide [12].

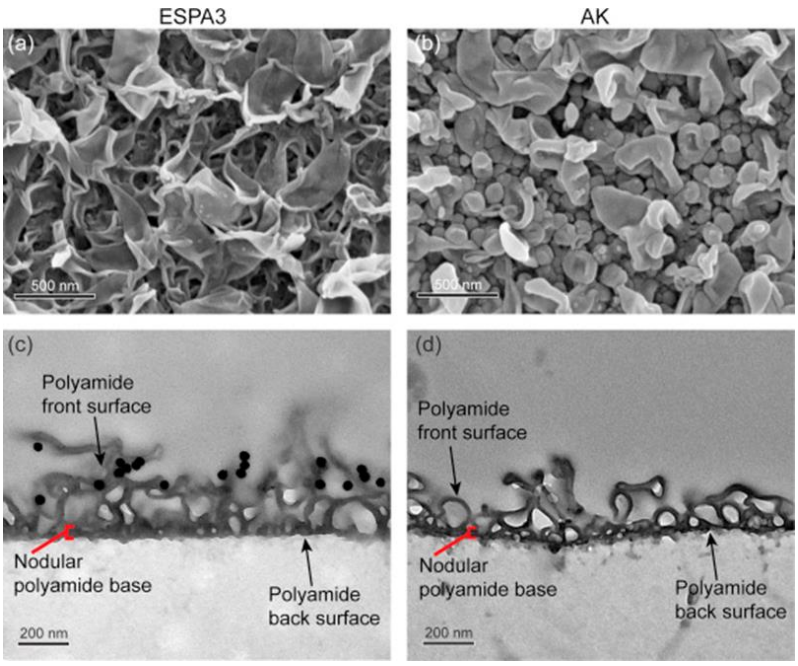

Figure 2.5 SEM image of the top surface (a and b), and TEM image of cross section (c and d) of fully aromatic TFC membrane ESPA3 (Hydranautics, Oceanside, CA, USA) and AK (GE Minnetonka, MN, USA) brackish water RO. Black dots in (c) are 30 nm gold NP [16].

2.2.4. Major drawbacks of PA-TFC-RO membranes

Despite the improvements in the performance and physiochemical properties of the RO membranes, there are still major challenges related to their performance and efficiency, which have limited further development of RO technology, and desalination industry in general. The primary drawbacks of these membranes are the trade-off relation between permeance and salt rejection, membrane fouling and practically no resistance to chlorination [17,18].

It is commonly known that increase in the water flux causes a decrease in the selectivity of the PA-TFC membranes. Overcoming this “trade-off” relation, by having both higher water flux and salt rejection is a desirable improvement in the performance of these membranes. Membrane fouling and scaling occurs due to the precipitation and accumulation of the foulants on the top surface of the membrane, which causes permeate flux decline. Deposition of organic and biological material, colloidal and particulate matter, insoluble inorganic salts or metal oxides are some of the main fouling sources. Membrane surface hydrophilicity, charge and roughness are some of the variables that affect membrane fouling and scaling [19–21]. Chlorination of feed water is a common way for controlling the biofouling; however, as it was mentioned before, PA is very susceptible to chlorine and undergoes degradation. Many studies have been conducted to explain the mechanism of the PA chlorination [22,23]. Xu et al. categorized the routes in which active chlorine species attack the structure of PA: 1- formation of N-chloroamide by substitution of hydrogen of the amide group with chlorine atom, 2- direct chlorination of aromatic rings of MPD 3- rapid N-chlorination followed by mitigation of chlorine to the aromatic ring through the intramolecular rearrangements, known as Orton rearrangements and 4- facilitated hydrolysis of PA layer by chlorine (Figure 2.6) [17] . The exact mechanisms of chlorine – PA matrix interactions are not yet fully understood. However, in general, chlorine attacks the amide nitrogen and aromatic ring in the PA layer, which results in deformation in the polymer chain or chain cleavage at the amide linkages [22].

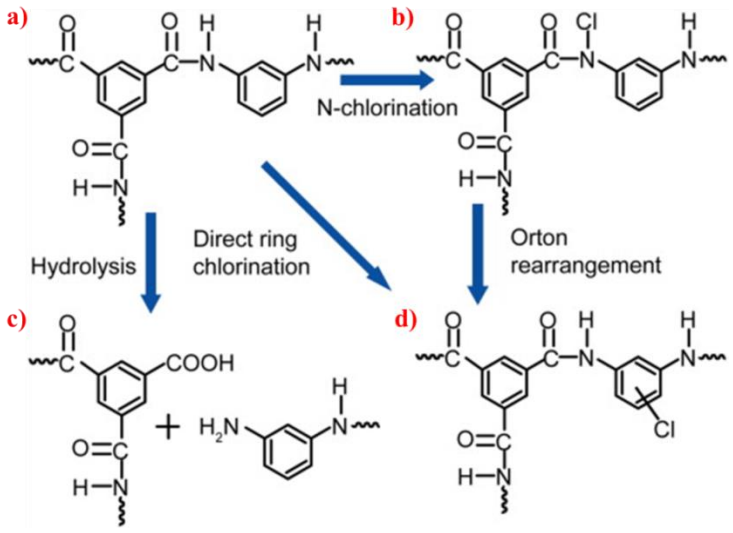

Figure 2.6 Chlorination of PA structure via four routs. a) PA structure, b and d) chain deformation by N-chlorination, and c) chain cleavage [17].

2.2.5. Strategies to enhance the performance of the PA-TFC RO membranes

Parameters in governing surface properties of the PA layer in TFC membranes include suitable support layers, monomers, additives, nanofillers, and reaction conditions [6]. Many approaches have been proposed to surpass the explained limitations of the PA-TFC RO membranes. One of the advantages of the TFC membranes is the ability to tune the properties of the TFC membrane by tailoring the porous substrate and the PA layer separately [6]. Here, some of the approaches to modify the PA layer are briefly mentioned.

Monomers

The search for newly synthesized monomers to enhance the properties of PA thin films is still an ongoing research area [6,13,24,25]. Table 2.1 provides a list of some of the proposed monomers. For example, in order to increase the hydrophilicity of the top selective layer, Wang et al. used triamine 3,5-diamino-N-(4-aminophenyl) benzamide (DABA) as an additional monomer to the diamine phase, MPD, in fabrication of TFC RO membranes with TMC [26]. They reported an increased permeance (37.5 to 55.4 L/m^2 h) with a slight decrease in the salt rejection (98.4 to 98.1%) with an increase in the concentration of DABA monomer in the amine phase from 0% to 0.25% (w/v). With regard to chlorine resistance, Konagaya and Watanabe investigated isophthaloyl dichloride and aliphatic, cycloaliphatic and aromatic diamines for fabrication of the PA RO membranes [27]. The chlorine resistance tests suggested that membranes fabricated using aromatic diamine compounds with an ortho positioned mono CH_3 or Cl substituents, had improved chlorine resistance. In another work, Yu et al. suggested m-phenylenediamine-4-methyl (MMPD) and cyclohexane-1,3,5-tricarbonyl chloride (HTC) for a synthesis of aromatic-cycloaliphatic PA-TFC RO membranes [28]. In their work, at the optimum performance, MMPD-HTC membrane showed a significant increase in the chlorine tolerance, up to 3000 ppm-hour Cl. They attributed the high chlorine resistance to the reduced probability of N-chlorination and Orton-rearrangement by utilizing MMPD.

Table 2.1 Some of the commonly used and recently reported monomers for synthesis of PA layer [6].

Amine monomer (abbreviation)	Chemical structure	Molecular weight	Acyl chloride monomer (abbreviation)	Chemical structure	Molecular weight
Piperazine (PIP)		86.14	Trimesoyl chloride (TMC)	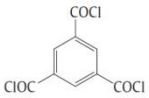	265.48
M-Phenylenediamine (MPD)	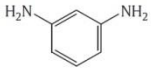	108.10	Isophthaloyl chloride (IPC)		203.02
P-Phenylenediamine (PPD)	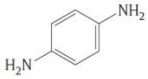	108.10	5-isocyanato-isophthaloyl chloride (ICIC)	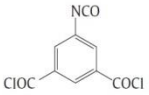	244.04
Sulfonated cardo poly(arylene ether sulfone) (SPES-NH_2)	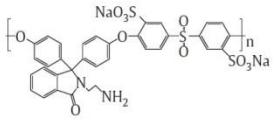	774.71	*mm*-Biphenyl tetraacyl chloride (*mm*-BTEC)	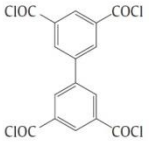	404.03
3,5-diamino-N-(4-aminophenyl) benzamide (DABA)	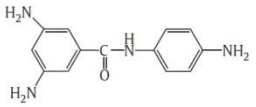	242.27	*om*-Biphenyl tetraacyl chloride (*om*-BTEC)	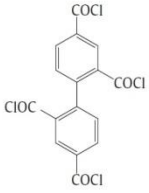	404.03
Triethanolamine (TEOA)	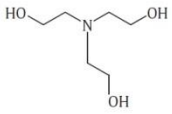	149.19	*op*-Biphenyl tetraacyl chloride (*op*-BTEC)	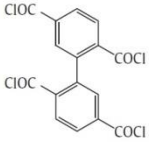	404.03
Methyl-diethanolamine (MDEOA)	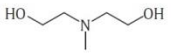	119.16	Cyclohexane-1,3,5-tricarbonyl chloride (HTC)	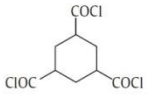	271.53
1,3-cyclohexanebis (methylamine) (CHMA)	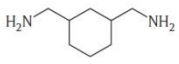	142.24	5-chloroformyloxy-isophthaloyl chloride (CFIC)	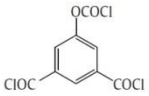	281.48
m-phenylenediamine-4-methyl (MMPD)	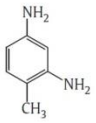	122.17			
Hexafluoroalcohol-m-Phenylenediamine (HFA-MPD)	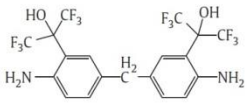	530.31			

Surfactants and additives/co-solvents

Addition of co-solvents and surfactants to the hydrocarbon solution is another commonly reported approach for improving the properties of PA-TFC-RO membranes [6,17]. Surfactants and co-solvents can modify the polymerization reaction. These materials can fill the miscibility gap between the amine, i.e. MPD and organic acid, i.e. TMC, solutions and provide a wider area/volume ratio for the reaction. For example, Kong et al. suggested that mixing acetone in the organic phase generates additional controllable MPD-TMC miscible/reaction zones which make the thickness of active PA layer regulated, Figure 2.7 [29]. Under these circumstances, they reported generation of thinner, less than 100 nm, and denser PA layer, which led to a three-fold increase in the permeate flux without a significant decrease in salt rejection.

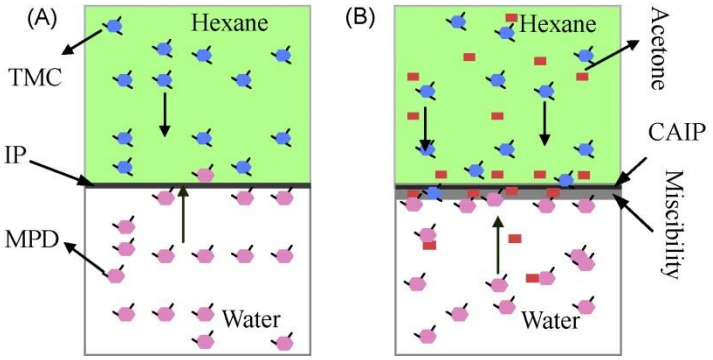

Figure 2.7 Schematic of conventional interfacial polymerization of MPD and TMC a) conventional method b) co-solvent assisted technique [29].

Surface modification

Due to incomplete crosslinking of the polyamide, the top surface of the TFC RO membrane has a large number of amino (-NH_2), and carboxylic (-COOH) groups, and it is negatively charged [17,30]. These unsatisfied groups can be reactive sites for binding with surface coating and nanoparticles. In general, the currently applied surface modification technologies include surface coating by thin films or self-assembled monolayers, and polymer grafting by chemical treatment such as UV or plasma treatment. In recent years, many researchers have worked on various functional coating layers such as hyperbranched and polyethylene glycol (PEG) based hydrophilic materials, polydopamine coating, zwitterionic-based coating, layer-by-layer assembly coating, and

chlorine resistance coating. These surface modifications are mainly focused on increasing the hydrophilicity of the top surface, and increasing the fouling resistance. However, even though increased hydrophilicity of the membrane leads to higher permeance, coating layers may affect the permeance of the membrane due to the additional resistance to mass transfer [17,29,30].

Incorporation of nano-scaled material in membranes

Nanoparticles (NP) are materials which are between 1 to 100 nm in at least one dimension. The most lucrative properties of NP are their very large specific surface area, antibacterial and adsorption properties [31,32]. In recent years, applications of nano-scaled materials in the membrane separation processes have harnessed many attentions. Here, the term "nano" in nano-enhanced or nanocomposite membranes refers to the added NP or nanotubes to functionalize the membranes and not the internal structure and pores of the membrane [33]. Depending on the structure and location of the NP, Yin and Deng categorized polymeric nanocomposite membranes into four groups: 1) conventional mixed matrix nanocomposite membranes, 2) thin film composite (TFC) membrane with nanocomposite substrate, 3) surface located nanocomposite membranes, and 4) thin-film nanocomposite (TFN) membranes. These groups are illustrated in the Figure 2.8 [34].

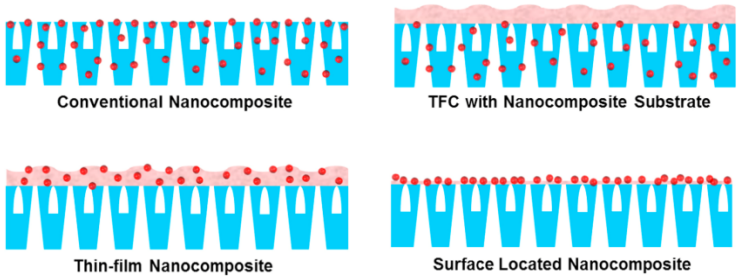

Figure 2.8 Schematic of different types of nanocomposite RO membranes [34].

Conventional nanocomposite or mixed matrix membranes are mostly made by phase inversion method for synthesis of porous membranes for water treatment. Nanofillers can improve the thermal, chemical and mechanical stability of the membranes as well as the membrane selectivity, and permeance. Also, NP such as molecular sieve can increase the hydrophilicity of the membranes, improve antifouling capacity and enhance structure of the membrane by influencing membrane porosity and pore interconnectivity [24,35,36].

TFC membranes with nanocomposite substrate were first developed to study the effects of membrane compaction. It is reported that incorporation of silica particles led to higher initial permeance and less membrane compaction in comparison with a similar TFC membrane with no added NP. This category of membranes is also used in forward osmosis membranes especially to reduce internal concentration polarization, which occurs within the pores of the membranes.

Properties of the membrane's top surface such as hydrophilicity, charge density and roughness have a large effect on the overall performance of the membrane [34,36]. These properties can be modified and tailored by incorporation of NP. So far, several methods have been suggested for integrating NP to the surface on the membranes including, NP self-assembly, coating/deposition, chemical grafting, electrostatic attraction, and layer-by-layer assembly [34,37]. For example, Kwak and Kim integrated TiO_2 NP onto the TFC RO membranes by self-assembly of particles through ionic interactions and hydrogen bonding forces with the carboxyl groups from the aromatic PA layer [38]. They reported that the tightly adsorbed TiO_2 particles increased the water flux, and provided the membranes with photocatalytic properties. In another study by Yin et al., Ag NP were grafted to the PA layer via covalent bonding using cysteamine bridging agent (thiol derivated, NH_2–$(CH_2)_2$–SH) [39]. They reported that in comparison with pristine TFC membrane, Ag-grafted membranes had improved antibacterial properties with higher permeance and slightly lower salt rejection. Figure 2.9 illustrates the grafted membranes. The fourth category of nano-enhanced composite membranes is the TFN membranes, which are thoroughly described in the next section.

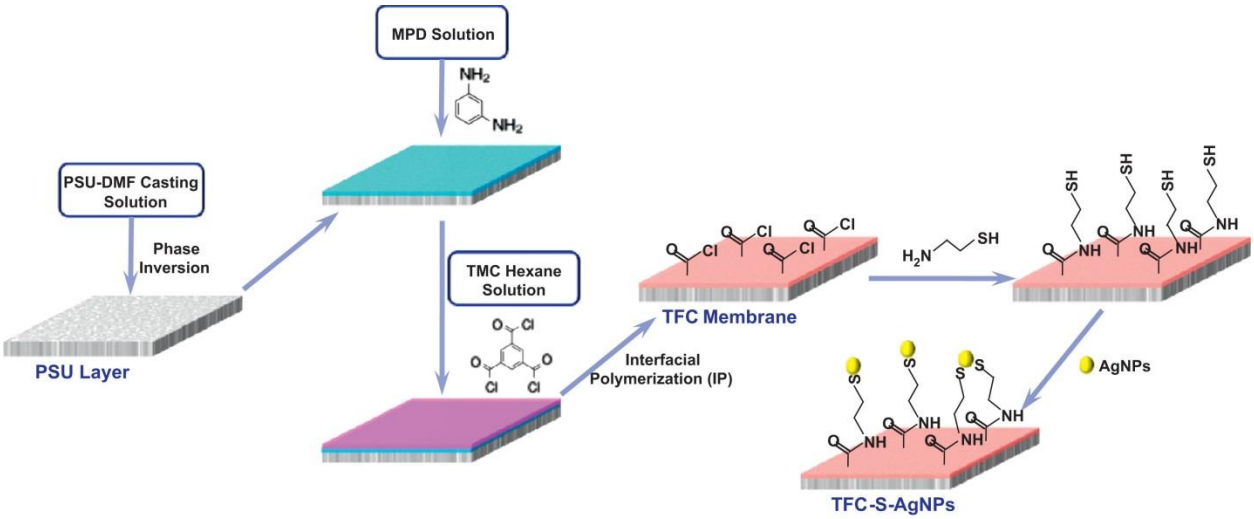

Figure 2.9 Schematic of immobilization of Ag NP onto the surface of PA TFC membrane [39].

2.3. Thin film nanocomposite (TFN) membranes

2.3.1. Overview of TFN membranes

TFN membranes are formed by the incorporation of NP into the selective PA layer of TFC membranes. This concept was first introduced by Hoek and coworkers, and the term "Thin Film Nanocomposite (TFN) membrane" was first used in their publication in 2007 [40]. Use of NP adds more degrees of freedom to the material properties and separation performance of the membranes, which helps to surpass the limitations of TFC membranes. In the last decade, TFN membranes have generated a lot of interest; studies are mostly focused on applications of these membranes for reverse osmosis (RO), nanofilteration (NF), and forward osmosis (FO) processes. There are, also, few reports on the application of TFN membranes for pervaporation and gas separation [36]. According to the literature, nano-scaled fillers can modify the performance and properties of the TFN membranes, and overcome trade-off relationship between the permeability and selectivity, and enhance antifouling properties, antimicrobial activity, chlorine resistance, and the mechanical and thermal stability. Table 2.2 shows a list of some reported NP used in TFN membranes.

The first industrial application of TFN membranes was tested by NanoH_2O Inc. at Port Hueneme United States Navy Facility in September 2008. It was reported that TFN membranes showed a 2-fold higher water flux than the conventional PA-TFC membranes and the salt rejection was 99.7%. NanoH_2O Inc. was later acquired by LG Chem, and under QuantumFlux brand name; they manufacture TFN membranes for water desalination [32,36].

Table 2.2 Some of the reported TFN membrane [34].

TFN		Particle size	Loading wt% (Best performance)	Fabrication method	Application	Performance	Published year and Reference
Filler	Polymer						
Oxidized MWNTs	Pebax 1074 or PVA	OD=20–40 nm L=5–15 μm	0–20% of polymer (10% of PVA)	Coating+Solvent evaporation	Water/oil emulsion separation	Under 100 psi, optimal water flux is 330 L/m^2 h, organic solute rejection is 99.8%; Fouling resistance ↑	2005
Zeolite (NaA)	PA	50–150 nm	0.004–0.4% (w/v) in organic phase	IP	RO	Surface hydrophilicity ↑; P_w ↑; Salt rejection no change; New concept: TFN	2007
Ag NPs	PA	50–100 nm	10% of polymer in organic phase	IP	NF	Water flux and salt rejection no change; Good antibiofouling property	2007
TiO_2 (P25)	PA	30 nm	1.0–9.0% (5.0%) Organic phase	IP	NF	Under 87 psi, optimal water flux is 9.1 L/m^2 h, $MgSO_4$ rejection (95%, 2000 mg/L)	2008
Silica (LUDOX® HS-40)	PA	~13.2 nm	5–28% of PA	IP	Dioxane solution filtration	P_w ↑; Solute rejection ↓	2008
Zeolite (NaA and AgA)	PA	50–250 nm	0.4% (w/v) in organic phase	IP	RO	P_w ↑; Salt rejection no change; AgA-TFN membranes exhibited more hydrophilic and smooth surfaces.	2009
Zeolite	PA	97, 212, and 286 nm	0.2% (w/v) in organic phase	IP	RO	Smaller NPs produced higher permeability enhancements, but larger NPs produced more surface properties change	2009
Silica	PA	3 and 16 nm	0–0.4% (3 nm) and 0–0.5% (16 nm) in aqueous phase	IP	RO	P_w ↑; NaCl rejection ↗↘; Thermal stability↑	2009
Oxidized MWNTs or Cellulose Nanofibers	PVA	OD=8–15 nm L=10–50 μm OD=~5 nm L<10 μm	10% of PVA 0.25% and 1.25% of PVA	Coating+Cross-linking	UF of oil/water emulsion	P_w ↑; Solute rejection slightly decreased; Suggested the presence of directional water channels through the interface between filler and PVA matrix	2010
Carboxylic MWNTs	Polyester	OD<8 nm L=10–30 μm	0.05% (w/v) in aqueous phase	Modified IP O/A/O	NF	P_w ↑; Na_2SO_4 rejection↑; Immerse support layer into organic phase before conventional IP process improved TFN performance	2010
MWNTs	PA	OD=9–12 nm L=10–15 μm	0.1, 0.5, 1, 5% (w/v) in aqueous phase	IP	RO	Surfactant (Triton X-100) was used to facilitate the dispersion of MWNTs; Chlorine resistance ↑	2010
Zeolite (LTA)	PA	~250 nm	0.2% in organic phase	IP	Seawater RO	Under 800 psi, optimal permeate flux is around 42 L/m^2 h, NaCl rejection (99.4%, 32,000 mg/L); Defects and molecular-sieving largely govern transport through zeolite-TFN membranes	2010
Functionalized Silica	PA	–	0.04, 0.4% in aqueous phase	IP	RO; PV	Small-angle neutron scattering (SANS) was used to study the dispersion of silica NPs in thin-film layer Thermal stability ↑; P_w ↑; NaCl rejection ↓	2010
Functionalized MWNTs	PA	OD=~ 30 nm L_1=10–30 μm L_2=0.5–2.0 μm	0.01–0.06% in aqueous or organic phase	IP	NF	P_w ↑; Solute rejection no change Nanogaps around the external surface of fillers provide a low resistance solvent pathway	2011
Oxidized MWNTs	PA	–	0–0.2% (w/v) in aqueous phase	IP	RO	Surface hydrophilicity ↑; P_w ↑; NaCl rejection ↓	2011
Metal alkoxide (TTIP, BTESE, PhTES)	PA	–	0–5% in organic phase	IP	NF/RO	Pore size ↑; P_w↑; With PhTES, P_w ↑, NaCl rejection no change	2011
Zeolite (NaX)	PA	40–150 nm	0.004, 0.01, 0.04, 0.2% (w/v) in organic phase (0.2%)	IP	RO	Thermal stability ↑; Hydrophilicity ↑; P_w ↑; NaCl rejection no change	2011
Hydrophilized ordered mesoporous carbon (OMC)	PA	–	0–10% in aqueous phase (5%)	IP	NF	Hydrophilicity ↑; Protein adsorption↓; P_w ↑; NaCl rejection ↓; Na_2SO_4 rejection slightly ↓	2011
Hydrophilic macromolecules+Ag^+	PA	11,000 Da	0.25% of (MDI+PEG) in organic phase 0.25% of $AgNO_3$ in aqueous phase	IP	Seawater RO	Good seawater desalination performance Fouling resistance ↑; Biofouling resistance ↑	2011
Ag NPs	PA	Several nanometers	Dispersed in aqueous phase Finally, 10% in PA	IP	NF	Surface hydrophilicity ↑; P_w ↑; Salt rejection no change Biofouling resistance ↑	2012

Table 2.4 (continued)

TFN		Particle size	Loading wt% (Best performance)	Fabrication method	Application	Performance	Published year and Reference
Filler	Polymer						
Mesoporous silica (MCM-41) and nonporous silica	PA	~100 nm ~100 nm	0–0.1% in organic phase (0.05%)	IP	RO	Surface hydrophilicity ↑; P_w ↑; Salt rejection no change Under 300 psi, optimal permeate flux is 46.6 L/m^2 h, NaCl rejection (97.9, 2000 mg/L) Porous structures of filler contributed significantly to the water flux enhancement	2012
Proteoliposome with aquaporin	PA	< 150 nm	10 mg/ml in aqueous phase	IP	RO	P_w ↑; Salt rejection no change Under 72.5 psi, water flux is 20 L/m^2 h, NaCl rejection (~97%, 584.4 mg/L)	2012
Aluminosilicate SWNTs	PVA	OD = 2.7 nm L > 200 nm	0–20% (v/v) in PVA solution	Coating + Cross-linking	NF	Surface hydrophilicity ↑; Roughness↓; P_w ↑; Salt rejection ↑	2012
Zeolite (NaY)	PA	40–150 nm	0–0.4% (w/v) in organic phase (0.1%)	IP	FO	P_w ↗↘; NaCl rejection ↘; Surface roughness ↗↘	2012
Alumina NPs	PA	~14 nm	1% in organic phase	IP	NF	Surface hydrophilicity ↑; P_w ↑; Salt rejection no change	2012
Oxidized MWNTs	PA	OD = 5–10 nm L = 10–30 μm	5% of PA	IP	Oil sand process-affected water treatment	Water flux ↑; Organic fraction rejection↑; Fouling resistance ↑	2013
Zwitterion functionalized CNTs	PA	OD = 1.5 nm L = 1 μm	0%, 9%, 20% of PA (20%)	Deposition + IP	RO	Water flux and salt rejection↑; Under 530 psi, optimal water flux is 48.8 L/m^2 h, NaCl rejection (98.6%, 2542 mg/L)	2013
Carboxylic MWNTs	PA	OD < 8 nm L = 10–30 μm	3 mg per membrane sample	Deposition + IP	RO	High electrical conductivity (~400 S/m), NaCl rejection (> 95%, 1000 mg/L), high water flux; Biofouling resistance↑under electric potential	2013
Oxidized MWNTs	PVA	OD = 10–30 nm L = 0.5–2 μm	0%, 5%, 10%, 15% of PVA	Electrospinning + Cross-linking	UF	Water flux ↑; Organic fraction rejection (99.5%) Good mechanical properties	2013
PMMA modified MWNTs	PA	OD = 20–30 nm L < 50 μm	0–5.4 g/L in organic phase (0.67 g/L)	IP	NF	P_w and selectivity ↑	2013
PMMA modified MWNTs	PA	OD = 20–30 nm L < 10 μm	0.67, 1.33, 2.0 g/L in organic phase (0.67)	IP	NF	Under 145 psi, optimal water flux is 69.7 L/m^2 h, Na_2SO_4 rejection (99.0%, 2000 mg/L)	2013
Carboxylic MWNTs	PA	OD < 8 nm L = 10–30 μm	0–2.0 mg/ml in aqueous phase (0.5)	Modified IP O/A/O	NF	P_w ↗↘; Hydrophilicity ↗↘ Under 87 psi, optimal water flux is 21.2 L/m^2 h, Na_2SO_4 rejection (> 70%, 5 mmol/L)	2013
Amine functionalized MWNTs	PA	OD = ~5 nm L = ~50 μm	0.01%, 0.05%, 0.1% in aqueous phase	IP	FO	Hydrophilicity ↑; S value↓; P_w and salt rejection↑ in both AL-FS and AL-DS modes	2013
Zeolite (Silicalite-1)	PA	–	0–0.2% in organic phase	IP	RO	P_w, hydrophilicity, and acid stability↑; Silicalite-1 is superior to NaA in fabricating TFN	2013
Zeolite (NaA)	PA	–	0–0.2%(w/v) in organic phase	IP	RO	Water flux and salt rejection ↑	2013
Aminated Zeolite	PA	≤ 100 nm	0.02% in aqueous solution	IP	RO	P_w ↑; Chlorine resistance↑; Under 800 psi, water flux is 37.8 L/m^2 h, NaCl rejection is 98.8% (32,000 mg/L)	2013
Zeolite A	PA	250 nm	0.2% in organic phase	IP	RO	P_w and salt rejection↑; Resistance to physical compaction ↑	2013
Modified mesoporous silica	PA	~100 nm	0–0.07% in aqueous phase (0.03%)	IP	NF	Under 87 psi, optimal water flux is 32.4 L/m^2 h, Na_2SO_4 rejection (> 80%, 5 mmol/L)	2013
Mesoporous silica	PA	~164 nm	0–0.1% (w/v) in organic phase (0.1)	IP	RO	P_w and hydrophilicity↑; Under 232 psi, optimal water flux is 53 L/m^2 h, NaCl rejection (> 96%, 2000 mg/L)	2013
Aminated hyper branched silica	PA	~7 nm	0.02% in aqueous solution	IP	RO	P_w ↑; Chlorine resistance↑↑Under 800 psi, water flux is 34.5 L/m^2 h, NaCl rejection is 97.7% (32,000 mg/L)	2013
Silica	Fluoropolyamide	–	0–1.0% (w/v) in aqueous phase (0.1)	IP	NF	P_w ↑; Na_2SO_4 rejection ↗↘ Under 87 psi, optimal water flux is 15.2 L/m^2 h, Na_2SO_4 rejection (85.0%, 2000 mg/L)	2013
Aluminosilicate SWNT	PA	OD = ~2.7 nm L = 150 nm	0.05%, 0.1%, 0.2% (w/v) in organic phase	IP (single pass flow)	Low pressure RO	P_w and salt rejection ↑	2013
Aminosilanized TiO_2	PA	~21 nm	0.005%, 0.05%, 0.1% in aqueous solution (0.005%)	IP	NF	P_w and selectivity ↑; Thermal stability↑; Under 110 psi, optimal water flux is 12.3 L/m^2 h, NaCl rejection is 54% (2000 mg/L)	2013
Organoclay (Cloisite 15A and 30B)	Chitosan	–	0.5%, 1%, 2% in casting solution	Coating on PVDF substrate	NF for dye removal	Dye removal↑; Adsoption is the dominating removal mechanism	2013

Table 2.4 (continued)

Proteoliposome containing Aquaporin Z	PEI	~107.8 nm	0, 50, 200, 400 in Lipid-to-protein ratio (200)	PEI crosslinking	NF	Under 14.5 psi, optimal water flux is 36.6 L/m^2 h; $MgCl_2$ rejection (95%, 100 mg/L)	2014
Carboxylic MWNTs	PA	OD=20–40 nm L=1–5 μm	0–0.1% in MPD solution	IP	RO	Hydrophilicity ↑; Water flux↑; Solute rejection no change; Better antifouling and antioxidative properties	2014

2.3.2. Separation properties of TFN membranes: permeability and selectivity

The effects of nanofillers on the permance and selectivity of the TFN membranes is due to a combination of changes in the physicochemical properties of the PA layer such as hydrophilicity, surface charge, thickness and density of the PA layer, extent of cross linking, porosity, and special water channels within the membrane [32,36].

In the pioneering work by Jeong et al., they added 0.004% to 0.4% (w/v) zeolites NPs (NaA type) to the solution of TMC and hexane to fabricate the TFN membranes. The incorporated zeolites were characterized as super-hydrophilic, negatively charged and with three-dimensional molecular sieve network [40]. They reported that incorporation of zeolites led to higher water permeance with similar salt rejection in comparison with the neat polyamide TFC membrane. According to the authors, by increasing the loading of NP, TFN membranes became increasingly more hydrophilic, negatively charged, and smoother than TFC counterparts. Jeong and coworkers also investigated the effects of pore-opened and pore-filled zeolite NP in the TFN membranes. They reported that TFN membranes with the pore-opened zeolites had a higher permeance than the pore-filled NP, but both types of TFN membranes still had higher water permance than the base TFC membranes. These results support the idea that the structure of the zeolites and properties of the molecular sieves have an active role in permeation of water. In general, a combination of effects contributes to the membrane permeance enhancement [32,35,36]. Lind et al., in a similar work, investigated the effects of the size of zeolites NP (97, 212 and 286 nm of Linde type A) on the performance of TFN membranes [41]. They found that all types of TFN membranes had higher permance than the TFC membrane. Larger NP produced membranes with highly desirable surface properties while smaller NP increased permeability by causing larger characteristic pores. For all cases, they reported that addition of zeolites resulted in thicker PA layers. Also, the extent of cross linking for all TFN membranes was less than the TFC membranes counterparts, which suggest that

TFN membranes had more open structure. This means that according to the size and type of the NP, they can be tailored for particular membrane applications [20,41].

Theoretically, if the water permeability of the NP is higher than of the PA layer, the water permeability of the nanocomposite membrane will be improved due to the additional preferential flow paths through the cross section of the membrane (Figure 2.10) [33]. Impermeable nanofillers such as TiO_2 by blocking water flow paths can reduce the permeability of the membrane. In this case, however, other properties of the nanocomposite membrane such as enhanced hydrophilicity, higher surface roughness, lower fouling and defects in the PA layer caused by the NP can improve the overall water permeability of the TFN membrane. The defects in the TFN membranes can be a result of agglomeration of NP or the poor binding/adhesion of the NP to the matrix of the PA thin layer [20,33,36].

Based on the solution-diffusion theory of transport in dense membranes, higher hydrophilicity facilitates the sorption and diffusion of the water molecules in the membrane, which leads to a higher permeability [2,33]. The higher hydrophilicity of the TFN membranes is mostly due to two reasons. First, if hydrophilic NP are exposed to the surface of the membrane the overall hydrophilicity of the film will be increased. Second, NP can alter the chemical structure of the PA layer, for example, by increasing the local miscibility of the organic and aqueous phases. During the interfacial polymerization, unreacted acyl chloride groups undergo hydrolysis reaction and create carboxylic groups. Therefore, if more carboxylic acid functional groups remain on the top surface of the PA layer the hydrophilicity of the membrane increases [32,34,42].

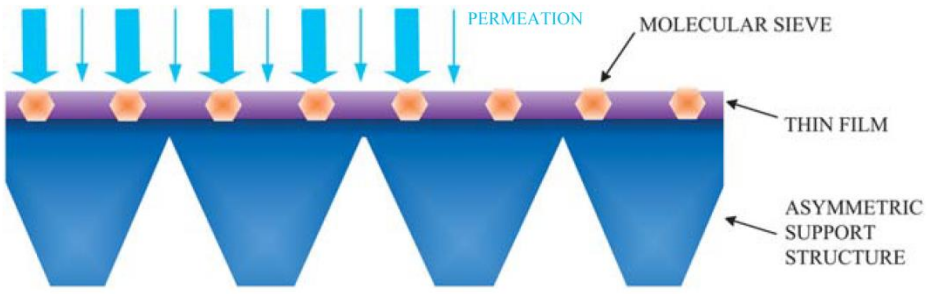

Figure 2.10 Conceptual schematic cross section of a TFN membrane including molecular sieves with preferential water flow paths, illustrated by arrows [20].

2.3.3. Antifouling and antibacterial properties of TFN membranes

The ability of a membrane to resist against fouling is function of some surface properties such as hydrophilicity, charge, structure and morphology. Therefore, by modifying these properties antifouling properties of the membrane can be improved [32,42] . There are several contradicting findings regarding the relationship between membrane fouling and surface roughness in the literature; however, in general a lower membrane surface roughness can decrease the fouling. Kim and Deng incorporated hydrophilized ordered mesoporous carbons (H-OMCs) into PA TFN membrane [43]. They reported a significant decrease in the adsorption of bovine serum albumin (BSA), which was used as the fouling agent, on the TFN membrane in comparison with the TFC membrane counterpart. They suggested that the decrease in the water contact angle from 49^{o} to 46^{o}, implying a greater hydrophilicity, was the major reason for the improved antifouling properties. It is commonly reported that membranes with higher surface hydrophilicity have better antifouling properties. Recently, Vatanpour et al. investigated the effects of amine functionalized multi-walled carbon nanotubes (MWCT) on the performance of TFN-RO membrane [44]. To investigate the antifouling properties of the TFN membranes, they measured the water flux decrement during a 180 minute-filtration test in the presence of bovine serum albumin (BSA) in the feed solution, as well as pure water flux recovery after the fouling test. They reported that 0.002% (w/v) of MWCT-NH_2 in TFN membranes lowered the fouling and lead to a higher water flux recovery. This was attributed to a reduced surface roughness, increased negative charge, and hydrophilicity.

Many studies have investigated antibacterial properties of TFN membranes by incorporation of biocidal NP such as Ag and Cu [45–49]. For example, Lee et al. introduced Ag NP to the PA layer by homogeneously dispersing the particles in the organic monomer solution during the interfacial polymerization. TFN membranes demonstrated a drastic improvement in the anti-biofouling capability of TFN membranes on Pseudomonas bacteria as well as a good stability of the membranes with Ag NP [48].

2.3.4. Chemical and mechanical properties of TFN membranes

It is shown that incorporation of NP into the PA layer of TFC membranes can provide new dimensions for designing chlorine resistant RO membranes [17,36]. For example, Kim et al.

grafted silica NP with hyper-branched aromatic polyamide-grafted (HBP-g-silica), and incorporated them within the PA thin film layer [50]. They reported that the novel TFN membranes had a better chlorine resistance which, according to the authors, was due to two reasons: 1) the intermolecular hydrogen bonding between the PA matrix and the amine groups of the functionalized NP diminished the replacement of hydrogen by chlorine, and 2) since the amide bonds in the PA structure are the main target of the chlorine attack, additional amide bonds or amino groups, which are introduced by the aminated silica NP, made the TFN membrane more resistant to the chlorine attack.

In addition, TFN membranes can provide better resistance to physical compaction for RO application. In general, initial water permeation of nanocomposite membranes is higher; also, less flux decline due to the membrane compaction occurs. This means that lower overall operating energy is required [32,51]. Also, thermal stability of TFN membranes can be improved by use of NP in the PA matrix. Jadav et al. investigated the silica incorporated TFN membranes by thermal gravimetric analysis (TGA), and reported improved thermal stability, which can be attributed to the higher electrostatic and steric effects between the silica NP and PA structure [52].

2.3.5. Challenges of the TFN membrane fabrication

Despite a large number of studies on the fabrication of TFN membranes, and promising improvements in their separation performance, large scale use of this new class of membranes has not yet been achieved. One of the main of challenges in the fabrication of TFN membranes is the agglomeration of NP, which results in the reduction of the active surface area of the NP. Also, it causes poor distribution of NP throughout the active PA layer, and formation of defects in the membrane [36]. Another major complication in the synthesis of TFN membranes is the low adhesion and compatibility between NP and the PA matrix. This causes leaching out of the NP during the filtration process. Leaching out of NP compromise the strict drinking water safety regulations, and raises environmental concerns. Also, removal of NP from the membranes results in degradation of TFN membranes [36].

In order to incorporate NP to the PA matrix, NP are generally added to either aqueous amine-rich or organic acid solutions. Therefore, having well-dispersed suspensions of NP mitigates the formation of agglomerates in the PA layer.

2.3.6. Strategies to overcome the challenges upon fabrication of TFN membranes

Many studies have been conducted to overcome the mentioned issues concerning the fabrication of TFN membranes for large scale industrial applications. Some of the proposed approaches are surface modifications of incorporated NP, use of metal alkoxides, enhanced interfacial polymerization techniques, and alignment of nanotubes/fillers [36].

Surface modification and functionalization of nanofillers is a relatively simple and effective approach to enhance the dispersion of the NP in the used solutions during the interfacial polymerization process. Also, functional groups on the NP can bring about covalent bonds to the PA matrix. In the past few years, several researchers have focused on functionalization of nano-additives by amine groups, aiming for probable interactions between the NP and the PA backbone, and creating better casting suspensions [36,44,53–55].

Namvar-Mahboub et al. studied the synthesis of aromatic TFN membranes with UZM-5 zeolite NP. They functionalized NP with amino groups using 3-aminopropyl (diethoxy)methylsilane (APDEMS), which is an amino silane coupling agent [57]. Grafting NH_2 groups to NP led to a better dispersion of hydrophilic zeolites in the organic (hexane) phase. Also, they suggested possible formation of covalent bond between the NH_2 groups on the zeolite and the TMC molecules, illustrated in the Figure 2.11. In another study on surface modified NP, Zhao et al. incorporated MWNT, grafted with long chains of aliphatic carboxylic acid, in the TFN membrane. They suggested a better NP-PA matrix compatibility, but did not provide more information about the dispersion of the NP in the casting solution [36,56].

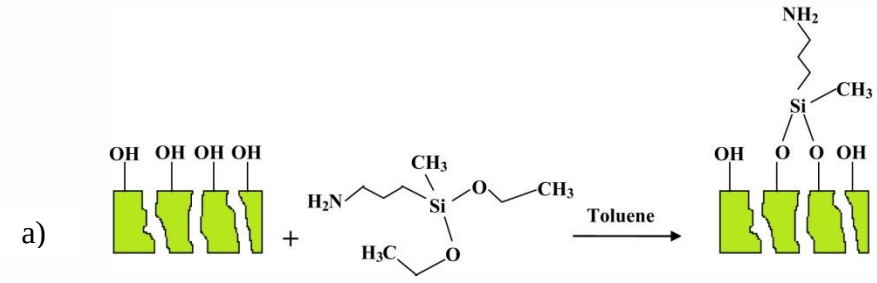

Figure 2.11 Schematic of a) amino functionalization of UZM-5 zeolites (green structure), and b) chemical reaction between functionalaized NP and TMC during polyamide synthesis [57]

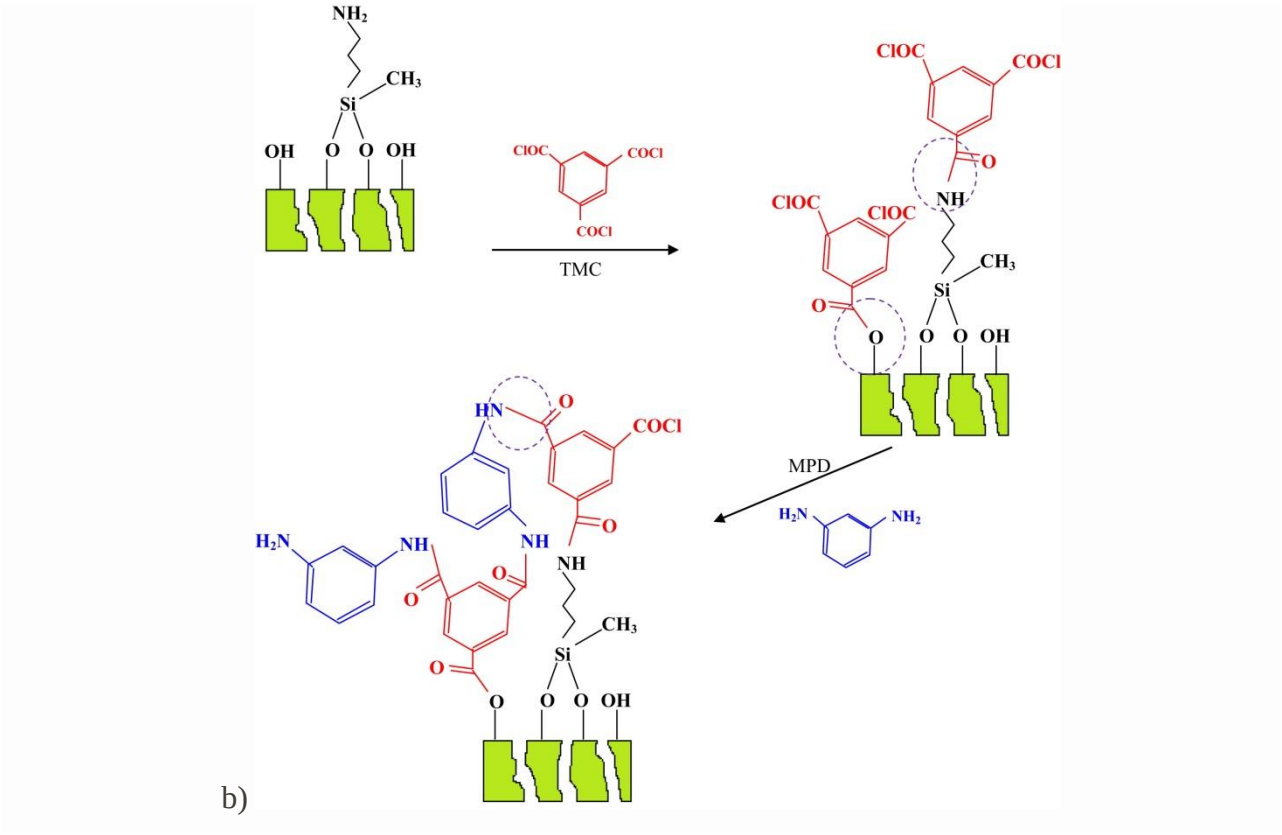

Figure 2.11 (continued) Schematic of a) amino functionalization of UZM-5 zeolites (green structure), and b) chemical reaction between functionalized NP and TMC during polyamide synthesis [57].

Another approach for overcoming the challenges associated with TFN membranes is to find modified fabrication methods [36]. For example, in order to minimize membrane defects, some researchers have suggested to introduce a secondary amine rich solution to the PA layer to react with the unreacted monomer (TMC) [58]. Another suggested fabrication method of TFN membranes is to pre-seed the NP in the PA layer [59]. In this method, after immersing the UF substrate with the amine rich solution, the membrane is contacted with an organic suspension consisting zeolite NP, ethanol and hexane and a low concentration of TMC (0.01 to 0.05 wt%). This step is the pre-seeding which enables well dispersed trapping of the NP on the substrate membrane. Afterwards, the membrane is contacted with the TMC solution having a conventional concentration of the monomer (0.1 wt%). According to the authors, this method led to a higher concentration of zeolites, up to 0.4 wt%, in the TFN membranes, which in turn showed an increase in the water flux and no considerable decrease in salt rejection (>95%).

2.4. Conclusions

This chapter provides a brief overview of RO membranes with focus on TFC and TFN membranes. The advantages and disadvantages of TFC membranes, as well as strategies to overcome the latter were discussed. One of the approaches to enhance the properties of TFC RO membranes is to embed NP into the PA layer; these membranes are called TFN membranes. Although TFN membranes have superior properties and separation characteristics, they are not used on a large scale. Leaching out of NP and agglomeration, due to low NP-PA adhesion/interaction, and low suspensibility of NP in casting solutions are the two major challenges for the TFN membrane fabrication. Surface modification of NP is one of the methods to overcome the problems associated with TFN membranes.

In the next two chapters, my attempts to incorporate CNC and PAMAM functionalized HNT into TFN membranes are presented. Considering the challenges with TFN membranes, CNC and HNT were chosen, since they are inherently safe, environmentally friendly, and inexpensive NP. Various functional group and PAMAM dendrimers were chosen to enhance the compatibility between the HNT NP and PA layer.

2.5. References

[1] J. Mulder, Basic Principles of Membrane Technology, Springer Science & Business Media, n.d.

[2] R.W. Baker, Membrane Science and Technology, John Wiley & Sons, Ltd, 2012. http://onlinelibrary.wiley.com/doi/10.1002/9781118359686.ch1/summary (accessed April 9, 2017).

[3] Mavis C.Y. Wong, Understanding the Relationship between Osmotic Membrane Structure and Separation Performance., UCLA: Civil Engineering 0300, 2014. http://escholarship.org/uc/item/4x61s703.

[4] J.C. Crittenden, R.R. Trussell, D.W. Hand, K.J. Howe, G. Tchobanoglous, Reverse Osmosis, in: MWHs Water Treat. Princ. Des. Third Ed., John Wiley & Sons, Inc., 2012: pp. 1335–1414. doi:10.1002/9781118131473.ch17.

[5] J. Kucera, Reverse Osmosis: Industrial Processes and Applications, Second Edition, Second, John Wiley & Sons, Inc., 2015. doi:10.1002/9781119145776.ch4.

[6] W.J. Lau, A.F. Ismail, N. Misdan, M.A. Kassim, A recent progress in thin film composite membrane: A review, Desalination. 287 (2012) 190–199. doi:10.1016/j.desal.2011.04.004.

[7] L.F. Greenlee, D.F. Lawler, B.D. Freeman, B. Marrot, P. Moulin, Reverse osmosis desalination: Water sources, technology, and today's challenges, Water Res. 43 (2009) 2317–2348. doi:10.1016/j.watres.2009.03.010.

[8] S. Loeb, S. Sourirajan, Sea Water Demineralization by Means of an Osmotic Membrane, in: Saline Water Conversion—II, AMERICAN CHEMICAL SOCIETY, 1963: pp. 117–132. doi:10.1021/ba-1963-0038.ch009.

[9] S. LOEB, The Loeb-Sourirajan Membrane: How It Came About, in: Synth. Membr., AMERICAN CHEMICAL SOCIETY, 1981: pp. 1–9. doi:10.1021/bk-1981-0153.ch001.

[10] P.W. Morgan, S.L. Kwolek, Interfacial polycondensation. II. Fundamentals of polymer formation at liquid interfaces, J. Polym. Sci. 40 (1959) 299–327. doi:10.1002/pol.1959.1204013702.

[11] J.E. Cadotte, R.J. PETERSEN, Thin-Film Composite Reverse-Osmosis Membranes: Origin, Development, and Recent Advances, in: Synth. Membr., AMERICAN CHEMICAL SOCIETY, 1981: pp. 305–326. doi:10.1021/bk-1981-0153.ch021.

[12] L. Lin, R. Lopez, G.Z. Ramon, O. Coronell, Investigating the void structure of the polyamide active layers of thin-film composite membranes, J. Membr. Sci. 497 (2016) 365–376. doi:10.1016/j.memsci.2015.09.020.

[13] T. Matsuura, Synthetic Membranes and Membrane Separation Processes, CRC Press, 1993.

[14] J.E. Cadotte, Interfacially synthesized reverse osmosis membrane, US4277344 A, 1981. http://www.google.com/patents/US4277344.

[15] K. Scott, R. Hughes, Industrial Membrane Separation Technology, Springer Science & Business Media, 2012.

[16] F. Pacheco, R. Sougrat, M. Reinhard, J.O. Leckie, I. Pinnau, 3D visualization of the internal nanostructure of polyamide thin films in RO membranes, J. Membr. Sci. 501 (2016) 33–44. doi:10.1016/j.memsci.2015.10.061.

[17] G.-R. Xu, J.-N. Wang, C.-J. Li, Strategies for improving the performance of the polyamide thin film composite (PA-TFC) reverse osmosis (RO) membranes: Surface modifications and nanoparticles incorporations, Desalination. 328 (2013) 83–100. doi:10.1016/j.desal.2013.08.022.

[18] L.F. Greenlee, D.F. Lawler, B.D. Freeman, B. Marrot, P. Moulin, Reverse osmosis desalination: Water sources, technology, and today's challenges, Water Res. 43 (2009) 2317–2348. doi:10.1016/j.watres.2009.03.010.

[19] B. Peñate, L. García-Rodríguez, Current trends and future prospects in the design of seawater reverse osmosis desalination technology, Desalination. 284 (2012) 1–8. doi:10.1016/j.desal.2011.09.010.

[20] M. M. Pendergast, E. M.V. Hoek, A review of water treatment membrane nanotechnologies, Energy Environ. Sci. 4 (2011) 1946–1971. doi:10.1039/C0EE00541J.

[21] G. Kang, Y. Cao, Development of antifouling reverse osmosis membranes for water treatment: A review, Water Res. 46 (2012) 584–600. doi:10.1016/j.watres.2011.11.041.

[22] J. Glater, The search for a chlorine-resistant reverse osmosis membrane, Desalination. 95 (1994) 325–345.

[23] V.T. Do, C.Y. Tang, M. Reinhard, J.O. Leckie, Degradation of Polyamide Nanofiltration and Reverse Osmosis Membranes by Hypochlorite, Environ. Sci. Technol. 46 (2012) 852–859. doi:10.1021/es203090y.

[24] K.P. Lee, T.C. Arnot, D. Mattia, A review of reverse osmosis membrane materials for desalination—Development to date and future potential, J. Membr. Sci. 370 (2011) 1–22. doi:10.1016/j.memsci.2010.12.036.

[25] D. Wu, Thin Film Composite Membranes Derived from Interfacial Polymerization for Nanofiltration and Pervaporation Applications, University of Waterloo, 2015. https://uwspace.uwaterloo.ca/handle/10012/9244.

[26] H. Wang, L. Li, X. Zhang, S. Zhang, Polyamide thin-film composite membranes prepared from a novel triamine 3,5-diamino-N-(4-aminophenyl)-benzamide monomer and m-phenylenediamine, J. Membr. Sci. 353 (2010) 78–84. doi:10.1016/j.memsci.2010.02.033.

[27] S. Konagaya, O. Watanabe, Influence of chemical structure of isophthaloyl dichloride and aliphatic, cycloaliphatic, and aromatic diamine compound polyamides on their chlorine resistance, J. Appl. Polym. Sci. 76 (2000) 201–207. doi:10.1002/(SICI)1097-4628(20000411)76:2<201::AID-APP9>3.0.CO;2-8.

[28] S. Yu, M. Liu, Z. Lü, Y. Zhou, C. Gao, Aromatic-cycloaliphatic polyamide thin-film composite membrane with improved chlorine resistance prepared from m-phenylenediamine-4-methyl and cyclohexane-1,3,5-tricarbonyl chloride, J. Membr. Sci. 344 (2009) 155–164. doi:10.1016/j.memsci.2009.07.046.

[29] C. Kong, M. Kanezashi, T. Yamomoto, T. Shintani, T. Tsuru, Controlled synthesis of high performance polyamide membrane with thin dense layer for water desalination, J. Membr. Sci. 362 (2010) 76–80. doi:10.1016/j.memsci.2010.06.022.

[30] A. Sarkar, P.I. Carver, T. Zhang, A. Merrington, K.J. Bruza, J.L. Rousseau, S.E. Keinath, P.R. Dvornic, Dendrimer-based coatings for surface modification of polyamide reverse osmosis membranes, J. Membr. Sci. 349 (2010) 421–428. doi:10.1016/j.memsci.2009.12.005.

[31] M. Bhadra, S. Mitra, Chapter 7 - Advances in Nanostructured Membranes for Water Desalination, in: A. Street, R. Sustich, J. Duncan, N. Savage (Eds.), Nanotechnol. Appl. Clean Water Second Ed., William Andrew Publishing, Oxford, 2014: pp. 109–122. doi:10.1016/B978-1-4557-3116-9.00007-X.

[32] E.M.V. Hoek, M.T.M. Pendergast, A.K. Ghosh, Chapter 9 - Nanotechnology-Based Membranes for Water Purification, in: A. Street, R. Sustich, J. Duncan, N. Savage (Eds.), Nanotechnol. Appl. Clean Water Second Ed., William Andrew Publishing, Oxford, 2014: pp. 133–154. doi:10.1016/B978-1-4557-3116-9.00009-3.

[33] M.G. Buonomenna, Nano-enhanced reverse osmosis membranes, Desalination. 314 (2013) 73–88. doi:10.1016/j.desal.2013.01.006.

[34] J. Yin, B. Deng, Polymer-matrix nanocomposite membranes for water treatment, J. Membr. Sci. 479 (2015) 256–275. doi:10.1016/j.memsci.2014.11.019.

[35] S. Sarkar, A. Sarkar, C. Bhattacharjee, 10 - Nanotechnology-based membrane-separation process for drinking water purification, in: A.M. Grumezescu (Ed.), Water Purif., Academic Press, 2017: pp. 355–389. doi:10.1016/B978-0-12-804300-4.00010-1.

[36] W.J. Lau, S. Gray, T. Matsuura, D. Emadzadeh, J. Paul Chen, A.F. Ismail, A review on polyamide thin film nanocomposite (TFN) membranes: History, applications, challenges and approaches, Water Res. 80 (2015) 306–324. doi:10.1016/j.watres.2015.04.037.

[37] T.A. Saleh, V.K. Gupta, Chapter 4 - Synthesis, Classification, and Properties of Nanomaterials, in: Nanomater. Polym. Membr., Elsevier, 2016: pp. 83–133. doi:10.1016/B978-0-12-804703-3.00004-8.

[38] S.-Y. Kwak, S.H. Kim, S.S. Kim, Hybrid Organic/Inorganic Reverse Osmosis (RO) Membrane for Bactericidal Anti-Fouling. 1. Preparation and Characterization of TiO2 Nanoparticle Self-Assembled Aromatic Polyamide Thin-Film-Composite (TFC) Membrane, Environ. Sci. Technol. 35 (2001) 2388–2394. doi:10.1021/es0017099.

[39] J. Yin, Y. Yang, Z. Hu, B. Deng, Attachment of silver nanoparticles (AgNPs) onto thin-film composite (TFC) membranes through covalent bonding to reduce membrane biofouling, J. Membr. Sci. 441 (2013) 73–82. doi:10.1016/j.memsci.2013.03.060.

[40] B.-H. Jeong, E.M.V. Hoek, Y. Yan, A. Subramani, X. Huang, G. Hurwitz, A.K. Ghosh, A. Jawor, Interfacial polymerization of thin film nanocomposites: A new concept for reverse osmosis membranes, J. Membr. Sci. 294 (2007) 1–7. doi:10.1016/j.memsci.2007.02.025.

[41] M.L. Lind, A.K. Ghosh, A. Jawor, X. Huang, W. Hou, Y. Yang, E.M.V. Hoek, Influence of Zeolite Crystal Size on Zeolite-Polyamide Thin Film Nanocomposite Membranes, Langmuir. 25 (2009) 10139–10145. doi:10.1021/la900938x.

[42] O.A. Sadik, N. Du, I. Yazgan, V. Okello, Chapter 6 - Nanostructured Membranes for Water Purification, in: A. Street, R. Sustich, J. Duncan, N. Savage (Eds.), Nanotechnol. Appl. Clean Water Second Ed., William Andrew Publishing, Oxford, 2014: pp. 95–108. doi:10.1016/B978-1-4557-3116-9.00006-8.

[43] E.-S. Kim, B. Deng, Fabrication of polyamide thin-film nano-composite (PA-TFN) membrane with hydrophilized ordered mesoporous carbon (H-OMC) for water purifications, J. Membr. Sci. 375 (2011) 46–54. doi:10.1016/j.memsci.2011.01.041.

[44] V. Vatanpour, M. Esmaeili, M.H.D.A. Farahani, Fouling reduction and retention increment of polyethersulfone nanofiltration membranes embedded by amine-functionalized multi-walled carbon nanotubes, J. Membr. Sci. 466 (2014) 70–81. doi:10.1016/j.memsci.2014.04.031.

[45] M. Ben-Sasson, K.R. Zodrow, Q. Genggeng, Y. Kang, E.P. Giannelis, M. Elimelech, Surface Functionalization of Thin-Film Composite Membranes with Copper Nanoparticles for Antimicrobial Surface Properties, Environ. Sci. Technol. 48 (2014) 384–393. doi:10.1021/es404232s.

[46] J. Yin, Y. Yang, Z. Hu, B. Deng, Attachment of silver nanoparticles (AgNPs) onto thin-film composite (TFC) membranes through covalent bonding to reduce membrane biofouling, J. Membr. Sci. 441 (2013) 73–82. doi:10.1016/j.memsci.2013.03.060.

[47] A. Mollahosseini, A. Rahimpour, A new concept in polymeric thin-film composite nanofiltration membranes with antibacterial properties, Biofouling. 29 (2013) 537–548. doi:10.1080/08927014.2013.777953.

[48] S.Y. Lee, H.J. Kim, R. Patel, S.J. Im, J.H. Kim, B.R. Min, Silver nanoparticles immobilized on thin film composite polyamide membrane: characterization, nanofiltration, antifouling properties, Polym. Adv. Technol. 18 (2007) 562–568. doi:10.1002/pat.918.

[49] L.Y. Ng, A.W. Mohammad, C.P. Leo, N. Hilal, Polymeric membranes incorporated with metal/metal oxide nanoparticles: A comprehensive review, Desalination. 308 (2013) 15–33. doi:10.1016/j.desal.2010.11.033.

[50] S.G. Kim, J.H. Chun, B.-H. Chun, S.H. Kim, Preparation, characterization and performance of poly(aylene ether sulfone)/modified silica nanocomposite reverse osmosis membrane for seawater desalination, Desalination. 325 (2013) 76–83. doi:10.1016/j.desal.2013.06.017.

[51] M.T.M. Pendergast, J.M. Nygaard, A.K. Ghosh, E.M.V. Hoek, Using nanocomposite materials technology to understand and control reverse osmosis membrane compaction, Desalination. 261 (2010) 255–263. doi:10.1016/j.desal.2010.06.008.

[52] G.L. Jadav, P.S. Singh, Synthesis of novel silica-polyamide nanocomposite membrane with enhanced properties, J. Membr. Sci. 328 (2009) 257–267. doi:10.1016/j.memsci.2008.12.014.

[53] B. Rajaeian, A. Rahimpour, M.O. Tade, S. Liu, Fabrication and characterization of polyamide thin film nanocomposite (TFN) nanofiltration membrane impregnated with TiO2 nanoparticles, Desalination. 313 (2013) 176–188. doi:10.1016/j.desal.2012.12.012.

[54] Y. Xu, X. Gao, X. Wang, Q. Wang, Z. Ji, X. Wang, T. Wu, C. Gao, Highly and Stably Water Permeable Thin Film Nanocomposite Membranes Doped with MIL-101 (Cr) Nanoparticles for Reverse Osmosis Application, Materials. 9 (2016) 870. doi:10.3390/ma9110870.

[55] J. Yin, Attachment of silver nanoparticles (AgNPs) onto thin-film composite (TFC) membranes through covalent bonding to reduce membrane biofouling, 441 (n.d.) 73–82.

[56] L. Zhao, W.S.W. Ho, Novel reverse osmosis membranes incorporated with a hydrophilic additive for seawater desalination, J. Membr. Sci. 455 (2014) 44–54. doi:10.1016/j.memsci.2013.12.066.

[57] M. Namvar-Mahboub, M. Pakizeh, S. Davari, Preparation and characterization of UZM-5/polyamide thin film nanocomposite membrane for dewaxing solvent recovery, J. Membr. Sci. 459 (2014) 22–32. doi:10.1016/j.memsci.2014.02.014.

[58] H. Zou, Y. Jin, J. Yang, H. Dai, X. Yu, J. Xu, Synthesis and characterization of thin film composite reverse osmosis membranes via novel interfacial polymerization approach, Sep. Purif. Technol. 72 (2010) 256–262. doi:10.1016/j.seppur.2010.01.019.

Chapter 3

Synthesis and characterization of novel cellulose nanocrystals (CNC)-based thin film nanocomposite (TFN) membranes for reverse osmosis applications

Farhad Asempour[a], Daryoush Emadzadeh[a,b], Takeshi Matsuura[a], Boguslaw Kruczek[a]*

[a] Department of chemical and Biological engineering, University of Ottawa, 161 Louis Pasteur St, Ottawa, ON K1N 6N5, Canada
[b] Department of Chemical Engineering, Gachsaran Branch, Azad University, Gachsaran, Iran

- Oral presentation - *11th International Congress on Membranes and Membrane Processes (ICOM 2017)*. Development and characterization of novel CNC-based TFN membranes, presenter: **Farhad Asempour**

*Corresponding author: Boguslaw.Kruczek@uottawa.ca

Chapter 3 - Synthesis and characterization of novel cellulose nanocrystals (CNC)-based thin film nanocomposite (TFN) membranes for reverse osmosis applications

3.1. Abstract

Addition of nanoparticles (NP) into the polyamide (PA) layer of the thin film composite (TFC) membranes is a relatively new approach to enhance the characteristics and the performance of TFC membranes. However, leaching out of the nano-sized additives is a major setback in fulfilling the strict regulations of drinking water and environmental safety. In this work, this issue is addressed by incorporating cellulose nanocrystals (CNC), which are inherently abundant, biodegradable, renewable and non-toxic, in the thin film nanocomposite (TFN) membranes for reverse osmosis (RO). Membrane characterization by Scanning Electron Microscopy (SEM), Atomic Force Microscopy (AFM), and water contact angle measurement showed improved morphology and surface properties of the CNC-TFN membranes. Membrane hydrophilicity was enhanced; water contact angle decreased from 73.5 ± 2.4 for TFC membrane to 55.5 ± 2.8 for TFN membrane with 0.1% (w/v) CNC. Also, successful incorporation of CNC in the active PA layer was confirmed by X-Ray Diffraction (XRD) analysis. Moreover, separation characteristics of membranes were studied by desalination of synthetic brackish water with a reverse osmosis system. It was found that addition of 0.1% (w/v) CNC in the TFN PA layer considerably enhanced the water flux (from 30 ± 5 to 63 ± 10 $L/m^2.h$ at 20 ± 1 bar(g)) without significantly compromising the salt rejection (97.8% ± 0.5). Also, embedding CNC in the TFN membrane improved antifouling properties of the membrane. In the fouling/filtration experiments with 300 ppm bovine serum albumin (BSA) in the feed solution, CNC-TFN membranes showed 11 % smaller water flux reduction in comparison with a control TFC membrane.

***Keywords*:** Cellulose nanocrystals, Thin film nanocomposite membrane, Reverse osmosis, Desalination, Brackish water

3.2. Graphical Abstract

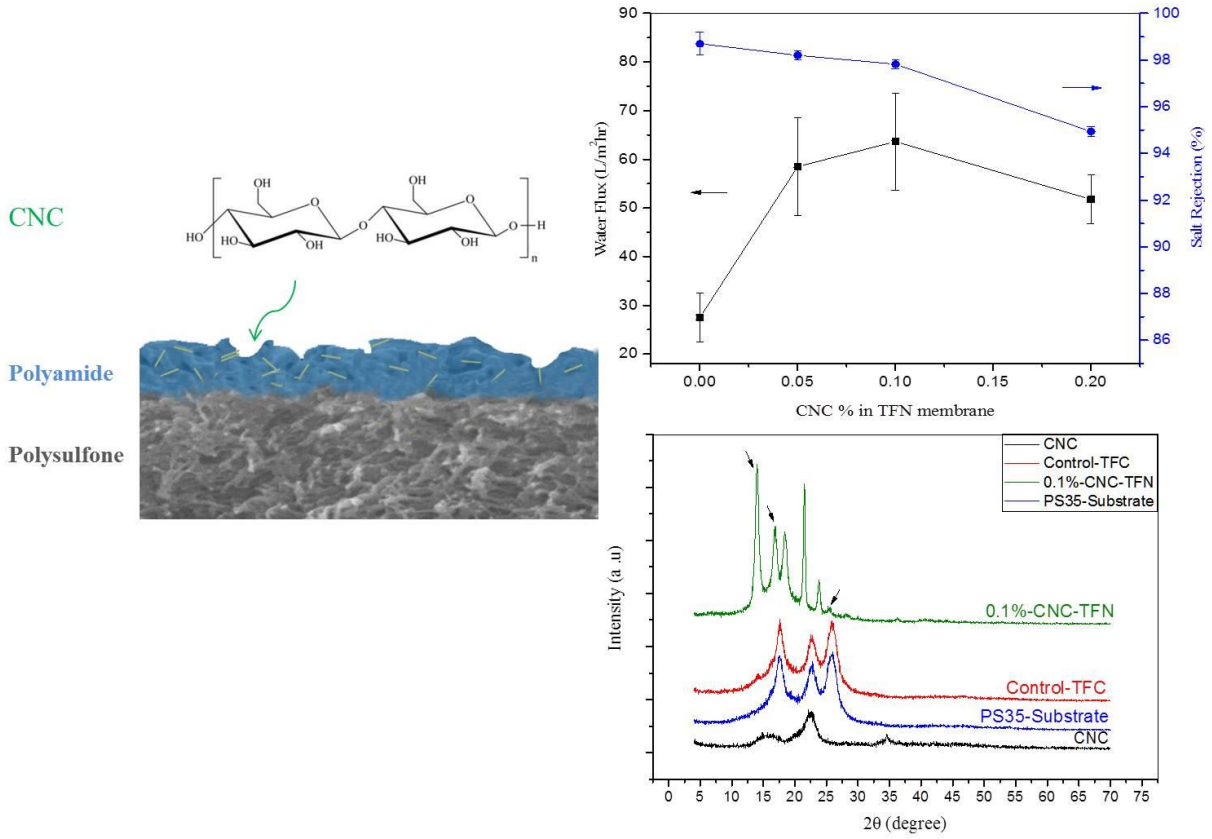

3.3. Introduction

Since the development of the thin film composite membranes by Cadotte in 1970, reverse osmosis membranes have gone through several improvements to surpass the trade-off relationship between permeance and selectivity, and to enhance membrane's antifouling properties and durability [1]. One of the major advancements in the fabrication of the TFC membranes is embedding nanoparticles (NP) within the polyamide (PA) layer. It is commonly reported that the use of nanoparticles leads to improvements of certain properties of the membranes such as hydrophilicity, surface charge density, surface roughness and degree of cross-linking of the polymer matrix and hence enhanced membrane performance [2]. Jeong et al., in their pioneering work introduced zeolite NaA as the nanosized additives in 2007 [3]. Since then various NPs such as TiO_2, SiO_2, silver nanoparticles, carbon nanotubes, and zeolites have been employed in the so called thin film nanocomposite (TFN) membranes [2,4]. However, the major challenge in further industrialization of TFN membranes is leaching out of the toxic nanoparticles into the downstream (permeate and retentate) which compromises the drinking water safety regulations. Besides, These commonly used inorganic nanoparticles are typically quite expensive and difficult to produce [5]. Therefore, the introduction of nano-scaled additives, which overcome these limitations, is greatly needed. In this work, for the first time we introduced cellulose nanocrystals (CNC) to TFN membranes.

Cellulose nanocrystals (CNC), also known as nanocrystalline cellulose (NCC), are natural rod-like particles which are obtained from acid hydrolysis of biomass. When biomass (cellulose) is treated in a harsh acid environment, the amorphous part of the cellulose consisting of cellulose fibers, lignin, waxes, etc. dissolves, and a highly crystalline residue remains. Depending on the source of the cellulose and the conditions of the acid treatment, the size of the CNC varies, but in general, CNC are few hundred nanometers long and few nanometers in diameter. These NP are abundant, biodegradable, renewable, non-toxic, and carbon neutral. They possess high specific strength, Young's modulus, surface area, and zeta potential. They also have a highly reactive surface due to the existence of the (-OH) groups, which makes them favorable for chemical functionalization. Figure 3.1 presents the chemical structure of the cellulose chain. The intriguing properties of CNC have harnessed a tremendous attention for a wide range of potential applications, for example, in nanocomposite polymers with enhanced properties, protective coating, drug delivery, tissue engineering, solar cells, etc. [6,7].

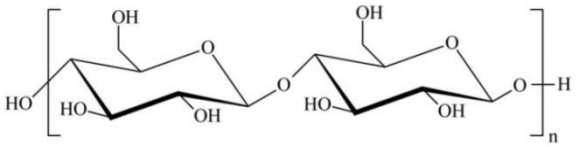

Figure 3.1 Molecular structure of cellulose [6]

Although CNC have been widely used in nonocomposite polymers, their application, particularly in hydrophobic polymeric membranes, has not been thoroughly investigated [8]. Bai et al. studied CNC/PVDF ultrafiltration membranes for water treatment [9]. They reported that addition of 0.1 wt% CNC in the membrane led to a 47.5% water flux improvement in comparison with the neat control membrane without a significant BSA rejection decrease. In another study on UF membranes, Li et al., prepared CNC/polysulfone for dialysis applications [10]. They noted that incorporation of 0.3 wt% CNC in the composite membrane doubled the ultrafiltration coefficient (from 24 to 48.4 L/m^2.h.mmHg), and the urea rejection increased by 44% (from 62.9% to 90.4%). It was also reported that CNC changed the structure of the UF composite membranes by increasing the size of the finger-like pores and improving their connectivity as well as increasing the hydrophilicity. Lately, Daraie et al. fabricated the CNC-polyether sulfone (PES) nanofiltration membrane by the phase inversion method. They suggested that CNC/PES membranes (0.8% to 1.2% CNC in the dope solution) showed two folds higher water permeability, and a 30% higher bivalent salt rejection than the pure PES control membrane. Moreover, it is reported that CNC/PES membranes had superior antifouling properties, showing complete recovery of water flux after fouling tests [11].

The purpose of this work is to study the possibility of incorporating CNC in the thin film PA layer, and their effect on the performance of the TFN membrane. To our best knowledge, there is no article reporting the use of CNC in the TFC membranes, fabricated by the interfacial polymerization method. The permeance (water flux) and the salt rejection of the membranes were tested with a reverse osmosis system using synthetic brackish water as a feed. Antifouling properties of the optimized TFN membrane were examined and compared with the control TFC membrane. The surface morphology of the synthesized membranes was characterized by SEM, AFM and contact angle measurements. Also, the presence and effects of CNC on the PA layer were investigated by XRD.

3.4. Experimental

3.4.1 Materials

A polysulfone ultrafiltration membrane (PS-35) with the molecular weight cut off (MWCF) of 20 kDa, which was used as the substrate, was obtained from Nanostone Water, Waltham Massachusetts, USA. The monomers M-phenylenediamine (MPD, purity of 99%) and 1,3,5-benzenetricarbonyl trichloride (TMC, purity > 98%) were procured from Sigma-Aldrich. The organic solvent was N-hexane (purity >99%) was also purchased from Sigma-Aldrich. Cellulose nanocrystals (CNC) were purchased from Celluforce, Montreal, Quebec, Canada. Sodium chloride (purity > 99.5%) was used as the solute in the feed. Bovine serum albumin (BSA) with the molecular weight of 66 kDa was acquired from Sigma-Aldrich and utilized as the organic foulant representing proteins in the effluent organic matters (EfOM).

3.4.2. Synthesis of TFN membranes

The polyamide selective layer was synthesized via in situ interfacial polymerization on top of the ultrafiltration membrane, PS-35. In this study, the aqueous solution consisted of 2% (w/v) MPD in deionized water, and the organic solution was comprised of TMC (0.05% w/v) and different amounts of the CNCs (0.05%, 0.1%, 0.2% w/v) in n-hexane. The organic solution containing CNC was sonicated for 2 hours to minimize formation of agglomerates. First, the aqueous solution was poured on the top surface of the substrate membrane and kept there for 2 minutes. This was followed by draining off the excess solution and removing the visible droplets from the substrate with a Teflon roller. Then, the top surface of the membrane was completely contacted with the organic solution containing the dispersed CNC for 1 minute. The residual organic solution was removed, and the surface was rinsed with pure n-hexane and drained off. Afterwards, the membrane was held at ambient conditions for 1 minute, before it was placed in an oven at 95°C for a 10 minute curing period. Finally, the membrane was rinsed thoroughly with deionized (DI) water and stored in the DI water.

According to the CNC loading, TNF membranes are coded as n%-CNC-TFN membrane, where n is the percent of CNC in the organic phase. When n is zero, the membrane is a control-TFC membrane.

3.4.3. Evaluation of membrane performance by desalination of synthetic brackish water

The RO performance of the synthesized TFN membranes was evaluated by using a continuous cross-flow system, consisting of 3 RO cells arranged in parallel, each with the effective surface area for permeation of 17.35 cm^2, Figure 3.2. Synthetic brackish water (3000 ppm aqueous sodium chloride solution) was used as the feed, and its flow rate was maintained at 2.4 ± 0.2 L/min to minimize the effects of concentration polarization and to achieve zero recovery conditions [12]. The experiments were conducted at 25 ± 2 ºC and 20 ± 1 bar(g) [12].

Permeate flux, J_w $\left[\frac{L}{h.m^2}\right]$, was calculated by Equation (1) using the volume of collected permeate (V_p $[L]$) in time (t $[h]$), per area of the membrane, A_p [m^2]. Salt rejection, R, was evaluated by Equation (2) in which C_p and C_f are the concentrations $\left[\frac{mg}{L}\right]$ of permeate and feed, respectively [13].

$$J_w = \frac{V_p}{A_p \times t} \tag{1}$$

$$R = 1 - \left(\frac{C_p}{C_f}\right) \times 100\% \tag{2}$$

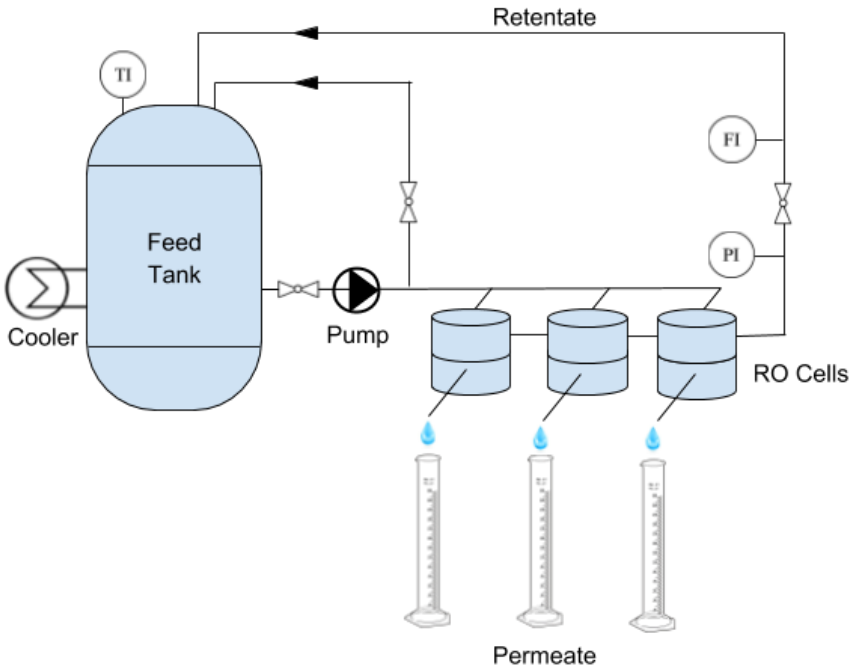

Figure 3.2 A continuous cross-flow membrane testing system.

3.4.4. Fouling experiments

Fouling experiments were carried out with the same cross-flow RO system for 20 hours at 25 ± 1ºC and 20 ± 1 bar(g). Concentrations of the salt and BSA, representing the effluent organic matter, in the feed, were 3000 and 300 mg/L respectively [14]. The feed flow rate was reduced to 1.6 ± 0.2 L/min to facilitate fouling, but it was still higher than 200 mm/s on the surface of the membrane in the cell. 200 mm/s is approximately the minimum feed velocity required for avoiding concentration polarization [12]. Membrane compaction refers to the physical compression of the membrane due to the pressure which normally results in an increase of the membrane selectivity and a decrease in the permeance [15,16]. Therefore, in order to eliminate the effects of membrane compaction, and to differentiate it from the fouling, the membranes were pre-compacted for at least 2 hours at 55 ± 1 bar(g). After reaching a steady permeate flux, the pressure was reduced to 20 ± 1 bar(g), the general testing level in this work, and then the BSA solution was added to the feed tank. Afterwards, permeate samples were collected every 45 minutes to detect the decrease in the permeance due to the fouling by BSA.

3.4.5. Membrane characterization

CNC and surface properties of the membranes were characterized by AFM (AFM Park NX10), SEM (Tescan Vega-II XMU), and XRD (Rigaku Ultima IV Diffractometer). To investigate that if sonication deteriorate the CNC particles, 0.02% (w/v) CNC in n-hexane were sonicated for 2 h. Then, the CNC solution were dried in ambient condition and tested for XRD. The surface roughness (Ra) was measured with a tapping mode AFM, scanning over a 10×10 μm areas. For membrane cross-section SEM images, samples were cut in liquid nitrogen and then coated with gold sputtering. The water contact angle of the membranes was measured using a VCA Optima surface analysis system (AST Products, Inc., Billerica, MA). For each membrane, we measured contact angle of 20 droplets of DI water, each with the volume of 2 μL, at room temperature. Shape and size of the CNC were characterized by TEM (FEI Tecnai G2 Spirit Twin TEM) imaging. The X-ray diffraction of TFN membrane and CNCs powder was carried out at room temperature and Bragg-Brentano geometry, using Cu Kα radiation ($\lambda = 1.5418$ Å). The 2θ range of 4° to 70° was covered with 0.02° step width and 3°/min scan speed.

3.5. Results and discussion

3.5.1. Analysis of the CNC particles

The TEM image of the CNC particles is shown in Figure 3.3. Particles are rod shape with the length of 100 to 200 nm and the diameter of less than 10 nm.

Figure 3.3 TEM image of CNC particles

3.5.2. Effects of CNC particles on the TFN membrane

The morphology and structure of the top surface and cross-section of the control-TFC, and 0.1%-CNC-TFN membrane were investigated by SEM, and the images are shown in Figure 3.4. A typical ridge and valley structure of the TFC membrane is observed at the surface of both types of membranes. The control-TFC membrane has more leaf-like structures than the 0.1%-CNC-TFN membrane; however, globular structures are more dominant in the 0.1%-CNC-TFN. This can be attributed to the enhanced PA crosslinking triggered by CNC in the TFN membrane. Kwak et al. have suggested that crosslinking in the PA network is the main contributor to the formation of the globular structures [17]. Also, Linde et al. pointed out that the presence of hydrophilic particles in the organic phase increases the miscibility of the organic and aqueous solutions, which promotes diffusion of MPD in TMC, and hence interfacial polymerization [18]. As it can be seen in the cross section images (Figures 3b and 3d), the TFN membrane has a thicker PA layer, which is in

accordance with other reported works on TFN membranes suggesting that the presence of hydrophilic NP leads to an increase in the PA layer thickness [4,15,16] . Figure 3.5 represents 3D images of the membrane surface topography observed by AFM. The surface roughness (Rq) is nearly equal for all membranes except for the membrane with CNC loading of 0.05%, which shows a higher surface roughness than other membranes. It is suggested that high surface roughness is an indication of a larger skin area for permeation, and consequently enhancement of the membrane productivity is often correlated to the membrane surface roughness [17].

(a) control-TFC top surface

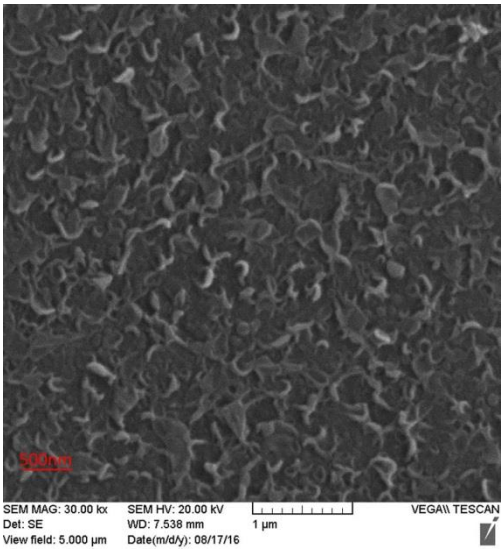

b) control-TFC cross section

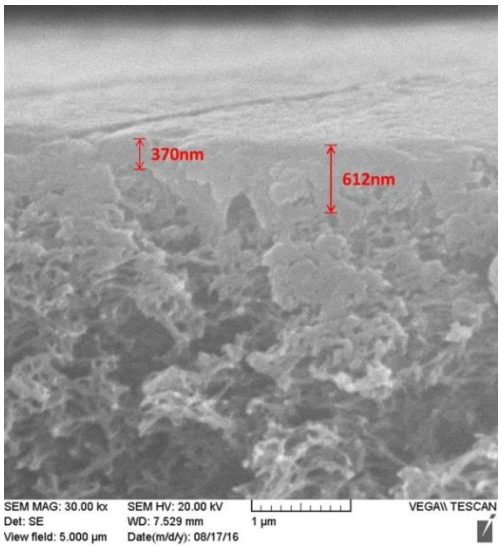

(c) 0.1%-CNC-TFN top surface

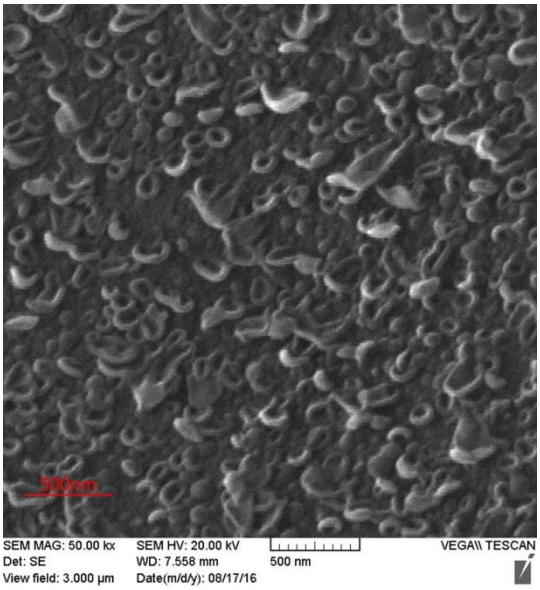

(d) 0.1%-CNC-TFN cross section

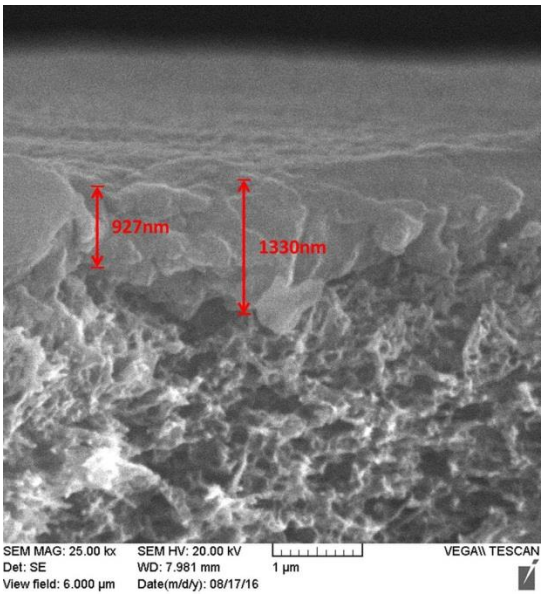

Figure 3.4 SEM images of the membranes a) control-TFC top surface, b) control-TFC cross section, c) 0.1%-CNC-TFN top surface, d) 0.1%-CNC-TFN cross section.

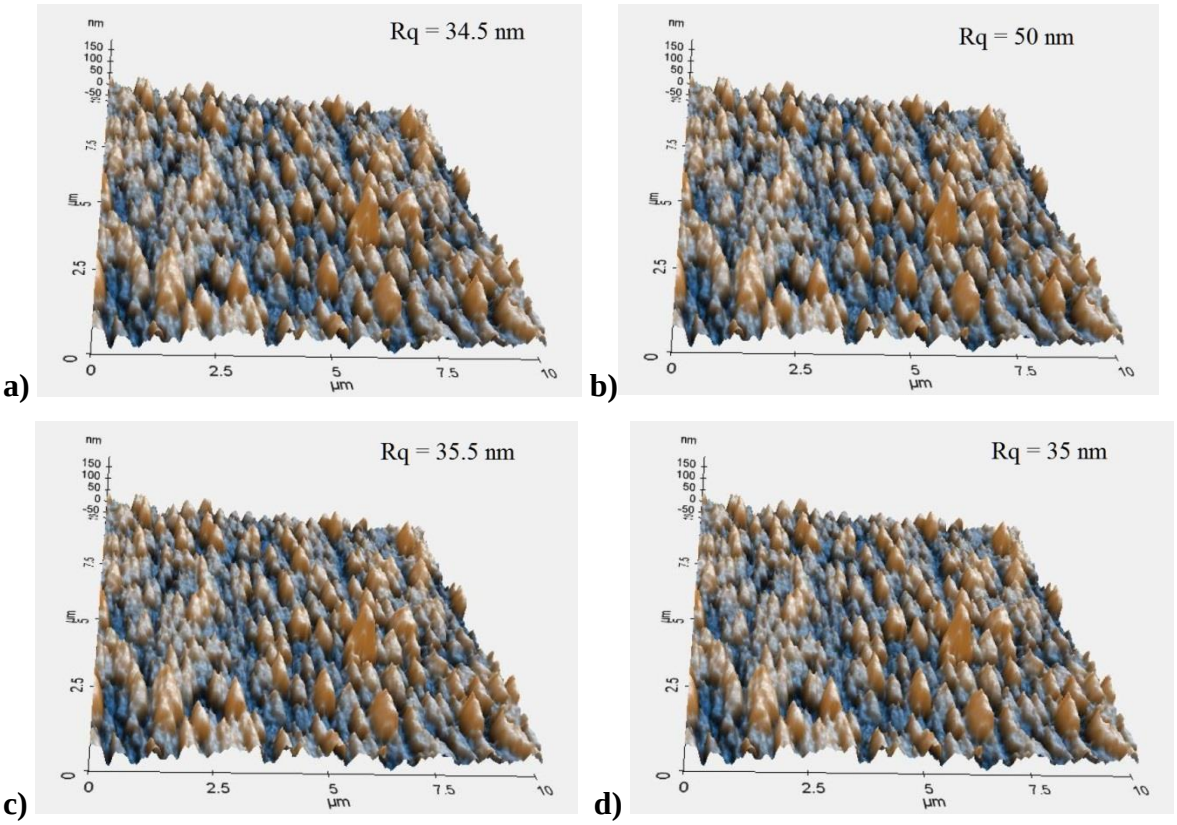

Figure 3.5 AFM image of top surface of a) control-TFC b) 0.05%-CNC-TFN c) 0.1%-CNC-TFN d) 0.2%-CNC-TFN.

Contact angle measurements for the control TFC and 0.1%-CNC-TFN membranes are shown in Table 1. Lower water contact angles correspond to more hydrophilic surfaces [21]. The average contact angles of all CNC-TFN membrane are lower than the control TFC membrane. It appears that the reduction of the contact angle is in line with the CNC loading, as the lowest and highest decrease of the contact angle are respectively for 0.05%-CNC-TFN and 0.2%-CNC-TFN membranes. The improved hydrophilicity of the TFN membranes can be attributed to the presence of hydrophilic CNC arising from the hydroxyl functional groups on their surface [2,6,8]. At the same time, a decrease of the average contact angles indicates a successful incorporation of the CNC into the PA layers during the interfacial polymerization.

Table 3.1 Average contact angle of membranes

CNC loading	0% (control)	0.05%	0.1%	0.2%
Contact Angle (°)	73.5	62.1	55.5	52.7
Standard Deviation	2.4	5.4	2.8	5.4

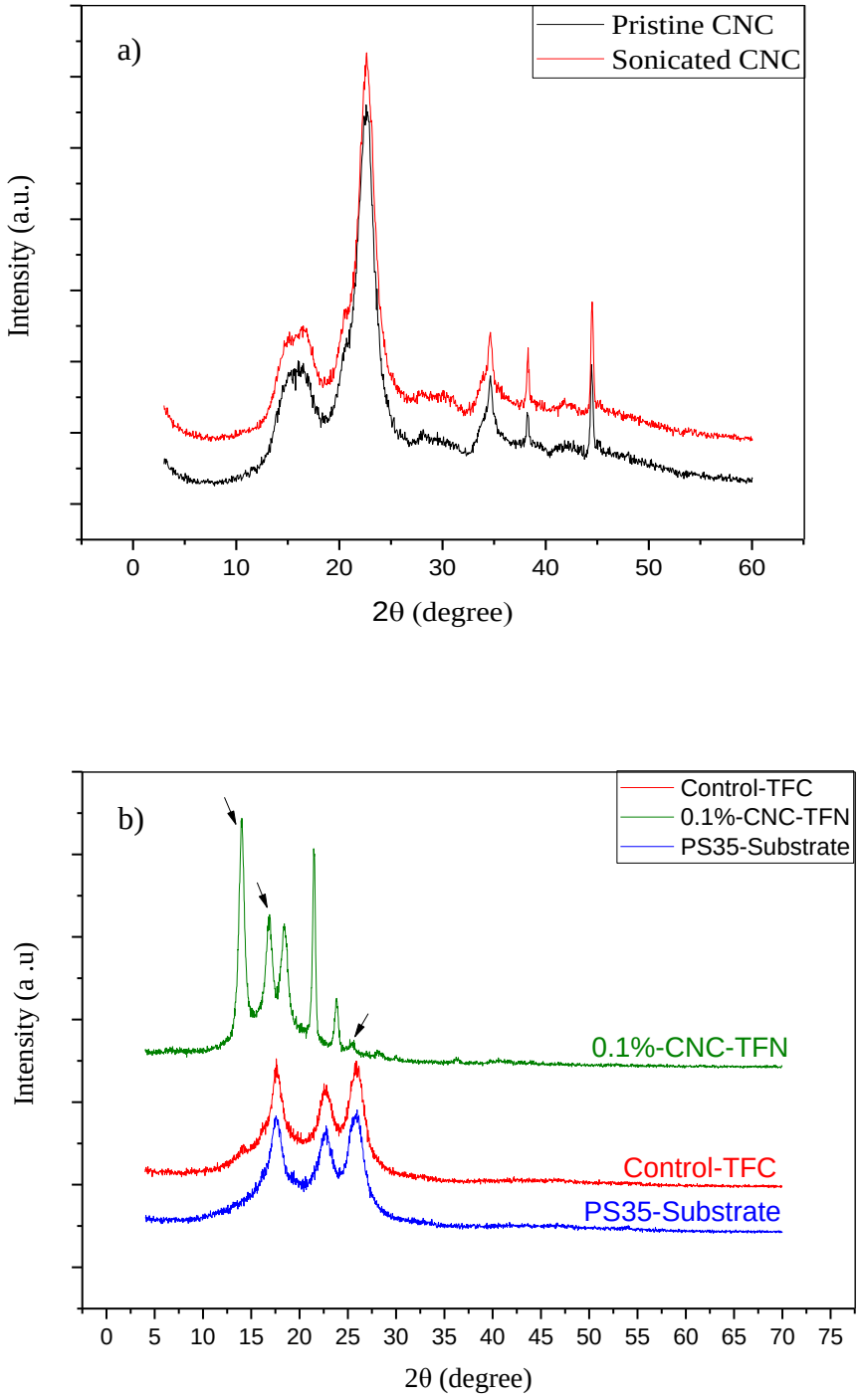

Figure 3.6 The XRD pattern of the a) pristine and 2 h sonicated CNC particles, b) PS substrate, control TFC and 0.1%-CNC-TFN membranes.

The XRD patterns of the CNC particles, the PS substrate membrane, the control TFC membrane and the 0.1%-CNC-TFN membrane are shown in Figure 3.6 a and b. According to the literature, cellulose type I has the characteristic diffraction peaks at 2θ = 15º, 17º, 21º, 23º and 34º, while peaks of the type II cellulose appear at 2θ = 12º, 20º, and 22º [22, 23]. The XRD spectrum of CNC particles shows three peaks at 2θ of approximately 16º, 22º and 34º. The peaks at 16º and 34º indicate the presence of cellulose type I. On the contrary, the fact that the highest intensity peak occurs at $2\theta \approx 22^{o}$ could be an indication of the presence of cellulose type II. One can thus conclude that CNC particles used in this study contain both types of cellulose I and II. The XRD spectra of the substrate and the control TFC membrane are similar showing peaks at 2θ = 17.5º, 22.5° and 25°, which indicate, not surprisingly, that polysulfone substrate determines the XRD spectrum of the TFC membrane. On the other hand, the XRD spectrum of the 0.1%-CNC-TFN membrane is significantly different from the spectra of the control membranes. There are five sharp peaks at 2θ =14°, 16.5°, 18.5°, 21.5° and 23.8°. It is likely that the peaks at 14^{o} and 16.5^{o} arise from the 15^{o} and 17^{o} of the added CNC. The shift to the smaller 2θ values indicates the interaction between CNC and the host PA polymer. The other peaks of the 0.1%-CNC-TFN membrane are either from the control TFC membrane or result from the overlap of TFC and CNC peaks [24]. The XRD analyses prove the successful incorporation of CNC into PA layer during interfacial polymerization. It is remarkable that a small amount of CNC causes such a significant change in the XRD spectrum of the CNC-based TFN membrane compared to the control TFC membrane. Also, comparison between the spectra of the sonicated CNC and pristine CNC shows that sonication did not deteriorate the structure and crystallinity of the CNC.

3.5.3. Desalination of synthetic brackish water

The RO performance of the control TFC and CNC-TFN membranes with synthetic brackish water solution as the feed is illustrated in Figure 3.7. In comparison with the control TFC membrane, the addition of the CNC particles (0.05% and 0.1% (w/v)) has significantly increased the permeate flux of the CNC-TFN membrane, from 30 ± 5 to 63 ± 10 $L/m^2.h$. However, further increase of CNC loading, 0.2% (w/v), caused a drop in water flux although it was still higher than the control TFC. This trend cannot be correlated with surface roughness determined using AFM. It is most likely interplay between increasing membrane hydrophilicity and increased thickness of the selective layer due to the presence of CNC particles. On the one hand, the increase in the

hydrophilicity of the membrane, confirmed by the contact angle analysis, tends to increase the water flux. On the other hand, an increase in the thickness of the selective layer in TFN membranes compared to the control TFC membrane, confirmed by the SEM analysis, increases the resistance to the water flux. Besides, CNC are not permeable particles, so excessive use of them within the matrix of the PA may lower the overall permeance of the membrane. As for the solute rejection, CNC loading resulted in a mild and almost a linear decrease up to 0.1% (w/v) loading, from 98.5 ± 0.5% to 97.8% ± 0.5% salt rejection. This was followed by a sharp decline to 95.5 ± 0.2% for the 0.2% (w/v) CNC loading. The decrease in the selectivity with an excessive filler loading is often observed which can be attributed to the formation of larger water flow channels between the NP agglomerates [2,25]. It is important to emphasize that salt rejection decreased despite of an increase in the thickness of the selective layer and presumed increase in membrane cross-linking due to the presence of hydrophilic CNC.

Considering the water flux and salt rejection, the TFN membranes with a 0.05-0.1% CNC loading appear to have an optimum performance. It is speculated that optimum performance in this range of CNC loading is interplay between increasing membrane hydrophilicity and thickness resulting from the presence of hydrophilic CNC, and a formation of CNC agglomerates in the selective layer of the membrane. Although more studies are required to better understand the optimum loading of CNC in TFN membranes, it is clear that adding CNC into the organic solution of TMC in n-hexane allows their incorporation into the resulting TFN membranes. More importantly, the performance of these TFN membranes is very sensitive to even as low CNC loading as 0.05% (w/v) in the organic solution of TMC monomer.

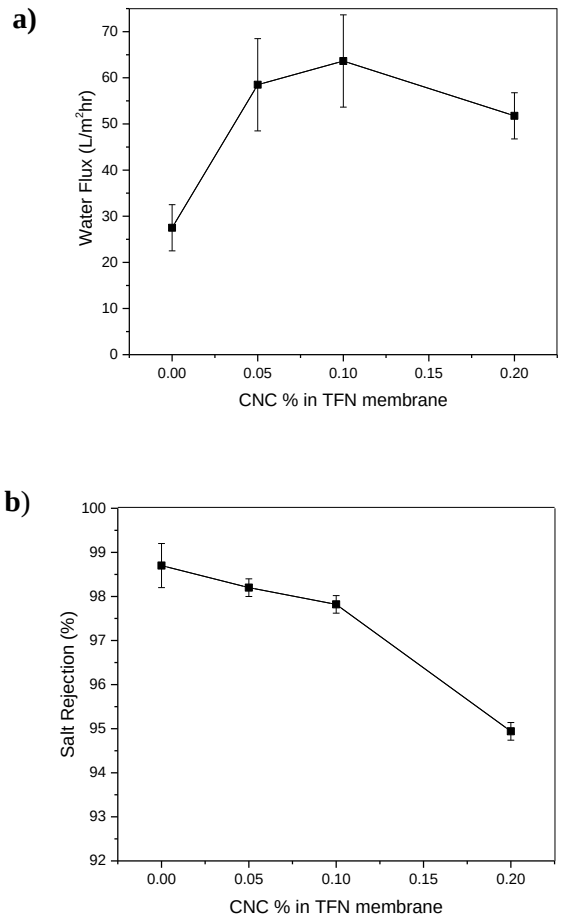

Figure 3.7 Performance of the TFC membrane and CNC-TFNs membranes with different CNC loadings; a) water flux and b) salt rejection. Each point represents the average flux / rejection of at least 3 tested membrane samples, each with 17.52 cm^2 active area.

The antifouling properties of the control TFC and 0.1%-CNC-TFN membranes with 0.1% (w/v) of CNC loading are compared in Figure 3.8. All the performance data are normalized with the corresponding initial permeate flux of the membranes. The flux decline is due to the BSA layer formation on the membrane surface, which causes an additional resistance for the permeate to flow through the membrane [13,26]. The 0.1%-CNC-TFN membrane had a less severe fouling than the control TFC membrane. After 1200 minutes of running the fouling-filtration test, water flux of the control TFC membrane declined to 0.74% of its initial value while this decrease was to 0.85% of the initial flux for the 0.1%-CNC-TFN membrane. In other words, although the presence of CNC in the selective layer of the membrane does not entirely prevent its fouling, it allows retaining 11% more of the original flux compared to the control TFC membrane. This improved antifouling

property can be associated with the negative surface charge of the CNC particles since the pH of the feed solution (~ 5.4) was slightly higher than the isoelecteric point (pI) of the BSA [14,26] .

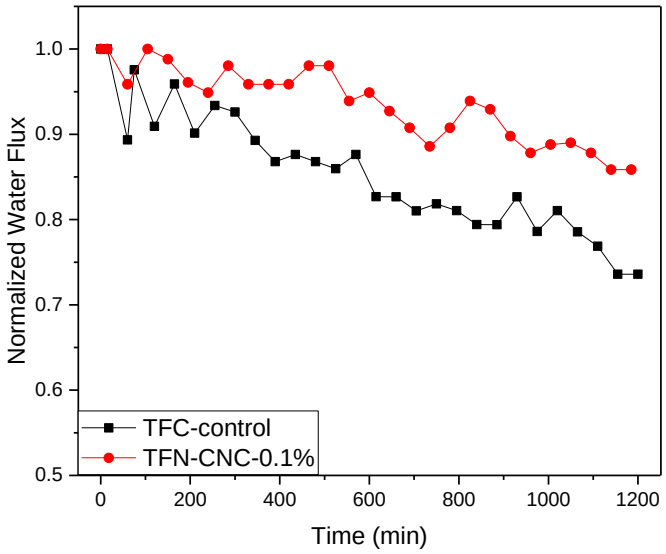

Figure 3.8 Change of normalized permeate flux with time for control TFC and 0.1%-CNC-TFN membrane. Each point represents the average flux / rejection of 3 tested membrane samples, each with 17.52 cm^2 active area.

3.6. Conclusions

Two of the major obstacles for commercialization of the nanocomposite RO membranes are the rising environmental concerns, due to the leaching out of the toxic NP into the permeate and retentate streams, as well as high production cost of NP. We tackled these issues by introducing CNC into the solution of TMC in n-hexane followed by interfacial polymerization of TMC and MPD. CNC are the nano-scale crystalline form of cellulose which is the most abundant natural polymer. Most importantly, CNC are considered as safe, non-toxic, biodegradable, and renewable particles.

In this work, for the first time, we embedded CNC into the PA layer of the TFN RO membranes. Membrane characterization by XRD analyses confirmed successful incorporation of CNC in the PA layer. From the SEM images, it was found that the CNC loading enhanced cross-linking of the PA, and increased the thickness of the PA layer. Also, membrane contact angle declined in line

with the amount of CNC loading, from 73.5 ± 2.4° for control TFC to 52.7 ± 5.4° for 0.2%-CNC-TFN membrane. The surface roughness showed no significant change except for the 0.05%-CNC-TFN. From the brackish water experimental results, the TFN membranes with CNC loading in the range of 0.05 - 0.1% (w/v) showed the optimum performance i.e., doubled permeate flux with only a modest decrease in the salt rejection. Also, the TFN membranes showed improved antifouling properties.

The unique properties of CNC and significant enhanced CNC-TFN water flux may open new doors to high performance TFN membranes for various applications. Further research is required to have a better understanding of the optimum CNC loading and to monitor long-term performance, stability, and probable applications of the CNC-TFN membranes.

3.7. Acknowledgement

The authors gratefully acknowledge the financial support for this project provided of Qingdao Wosai Seawater Desalination Technology Ltd. The authors would like to Mr. Du Bai, Mr. Andre Francois, Dr. Somaye Akbrari, Dr. Siamak Lashkari and Dr. Deepak Rana for their kind help in interpretation of some physical analyses. Also, would like thank Dr. Sara Dastjerdi and Dr. Marc Dubé for providing us with the TEM image of CNC.

3.8. References

[1] K.P. Lee, T.C. Arnot, D. Mattia, A review of reverse osmosis membrane materials for desalination—Development to date and future potential, J. Membr. Sci. 370 (2011) 1–22. doi:10.1016/j.memsci.2010.12.036.

[2] W.J. Lau, S. Gray, T. Matsuura, D. Emadzadeh, J. Paul Chen, A.F. Ismail, A review on polyamide thin film nanocomposite (TFN) membranes: History, applications, challenges and approaches, Water Res. 80 (2015) 306–324. doi:10.1016/j.watres.2015.04.037.

[3] B.-H. Jeong, E.M.V. Hoek, Y. Yan, A. Subramani, X. Huang, G. Hurwitz, A.K. Ghosh, A. Jawor, Interfacial polymerization of thin film nanocomposites: A new concept for reverse osmosis membranes, J. Membr. Sci. 294 (2007) 1–7. doi:10.1016/j.memsci.2007.02.025.

[4] D. Emadzadeh, W.J. Lau, M. Rahbari-Sisakht, A. Daneshfar, M. Ghanbari, A. Mayahi, T. Matsuura, A.F. Ismail, A novel thin film nanocomposite reverse osmosis membrane with superior anti-organic fouling affinity for water desalination, Desalination. 368 (2015) 106–113. doi:10.1016/j.desal.2014.11.019.

[5] L.Y. Ng, A.W. Mohammad, C.P. Leo, N. Hilal, Polymeric membranes incorporated with metal/metal oxide nanoparticles: A comprehensive review, Desalination. 308 (2013) 15–33. doi:10.1016/j.desal.2010.11.033.

[6] Y. Habibi, L.A. Lucia, O.J. Rojas, Cellulose Nanocrystals: Chemistry, Self-Assembly, and Applications, Chem. Rev. 110 (2010) 3479–3500. doi:10.1021/cr900339w.

[7] B.L. Peng, N. Dhar, H.L. Liu, K.C. Tam, Chemistry and applications of nanocrystalline cellulose and its derivatives: A nanotechnology perspective, Can. J. Chem. Eng. 89 (2011) 1191–1206. doi:10.1002/cjce.20554.

[8] M. Mariano, N. El Kissi, A. Dufresne, Cellulose nanocrystals and related nanocomposites: Review of some properties and challenges, J. Polym. Sci. Part B Polym. Phys. 52 (2014) 791–806. doi:10.1002/polb.23490.

[9] H. Bai, X. Wang, Y. Zhou, L. Zhang, Preparation and characterization of poly(vinylidene fluoride) composite membranes blended with nano-crystalline cellulose, Prog. Nat. Sci. Mater. Int. 22 (2012) 250–257. doi:10.1016/j.pnsc.2012.04.011.

[10] S. Li, Y. Gao, H. Bai, L. Zhang, P. Qu, L. Bai, Preparation and characterization of polysulfone dialysis composite membranes modified with nanocrystalline cellulose, BioResources. 6 (2011) 1670–1680. doi:10.15376/biores.6.2.1670-1680.

[11] P. Daraei, N. Ghaemi, H.S. Ghari, An ultra-antifouling polyethersulfone membrane embedded with cellulose nanocrystals for improved dye and salt removal from water, Cellulose. 24 (2017) 915–929. doi:10.1007/s10570-016-1135-3.

[12] J.C. Crittenden, R.R. Trussell, D.W. Hand, K.J. Howe, G. Tchobanoglous, Reverse Osmosis, in: MWHs Water Treat. Princ. Des. Third Ed., John Wiley & Sons, Inc., 2012: pp. 1335–1414. doi:10.1002/9781118131473.ch17.

[13] R.W. Baker, Membrane Science and Technology, John Wiley & Sons, Ltd, 2012. http://onlinelibrary.wiley.com/doi/10.1002/9781118359686.ch1/summary (accessed April 9, 2017).

[14] W.S. Ang, M. Elimelech, Protein (BSA) fouling of reverse osmosis membranes: Implications for wastewater reclamation, J. Membr. Sci. 296 (2007) 83–92. doi:10.1016/j.memsci.2007.03.018.

[15] M. Xie, J. Lee, L.D. Nghiem, M. Elimelech, Role of pressure in organic fouling in forward osmosis and reverse osmosis, J. Membr. Sci. 493 (2015) 748–754. doi:10.1016/j.memsci.2015.07.033.

[16] M.T.M. Pendergast, J.M. Nygaard, A.K. Ghosh, E.M.V. Hoek, Using nanocomposite materials technology to understand and control reverse osmosis membrane compaction, Desalination. 261 (2010) 255–263. doi:10.1016/j.desal.2010.06.008.

[17] S.-Y. Kwak, S.G. Jung, Y.S. Yoon, D.W. Ihm, Details of surface features in aromatic polyamide reverse osmosis membranes characterized by scanning electron and atomic force microscopy, J. Polym. Sci. Part B Polym. Phys. 37 (1999) 1429–1440. doi:10.1002/(SICI)1099-0488(19990701)37:13<1429::AID-POLB9>3.0.CO;2-B.

[18] M.L. Lind, A.K. Ghosh, A. Jawor, X. Huang, W. Hou, Y. Yang, E.M.V. Hoek, Influence of Zeolite Crystal Size on Zeolite-Polyamide Thin Film Nanocomposite Membranes, Langmuir. 25 (2009) 10139–10145. doi:10.1021/la900938x.

[19] G.N.B. Baroña, J. Lim, M. Choi, B. Jung, Interfacial polymerization of polyamide-aluminosilicate SWNT nanocomposite membranes for reverse osmosis, Desalination. 325 (2013) 138–147. doi:10.1016/j.desal.2013.06.026.

[20] S.-Y. Kwak, S.G. Jung, S.H. Kim, Structure-motion-performance relationship of flux-enhanced reverse osmosis (RO) membranes composed of aromatic polyamide thin films, Environ. Sci. Technol. 35 (2001) 4334–4340. doi:10.1021/es010630g.

[21] W.J. Lau, A.F. Ismail, P.S. Goh, N. Hilal, B.S. Ooi, Characterization Methods of Thin Film Composite Nanofiltration Membranes, Sep. Purif. Rev. 44 (2015) 135–156. doi:10.1080/15422119.2014.882355.

[22] H. Zhao, J.H. Kwak, Z. Conrad Zhang, H.M. Brown, B.W. Arey, J.E. Holladay, Studying cellulose fiber structure by SEM, XRD, NMR and acid hydrolysis, Carbohydr. Polym. 68 (2007) 235–241. doi:10.1016/j.carbpol.2006.12.013.

[23] W.P. Flauzino Neto, H.A. Silvério, N.O. Dantas, D. Pasquini, Extraction and characterization of cellulose nanocrystals from agro-industrial residue – Soy hulls, Ind. Crops Prod. 42 (2013) 480–488. doi:10.1016/j.indcrop.2012.06.041.

[24] Y. Yang, H. Zhang, P. Wang, Q. Zheng, J. Li, The influence of nano-sized TiO2 fillers on the morphologies and properties of PSF UF membrane, J. Membr. Sci. 288 (2007) 231–238. doi:10.1016/j.memsci.2006.11.019.

[25] H. Dong, L. Zhao, L. Zhang, H. Chen, C. Gao, W.S. Winston Ho, High-flux reverse osmosis membranes incorporated with NaY zeolite nanoparticles for brackish water desalination, J. Membr. Sci. 476 (2015) 373–383. doi:10.1016/j.memsci.2014.11.054.

[26] S. Jiang, Y. Li, B.P. Ladewig, A review of reverse osmosis membrane fouling and control strategies, Sci. Total Environ. 595 (2017) 567–583. doi:10.1016/j.scitotenv.2017.03.235.

Chapter 4

Synthesis and characterization of Thin Film Nanocomposite reverse osmosis membranes embedded with various functionalized Halloysite NanoTubes (HNT)

Farhad Asempour[1], Somaye Akbari[2], Du Bai[1], Daryoush Emadzadeh[1,3], Takeshi Matsuura[1,4], Boguslaw Kruczek[1*]

[1] Department of Chemical and Biological Engineering, University of Ottawa, 161 Louis Pasteur St, Ottawa, ON K1N 6N5, Canada

[2] Textile Engineering Department, Amirkabir University of Technology, 424 Hafez Ave, Tehran, Iran

[3] Department of Chemical Engineering, Gachsaran Branch, Azad University, Gachsaran, Iran

[4] Advanced Membrane Technology Research Centre (AMTEC), Universiti Teknologi Malaysia, 81310 Skudai, Johor, Malaysia

- **67th Canadian Chemical Engineering Conference (2017)**
  Preparation and characterization of a novel reverse osmosis thin film nanocomposite (TFN) membrane using dendritic functionalized halloysite nanotubes (HNT) presenter: **Farhad Asempour**

* Corresponding author: Boguslaw.Kruczek@uottawa.ca

Chapter 4. Synthesis and characterization of Thin Film Nanocomposite reverse osmosis membranes embedded with various functionalized Halloysite NanoTubes (HNT)

Keywords: Thin film nanocomposite membranes, reverse osmosis, halloysite nanotube, leaching, nanoparticle, dendrimer.

4.1. Abstract

Thin film nanocomposite (TFN) membranes are a relatively new category of high-performance membranes for reverse osmosis and nanofiltration applications. However, large-scale and long-term use of these membranes is remarkably limited. One of the major reasons for this constraint is the low compatibility and adhesion between the embedded NP and the polyamide matrix of membranes. Here, we addressed this issue by functionalization of the nanoscale additives to enhance their interactions with the polymer matrix and thus reducing NP leachability. Reverse osmosis TFN membranes were fabricated by in-situ interfacial polymerization of m-phenylenediamine (MPD) and trimesoyl chloride (TMC), and incorporation of functionalized Halloysite Nanotubes (HNT). Exterior surface of the HNT was modified by adding three different functional groups: amine groups (HNT-NH_2), the first generation of poly(amidoamine) (PAMAM) dendrimers (HNT-G1), and carboxylic acid (HNT-COOH). The modified HNT were characterized by Attenuated Total Reflection-Fourier Transform Infrared Spectroscopy (ATR-FTIR), Transmission Electron Microscopy (TEM), Scanning Electron Microscopy (SEM), zeta potential, and thermogravimetric (TGA) analyses. Besides, surface morphology and physicochemical properties of the membranes as well as reactions of the functionalized HNT with the monomers and the polyamide matrix were investigated by SEM, ATR-FTIR, XPS, and contact angle measurements. It was also attempted to study the HNT leachability from the membranes by using a leaching test in a batch incubator followed by tracing the HNT with Inductively Coupled Plasma Mass Spectrometry (ICP-MS). Furthermore, membrane selectivity and permeate flux were evaluated in cross-flow reverse osmosis (RO) desalination experiments using synthetic brackish

water. It was found that addition of HNT and modified HNT enhanced the water flux of all membranes without sacrificing the salt rejection (99.1 % ± 0.1 %). The membrane with HNT-COOH particles showed the maximum water flux increase (from 26.2 ± 2.5 L/m^2.hr to 49.6 ± 12.9 L/m^2.hr). TFN membranes with HNT-NH_2 and HNT-G1 had significantly lower HNT leaching in comparison with TFN membrane with non-functionalized HNT. These results were attributed to the increased membrane hydrophilicity and a formation of covalent bond between the amine groups of HNT-NH_2 and HNT-G1 with acyl chloride functional groups of TMC monomers.

4.2. Introduction

Although membrane separation processes are emerging in various water treatment applications, some obstacles are yet to be addressed for further growth of polymeric membrane technology and industry. Particularly for water desalination with aromatic polyamide thin film composite (TFC) membranes, low permeance, and salt rejection, likewise, membrane fouling and poor tolerance to chlorine are currently the major challenges [1–3]. Embedding nanoparticles (NP) in the selective polyamide (PA) layer is a strategy to enhance the performance and physiochemical properties of the resulting thin film nanocomposite (TFN) membranes. It is often reported that the addition of hydrophilic NP increases the surface wettability of the PA layer, and thus improves water flux and antifouling capacity of the membranes [4–6]. Also, NP can influence the properties of the PA layer such as its density, thickness and the degree of cross-linking [7]. Many studies on TFN membranes are focused on the development of novel nano-scale additives. Some of the studied materials in the past decade include carbon nanotubes (CNT) [8], graphene oxide (GO) [9], poly(amidoamine) (PAMAM) dendrimers (as nano-scale copolymers) [10], zeolites [11], titanium oxide (TiO_2) [9], silver (Ag) [12], aluminum oxide (Al_2O_3) [13], nanoclayparticles [14], silica NP [15], and zinc oxide (ZnO) [16–18].

Nevertheless, there are some complications associated with the nanocomposite membranes, which have greatly limited large scale applications of TFN membranes. NP tend to aggregate due to their high surface tension. This phenomenon results in uneven distribution of NP in the PA matrix, which may cause defects and deteriorate membrane selectivity. Therefore, it is essential that NP are well dispersed in the monomer's suspensions. Another major challenge of nanocomposite membranes is leaching out of the NP into the downstream, which causes membrane degradation, infringement of drinking water regulations, and rising environmental concerns. Polymer-NP compatibility and their interfacial interactions/adhesions play a critical role in controlling the membrane performance and leaching out of the NP [3,19,20]. Surface modification of the NP is one of the methods to overcome the above mentioned challenges. Functionalization of the NP prevents the formation of large NP aggregates and improves some other properties of the PA layer. It is reported that the functionalization of NP with hydrophilic groups such as amine, carboxylic acid, and sulfonic acid leads to TFN membranes with higher surface hydrophilicity and water permeance [3,21]. It is also suggested that functional groups on the NP can potentially take part in the interfacial polymerization generating covalent linkages with the PA matrix [3,14–17].

In this study, we have combined RO membrane technology with dendrimer nanotechnology. We examined functionalization of HNT and their incorporation into the TFN membranes for brackish water desalination. As mentioned earlier, it is believed that functionalization of the nano-fillers enhances their reactivity in the PA layer of the TFN membranes [3,24]. Therefore, the primary motivation of this work is to overcome the leachability of the HNT by functionalizing them and generating covalent bonds between the HNT and the PA matrix. Three different types of functional groups were utilized to modify the HNT. The first category, named HNT-NH_2, was the HNT which were grafted by amine groups via a single step silanization. The next type of functional group, noted as HNT-G1, was the first generation of amine terminated poly(amidoamine) (PAMAM) dendrimers. The dendritic structures were added to the surface of HNT via the divergent synthesis route. The last type of HNT functionalization was the addition of carboxylic acid groups. These functionalized HNT are noted as HNT-COOH and were prepared by adding succinic anhydride to HNT-NH_2. After functionalization of the HNT, they were incorporated in the TFN membrane by in situ interfacial polymerization of PA. Finally, the effects of the surface functionalized HNT on membrane performance as well as NP-PA interactions were studied. Reverse Osmosis (RO) desalination tests were conducted using synthetic brackish water to determine the permeance and selectivity of the membranes. Physicochemical properties of the TFN membranes and interactions between the HNT and monomers / PA matrix were characterized by SEM, XPS, ATR-FTIR and water contact angle measurement. Also, it was attempted to test the leachability of HNT from the membranes by shaking the membranes for 48 h in a batch incubator, and tracing the leached out HNT with ICP-MS.

4.3. Overview of embedded HNT and PAMAM dendrimers

HNT are naturally occurring multilayer aluminosilicates with the molecular formula of $Al_2Si_2O_5(OH)_4 \cdot nH_2O$. Owing to their low production cost, minimal environmental risks, unique structure and chemical properties, HNT are excellent nanofiller candidate for polymeric membranes to be used for water-treatment applications. As it is illustrated in Figure 4.1, HNT have a hollow tubular morphology with the length of 0.5 – 1.2 µm, and inner and outer diameter of 15-30 nm and 50-70 nm respectively. The gaps between layers in anhydrous HNT are 7 to 10 Å. The exterior surface of the HNT is composed of siloxane groups (Si-O-Si) with few hydroxyl groups, which enables their functionalization [25,26]. HNT have been employed in some studies on

synthesis of nanocomposite ultrafiltration and forward osmosis membranes, which led to an improvement of antifouling properties [27,28]. For instance, Ghanbari et al. utilized amine functionalized HNT for water desalination by TFN Forward Osmosis. They reported that incorporation of 0.05% (w/v) HNT to the PA layer led to 50% increase of the water flux. They also noted that the same membrane in an RO test at 2.5 bar had 66% higher water flux than the control membrane without HNT [14].

PAMAM dendrimers are a class of three dimensional, highly branched, symmetrical, and nanoscopic polymers. They are formed by iterative constructs of amidoamine and primary/terminal amine groups. Each of the outward repeating cycles is called a generation, and the number of terminal groups grows exponentially by increasing the generation number [29]. PAMAM dendrimers can be incorporated in or grafted onto the PA matrix since they have a high density of reactive terminal amine groups [30].

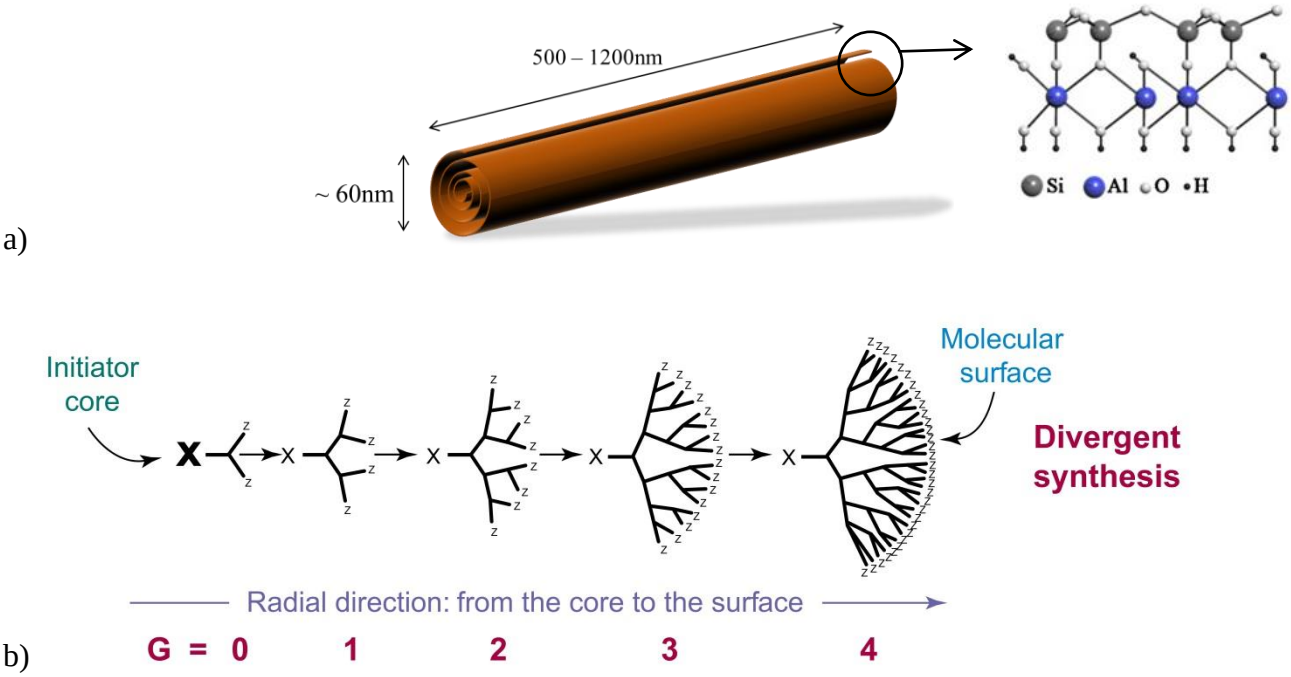

Figure 4.1 Structure of a) HNT and b) Generations 0 to 4 of PAMAM dendrimers; x and z are indicates the core and terminal amine functional groups respectively [25,29].

One of the first studies on the application of dendrimers in surface modification of TFC RO membranes was reported by Sarkar et al. They noted that hydrophilicity of the membranes was increased by coating them with PAMAM [30]. Also, there have been some studies to synthesize PA layer using different generations of PAMAM dendrimers as the main monomer or an additive. Sum et al. employed mixed monomers of zero generation PAMAM-NH_2 and void filling piperazine (PIP) [31]. In another work, Mansurpanah et al. applied various generations, 0 to 2, and concentrations of amine terminated PAMAM to the amine rich monomer (piperazine) solution to fabricate TFC membranes. They reported that with the growth of the PAMAM generation, interfacial polymerization was enhanced; also membrane selectivity and cationic surface charge were increased [10]. It was also reported that due to the open structure of the PAMAM dendrimers, TFC membrane permeance improved [10,31]. Figure 4.2 represents a schematic representation of 3 different generations of the PAMAM dendrimer grafted on an HNT particle.

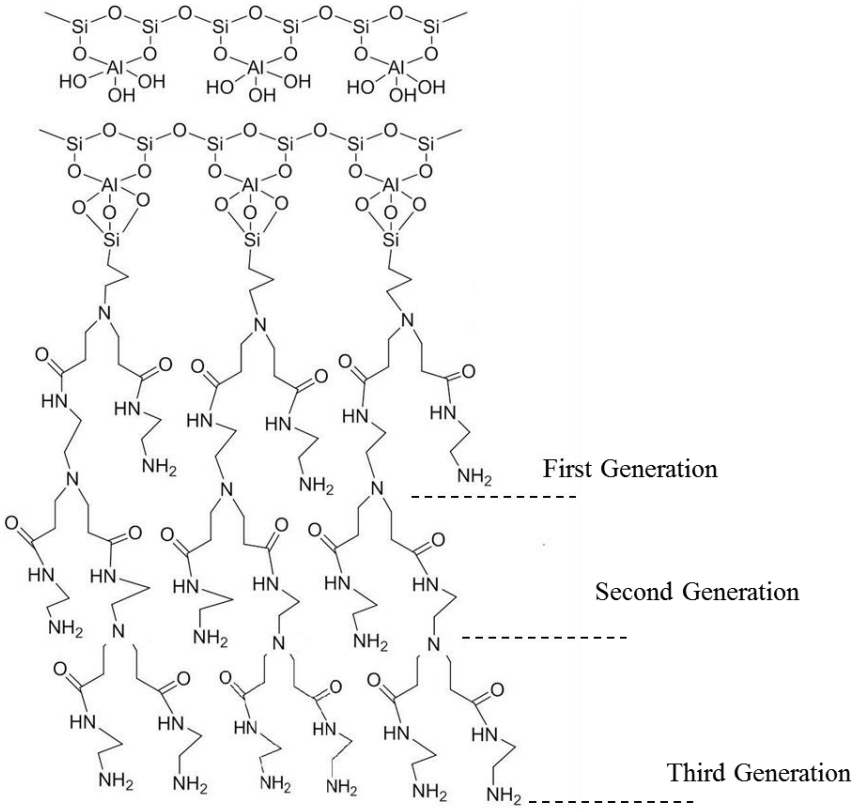

Figure 4.2 Schematic structure of an HNT grafted with third generation of the PAMAM dendrimers (due to spacial limit not all branches are shown)

4.4. Experimental

4.4.1. Materials

Polysulfone ultrafiltration membrane (PS35) with molecular weight cut-off of 20,000 was purchased from Nanostone Water, Waltham Massachusetts, U.S.A. The Halloysite NanoTubes (HNTs) were provided by Delta-Dolsk, Poland. M-phenylenediamine (MPD) and 1,3,5-benzenetricarbonyl trichloride (TMC), aminopropyltriethoxysilane (APTES), methyl acrylate (MA), ethanol, ethylene diamine (EDA), diethyl ether, n-hexane, succinic anhydride, and sodium chloride were all of the laboratory reagent grades and purchased from Sigma-Aldrich. Deionized water was used for making the aqueous MPD solution, and distilled water was utilized for washing the membranes and preparing the synthetic brackish water feed with NaCl as the solute.

4.4.2. Synthesis of modified HNT

The detailed synthesis procedure of dendrimers and functionalization of HNT are fully described in a previous work [32]. Briefly, acid treatment of HNT was carried out to remove contaminants such as iron in the first step of functionalization. In this stage, HNT were mixed with aqueous HCl solution (35%) for 24 h using a magnetic stirrer and washed three times with distilled water. For amine functionalization of HNT, the acid-washed and dried HNT were refluxed with APTES solution in toluene (4/15 v/v) at 60 ºC for 12 h to produce HNT-NH_2 [28]. HNT-G1were another type of functionalized NP, which was synthesized by the Michael addition of methyl acrylate to the HNT-NH_2, followed by amidation of the ester groups with ethylene diamine. In this technique, first HNT were amino functionalized with APTES. Then, MA (15 mL) and HNT-NH_2 (31.25 g) in ethanol solution at 60 ºC went under Michael reaction for 24 h. The resulted solution was put into a centrifuge, and the separated HNT were washed and centrifuged with diethyl ether, ethanol and methanol, each for 5 times to remove the impurities before being dried at 60 ºC. In the next step, ethylene diamine was added to the solution of ethanol and HNT and stirred for 24 h at 60 ºC. Finally, after centrifugation of the resulted slurry solution, separated HNT were washed with distilled water and dried. The last type of functionalized HNT was HNT-COOH. To synthesize HNT-COOH particles, 1 g of HNT-NH_2 reacted with 1.2 g of succinic anhydride in 50 mL of DMF at 90°C for 24 h under reflux. Finally, modified HNT were washed with DMF and dried at 60°C for 8h [25]. The Schematic structures of the functionalized HNT are illustrated in Figure 4.3.

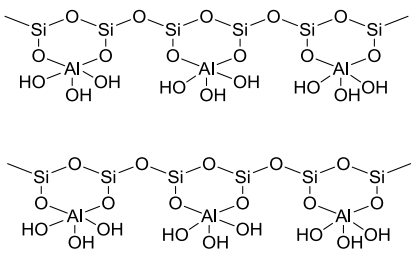

a) HNT

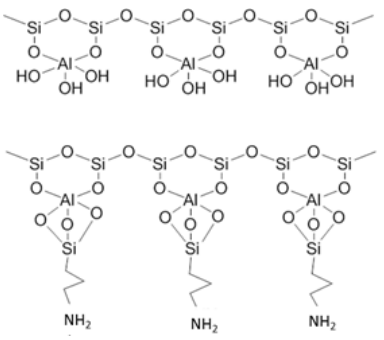

b) HNT-NH_2

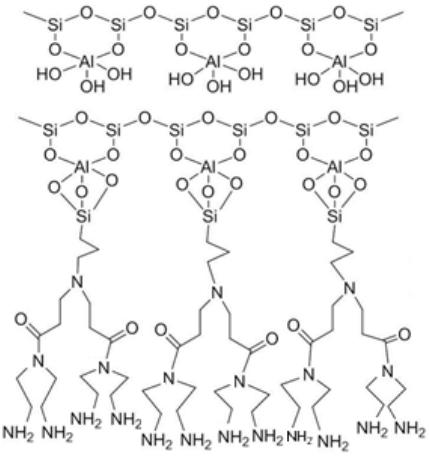

c) HNT-G1

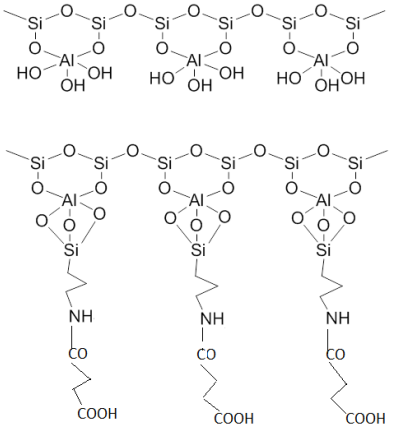

d) HNT-COOH

Figure 4.3 Schematic structure of the HNT.a) HNT (acid-washed), b) HNT-NH2, c) HNT-G1, and d) HNT-COOH**.**

4.4.3. Synthesis of the TFC and TFN membranes

The PS35 UF membrane was used as the substrate for the PA layer, which was synthesized by in-situ interfacial polymerization of MPD and TMC. Fabrication of TFC membrane started with contacting the substrate with a 2% (w/v) solution of MPD in deionized water for 5 minutes. Then, the excess aqueous solution was drained off from the substrate, and any residual droplets were further removed from the membrane with a Teflon roller. This was followed by pouring an organic solution, 0.05% (w/v) TMC in n-hexane, on the membrane. The organic solution was in contact with the membrane for 1 minute. Then, the excess solution was completely removed, and the

membrane was rinsed with pure n-hexane. Afterwards, the membrane was placed in an oven at 95°C for 10 minutes. Finally, the membrane was carefully washed with and stored in deionized water. To fabricate TFN membranes with either pristine HNT or modified HNT as the nano-scaled additive materials, organic solution, 0.05% (w/v) TMC and 0.05% (w/v) HNT in hexane, was used as the organic phase, and the solution was sonicated for 2 h to avoid agglomeration of the HNT. It should be noted that the concentration of 0.05% (w/v) was previously reported by Ghanbari et al. as the optimal amount of HNT for the synthesis of the forward osmosis TFN [8].

In this article the membranes are coded as: x-HNT-TFN where x indicates the functional group on the HNT. When no HNT is embedded in the PA layer, the membrane is coded as TFC. When pristine HNT are used as NP, the "x" is dropped.

4.4.4. Evaluation of membranes performance

Membranes were tested in a continues-cross-flow RO system to evaluate their selectivity and water flux. The testing system consists of 3 parallel cells, each with the effective permeation area of 17.35 cm^2. The feed was synthetic brackish water with 3,000 ppm NaCl. The temperature of the feed in the reservoir was controlled at 25 ± 2°C, and the trans-membrane pressure was kept at 20 ± 1 bar(g). To avoid concentration polarization in the cells, the feed flow rate was maintained at 2.4 ± 0.2 L/min, which provides the minimum linear velocity of 200 mm/s on the surface of the membrane [33].

Equations 1 is used to determine the permeate flux, J_w $\left[\frac{L}{h.m^2}\right]$. V_p $[L]$ is the collected permeate during the time t $[h]$, and $A_p[\mathrm{m}^2]$ is the active membrane area for permeation. Salt rejection, R, was evaluated by equation 2, in which C_p and C_f are the salt concentrations $\left[\frac{mg}{L}\right]$of the permeate and feed streams, respectively, measured by conductometry.

$$J_w = \frac{V_p}{A_p \times t} \qquad (1)$$

$$R = \left(1 - \frac{C_p}{C_f}\right) \times 100\% \qquad (2)$$

4.5. Characterization of membranes and NP

Top surface morphology of the membranes was studied by SEM (Tescan Vega-II XMU). All samples were coated by gold sputtering. The morphology of the acid washed HNT was characterized using TEM (Philips CM30). Also, the morphology of all NP were studied with SEM (Hitachi S-4160). The percentage of the functionalization of each HNT were evaluated by the thermogravimetric analyzer (TGA), TGA Q5000 (TA Instruments Ltd, USA) from 30°C to 800°C at a heating rate of 10°C/min under the nitrogen atmosphere. In order to investigate the chemical properties and probable interactions between the NP and the PA matrix, XPS analyses were also conducted. Elemental surveys were carried out over 1 × 1 mm area of the membranes using an XPS (Kratos Analytical model Axis Ultra DLD spectrometer) machine with monochromated aluminum-K α X rays at the power of 140 watts. In addition, a Nicolet 6700 FTIR (Thermo Scientific) with a diamond crystal was utilized to obtain the ATR-FTIR spectra of the PS35 substrate, TFN membranes, acid-washed and functionalized HNT, and HNT which reacted with monomers (MPD and TMC). All scans were recorded at the resolution of 4 cm^{-1} in a range of wave numbers between 650 and 4000 cm^{-1}. For having a better understanding of the interactions of the HNT with various functionalizations and the monomers, we studied the reaction of each monomer with NP prior to the fabrication of the PA layer by IP. To do so, 0.05 w/v% of NP were added to either the 0.05w/v% TMC solution or the 2 w/v% MPD solution. After 2 h of mixing and sonication, NP were removed from the dispersions by centrifugation and washed twice either with hexane (NP treated with the TMC solution) or with distilled water (NP treated with the MPD solution). Then, the HNT were characterized with FTIR to examine if the reaction took place between the NP and the monomer. For a quantitative ATR-FTIR analysis of the reacted NP, all ATR-FTIR spectra were normalized by the intensity of the band at 910 cm^{-1}, which is assigned to the bending vibration of Al-OH, as an internal standard [34]. For the quantitative analysis of the substrate, TFC, and TFN membrane, the spectra were normalized using the intensity of the polysulfone support at 1584 cm^{-1} [35]. Besides, the zeta potential measurement of the functionalized HNT was conducted by a zeta analyzer (Zetasizer PSS0012-22, Malvern Instruments) using frontal electrophoretic light scattering method to determine the surface charge. NP were added to distilled water and sonicated for 15 min prior to the surface potential analysis with the zeta analyzer. Also, sessile water contact angle of the membranes was measured using a VCA Optima surface analysis system (AST Products, Inc., Billerica, MA). At least 10 droplets of

deionized water with the volume of 2 µL were examined for the measurements at room temperature.

Furthermore, it the adhesion/interactions between the NP and the PA layer were studied by assessing the amount of NP leached out from the membrane. For this test, upon fabricating the TFN membranes and removing them from the oven, a circular sheet with the area of ≈17.5 cm^2 was cut from each membrane and placed in a batch container. Then, 50 mL of deionized water was added, and the container was sealed. The container with the membrane immersed in water was shaken in an incubator at 150 RPM for 48 hours. Finally, the water sample was collected from the container, acidified to ensure that all NP were in the liquid phase, and analyzed for the presence of Al using ICP-MS. This method was adapted from Yin et al.'s work to investigate the leaching of silver nanoparticles. Their TFC membranes, grafted with Ag and Ag^+ particles via covalent bonds, were shaken with distilled water in an incubator for 14 days at 100 RPM. They reported that after 14 days 12% of the embedded NPs leached out of the membrane [12].

4.6. Results and discussion

4.6.1. Characterization of nanoparticles

The TEM image of HNT is represented in Figure 4.4**.** As it is shown, the HNT exhibits a hollow tubular structure.

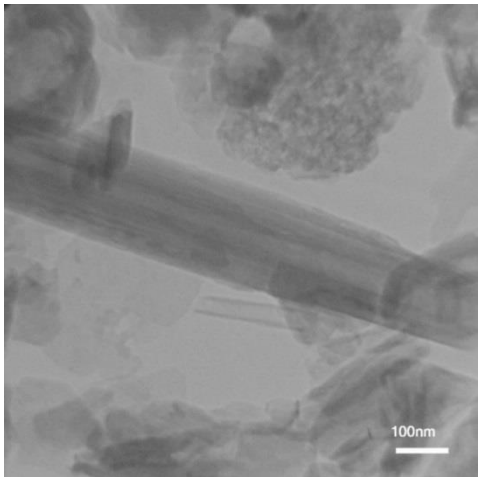

Figure 4.4 TEM image of the acid washed HNT.

SEM images of the HNT and HNT-G1are shown in Figure 4.5. From the images, it appears that the surface modification of the HNT has not changed the shape and morphology of the HNT. The arrows show the length and diameter of the HNT. It is commonly known that HNT are non-uniform in size [25].

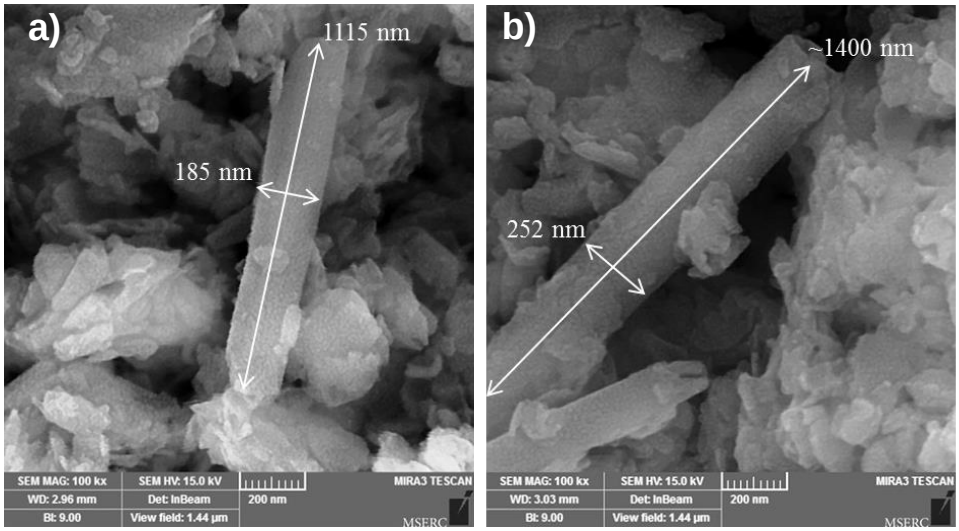

Figure 4.5 SEM image of a) HNT and b) HNT-G1

In order to evaluate the charge on the NP after functionalization, the zeta potential of the HNT with various functional groups was measured and the results shown in Table 4.1. These results indicate that the surface of HNT is negatively charged due to the presence of hydroxyl groups. The surface charge of the HNT-NH_2 became higher from -34.5 to -12.9 mV. Amino functionalization by APTES could not change the negative charge to the positive one. However, the addition of the first generation amine dendritic structures, HNT-G1, increased zeta-potential to +2.2(mV). This change is attributed to the existence of the positive amine groups which confirms the successful surface modification of HNT.

The percentage of functionalization of the HNT, HNT-NH_2, HNT-G1, and HNT-COOH were investigated by the TGA analyses. Table 4.1 illustrates the organic content of the mentioned samples. The organic increments (%) were calculated by subtracting the mass loss HNT from those of functionalized HNT. As it can be seen, HNT-COOH has the maximum organic content, which indicates the reaction of HNT-NH_2 with succinic anhydride.

Table 4.1 Zeta potential and TGA results of various functionalized HNT.

NP	Zeta potential (ζ)	Weight loss at 800°C (%)	Organic increment (%)
HNT	-34.5	17.65	0
HNT-NH_2	-12.9	19.07	1.42
HNT-G1	+2.2	22.94	5.29
HNT-COOH	-3.49	25.71	8.06

The ATR-FTIR analysis is a convenient way to determine the chemical reactions that occur when the HNT are functionalized. Also, it can be used to study the interactions between HNT and the IP monomers. Figure 4.6 illustrates the ATR-FTIR spectra of the HNT with various functional groups. The characteristic peaks of the HNT are the stretching vibration of the inner-surface Al-OH groups, which appear at 3621 and 3695 cm^{-1} [32]. Also, the peaks at 1630 and 910 cm^{-1} are attributed to the OH bending vibrations, which are associated with the HNT's interlayer molecules of water and Al-OH, respectively. The peak related to the stretching bond of Si-O appears at 1030 cm^{-1} [32]. In comparison with the acid-washed HNT, the main difference in the FTIR spectra of the functionalized HNT appeared within the wave number range between 1741 and 1480 cm^{-1} [32]. Regarding the HNT-NH_2, the modifications were confirmed by the presence of the new peak at 1489 cm^{-1} (the bending NH_2 vibration band). For HNT-G1 new peaks appeared at 1646 and 1562 cm^{-1} (the stretching vibrations of N–H bending vibrations and C–N bond, respectively). For HNT-COOH carbonyl vibrations new peaks appeared at 1580 and 1700 cm^{-1}, which correspond to the amide and carboxylic acid groups, respectively [32].

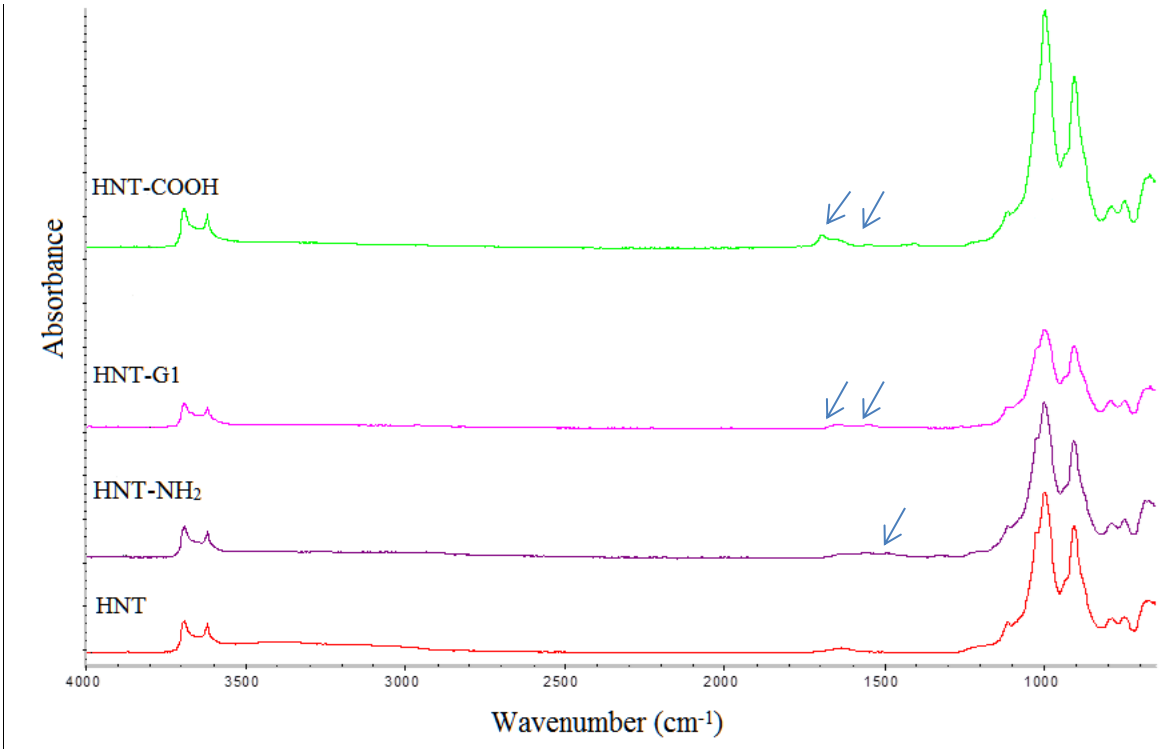

Figure 4.6 ATR-FTIR spectra of HNT, HNT-NH_2, HNT-G1, and HNT-COOH. The presence of new peak according to amid group reveals by flash point in the spectra**.**

The reactions between HNT, HNT-NH_2, HNT-G1, and HNT-COOH with the TMC and MPD monomers before the IP are also confirmed by the FTIR spectra shown in Figure 4.7 (a-d). The new peak at 1707 cm^{-1}, which corresponds to carbonyl groups, confirms the reaction of the hydroxyl groups at the surface of HNT with the carboxylic acid of TMC as shown in Figure 4.7-a. A broad peak around 3581 to 2797 cm^{-1} indicates the reaction with MPD.

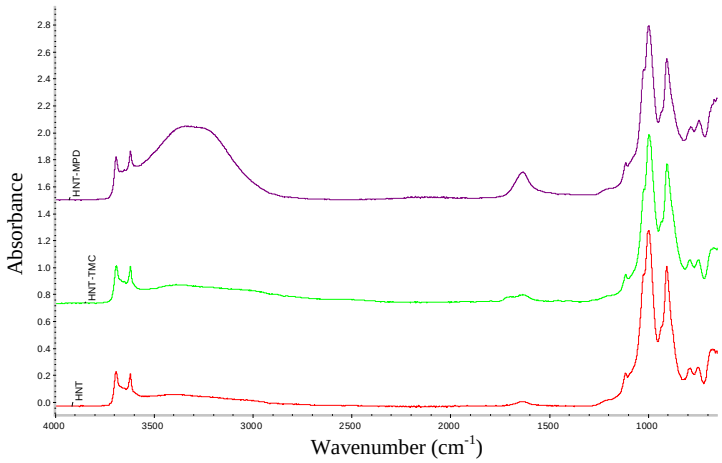

a) HNT, HNT-TMC, and HNT-MPD

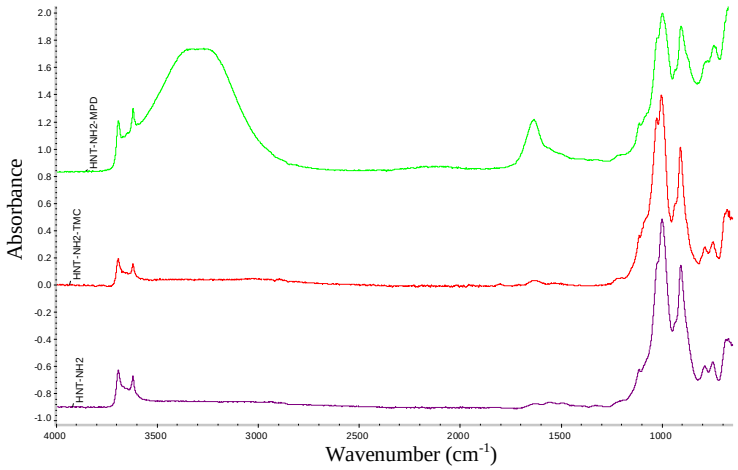

b) HNT-NH_2, HNT-NH_2-TMC, and HNT-NH_2-MPD

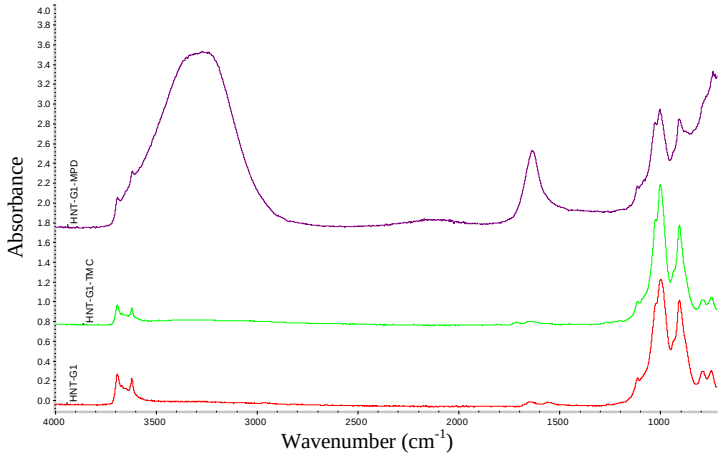

c) HNT-G1, HNT-G1-TMC, and HNT-G1-MPD

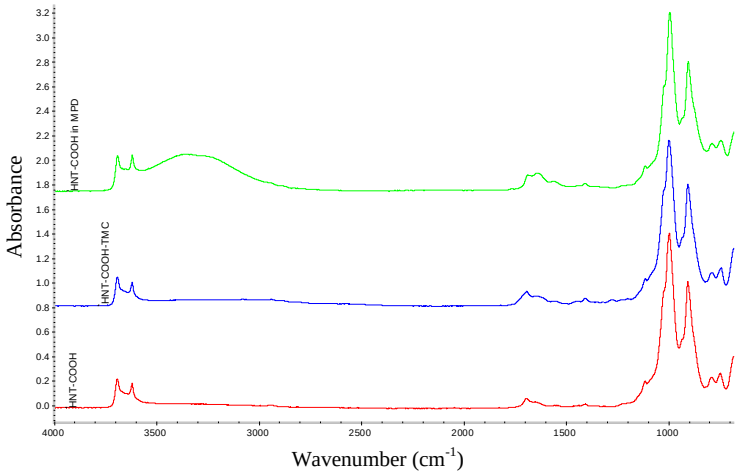

d) HNT-COOH, HNT-COOH -TMC, and HNT-COOH -MPD

Figure 4.7 ATR-FTIR spectra for a) HNT, HNT-NH2, HNT-G1, and HNT-COOH sonicated for 2 h in TMC and MPD solution, respectively.

The reactions of HNT-G1 with TMC illustrated in Figure 4.7-c. The new peak appeared at 1714 cm^{-1} in HNT-G1-TMC, corresponding to the carbonyl groups, confirms the reaction of amine group at the surface of HNT-G1 with the carboxylic acid of TMC in the monomer solution. Also, the reaction of HNT-COOH with TMC and MPD is illustrated in Figure 4.7-d. The new peaks at 1638 and 1556 cm^{-1} of HNT-COOH-MPD, corresponding to primary amine and secondary amide, show the reaction between the carboxylic acid groups at the surface of HNT-COOH with the amine group of MPD (secondary amide is also in HNT-COOH). Again, the wide peak between

3581 and 2797 cm^{-1} and the one at 1633 cm^{-1} are due to the reaction with MPD. The structure of the monomers and PA are given in Figure 4.8, while Figure 4.9 shows the proposed structure of interaction of HNT-G1 with PA; i.e., the reaction of amine groups of HNT-G1 with acyl chloride groups from the TMC section of the PA.

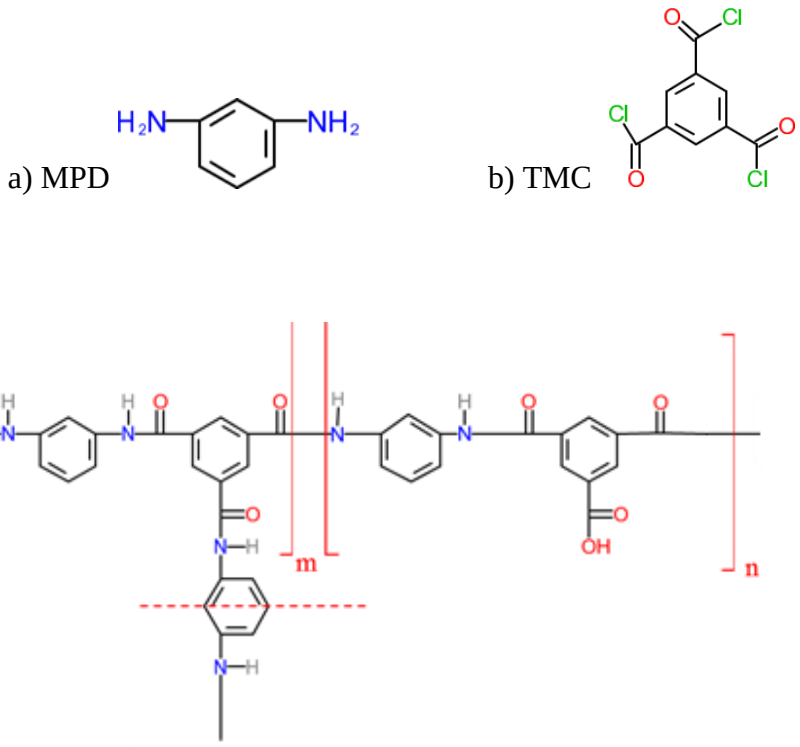

Figure 4.8 Molecular structure of a) MPD b) TMC and c) polyamide; m and n represent the cross-linked, and linear sections of the PA matrix.

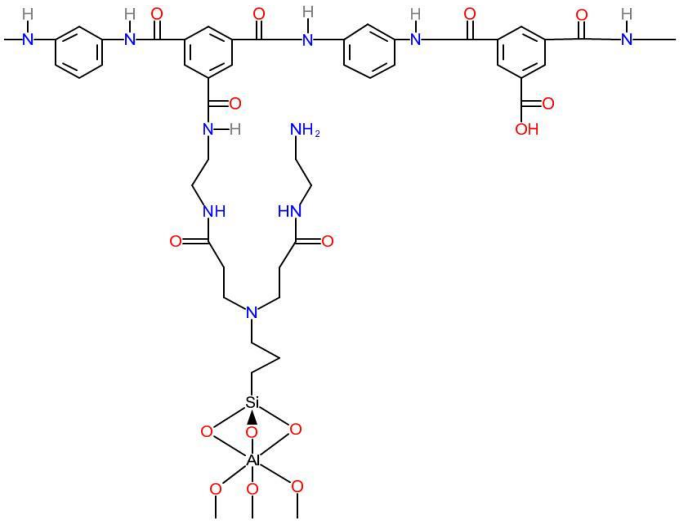

Figure 4.9 Proposed interaction of amine from HNT-G1 with the matrix of polyamide in TFN-HNT-G1

4.6.2. Characterization of the membranes

Figure 4.10 (a-e) illustrates the SEM images of the top surface and cross section of the TFC control membrane and TFN-HNT membranes with various functional groups. The typical ridge and valley structure, commonly reported for the PA TFC membranes, is observed in all images. However, there are some differences between the TFC and TFN membranes. It appears that the spaces between the "leaves" of the TFN-HNT-NH_2 and TFN-HNT-G1 are filled with broader dense layers than those of the control TFC membrane (compare Figure 4.10-c and 4.10-d with 4.10-a). Ghanbari et al. have reported the same trend in the morphology [13,14]. Kwak et al., in their study on the morphology of the polyamide TFC membranes, reported that the "leaf-like" structures are more common in polyamide TFC membranes with less cross-linked polymer chains [36]. Accordingly, the more leaf-like structures of TFN-HNT-NH_2 and TFN-HNT-G1 surface suggest the reaction of the HNT-NH_2 and HNT-G1 with TMC (see Figure 4.10 for G1) reduces the cross-linking in the PA layer. This is confirmed later by the XPS analysis.

As for the effect of HNT-COOH on the surface morphology, the surface of TFN-HNT-COOH membrane is similar to surface of the control TFC membrane (compare Figure 4.10-d with 4.10-a), suggesting that the presence of the HNT-COOH has not as much effect on the cross-linking as the HNT-NH_2 and HNT-G1. This will also be confirmed later by the XPS analysis.

It should be noted that, there are many discrepancies in the literature concerning the effects of the NP on the morphology of the PA layer [14,24,27]. However, it is generally believed that the NP can play an active role during the IP and formation of the PA layer. For example, Lind et al. suggested that hydrophilic NP increase the local miscibility of the aqueous (MPD) and organic (TMC) phases, and promote IP [27,37].

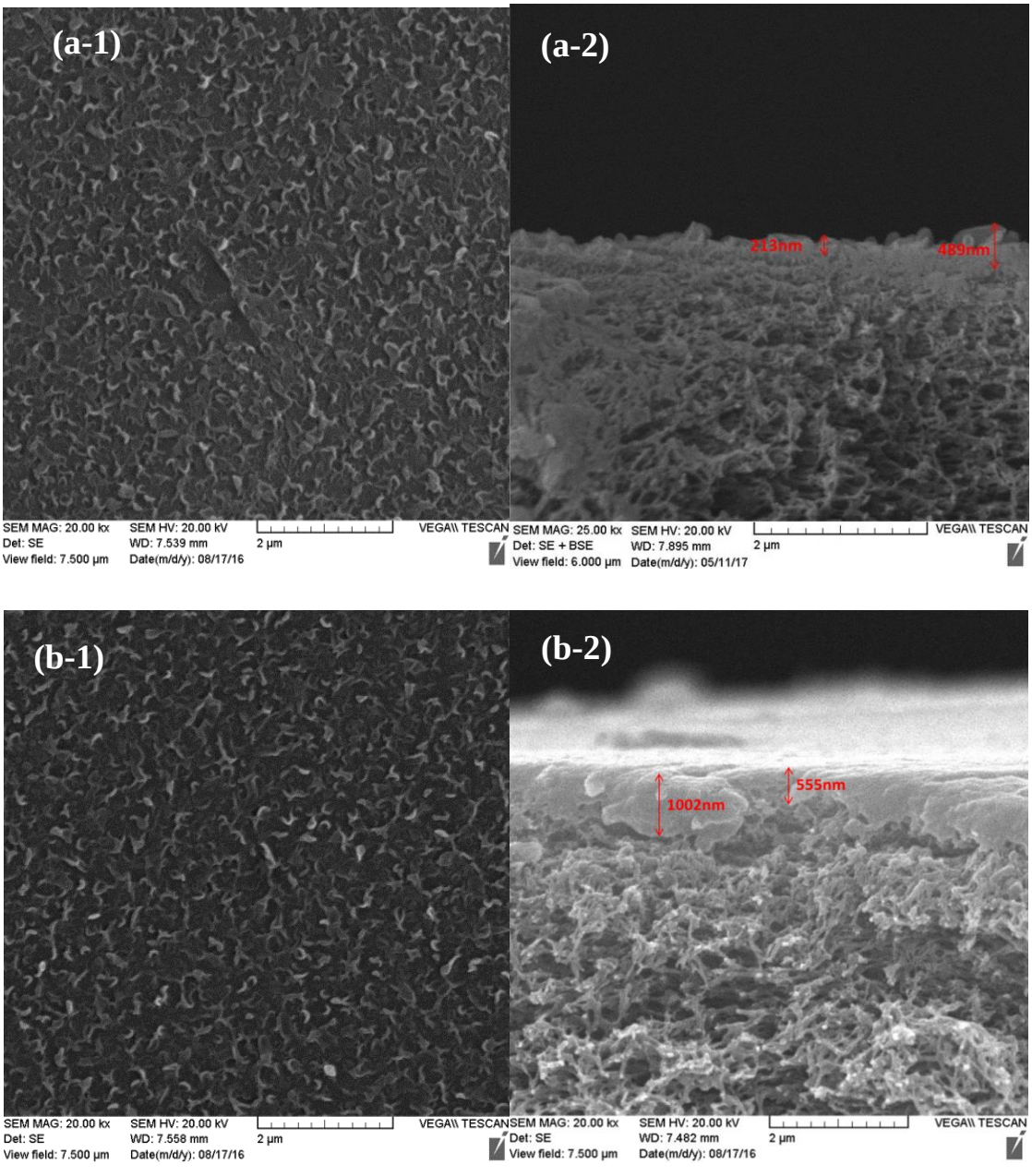

Figure 4.10 SEM images of top surface (noted with no.1) and cross section (noted with no.2) of a) TFC, b) TFN-HNT, c) TFN-HNT-NH_2, d) TFN-HNT-G1, e) TFN-HNT-COOH membranes**.**

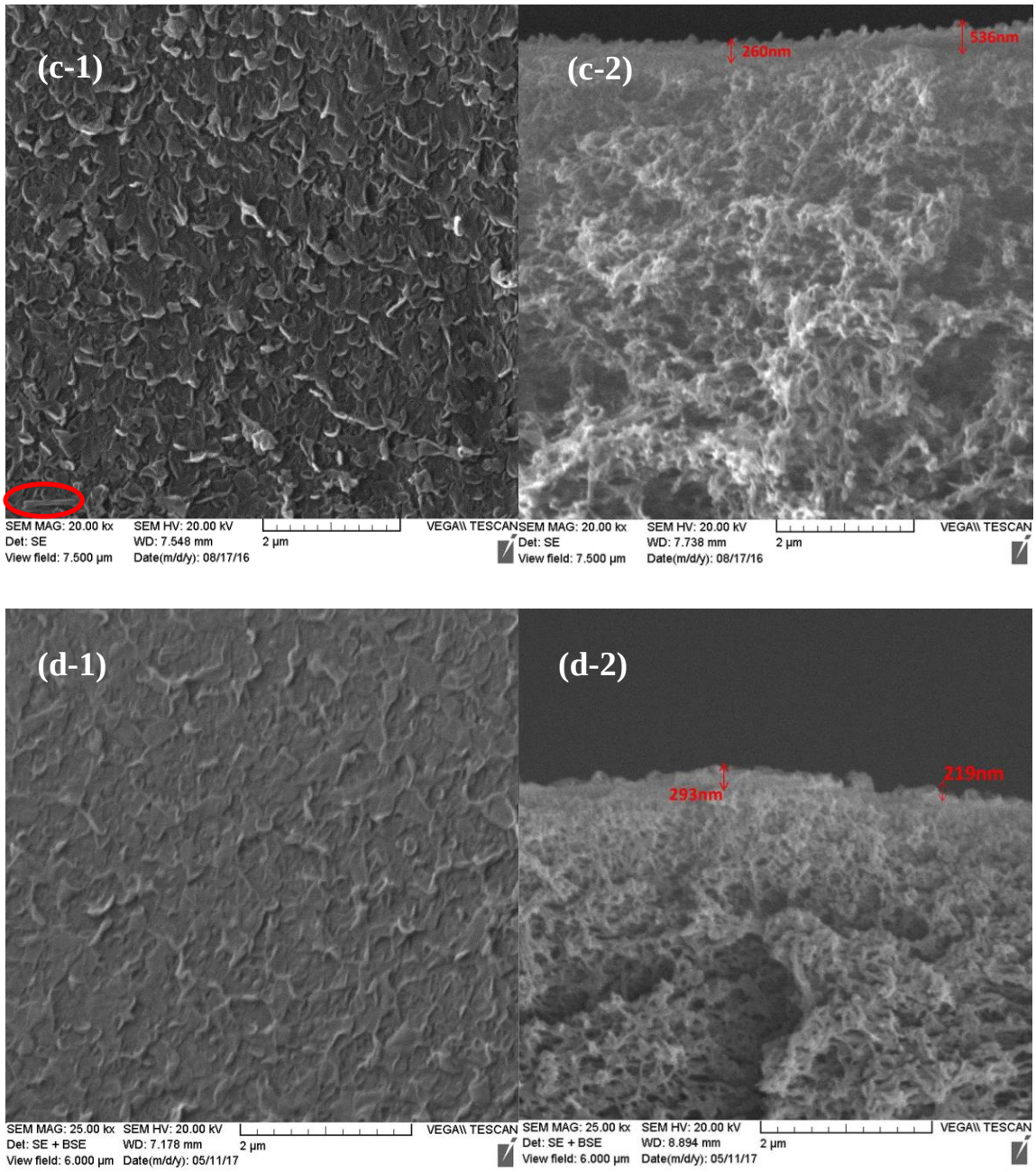

Figure 4.10 (countinued) SEM images of top surface (noted with no.1) and cross section (noted with no.2) of a) TFC, b) TFN-HNT, c) TFN-HNT-NH_2, d) TFN-HNT-G1, e) TFN-HNT-COOH membranes**.**

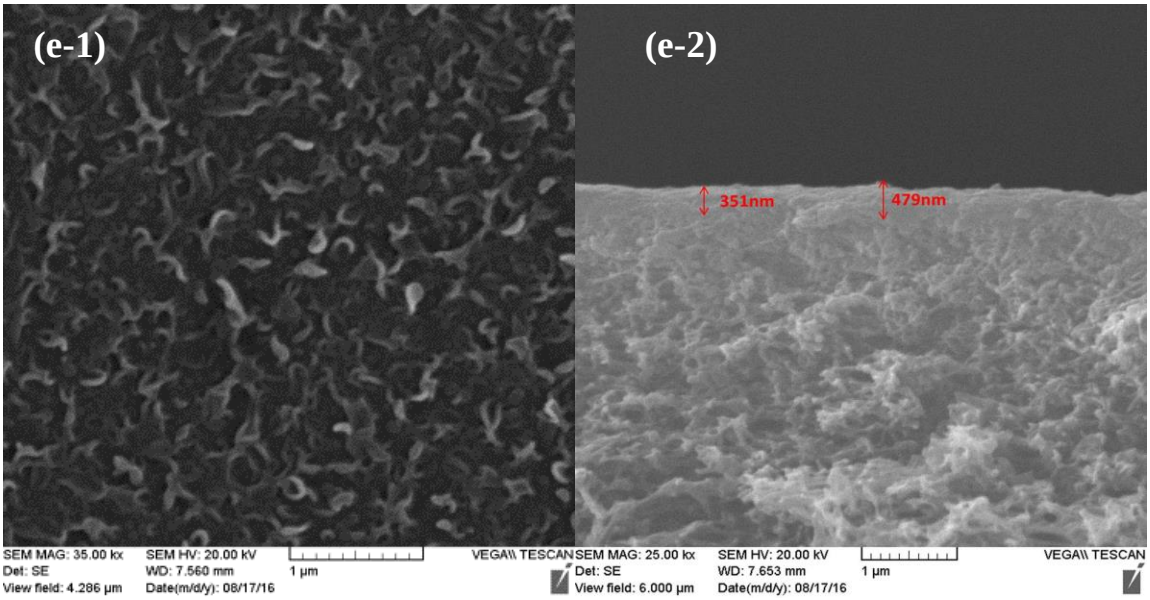

Figure 4.10 (continued) SEM images of top surface (noted with no.1) and cross section (noted with no.2) of a) TFC, b) TFN-HNT, c) TFN-HNT-NH_2, d) TFN-HNT-G1, e) TFN-HNT-COOH membranes**.**

The results of the contact angle measurement are summarized in Figure 4.11. The results revealed that surface hydrophilicity of the membranes was enhanced by adding the NP. The average contact angle of the TFC membrane was 73.0 ± 2.9° which was reduced to 56.6 ± 10.5 ° for the TFN-HNT membrane. The contact angles of the TFN membranes were further reduced by changing the functional groups of the HNT to amine or carboxylic acid. The largest contact angle decrease was observed for TFN-HNT-COOH (31.55 ± 1.7°). Higher hydrophilicity of the TFN-HNT-COOH compared to the other samples can be attributed to the highest organic content of HNT-COOH (Table 4.1). These observations are in accordance with the previous studies on the incorporation of hydrophilic NP in TFN membranes [3].

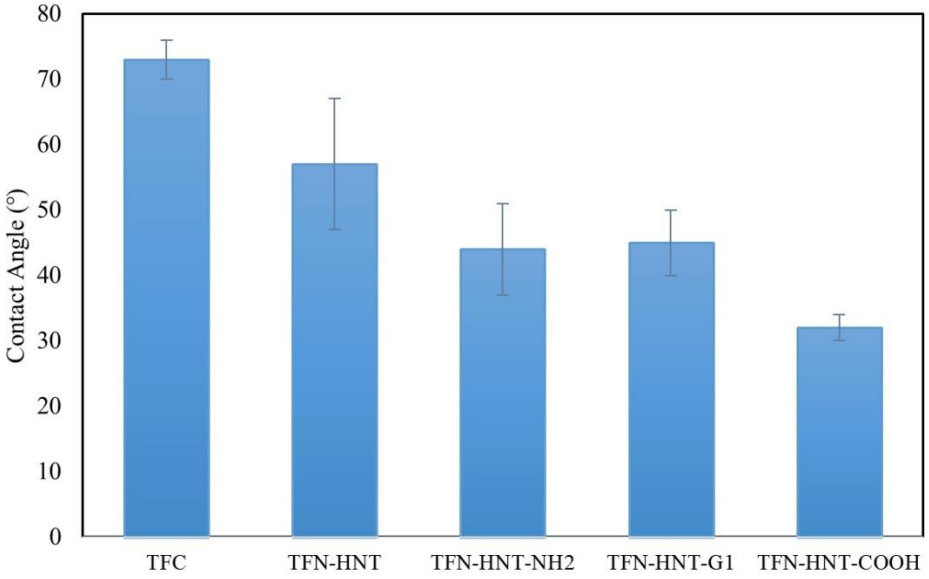

Figure 4.11 Contact angles of TFC and TFN membrane with various functional groups.

XPS is a surface sensitive method to investigate the elemental composition and chemical binding at the top ~5 nm layer of thin films. The elemental compositions of the TFC and TFN membranes are summarized in Table 4.2. The existence of Si and Al in the TFN membranes proves the successful incorporation of the HNT and functionalized-HNT in the PA layer. It should be noted that a small amount of Si and Al is also detected in the TFC membrane due to the noise, which shows the magnitude of error. The extent of cross-linking within the matrix of PA can be analyzed by of the C/N and O/N ratios. According to Figure 4.8, one acyl chloride group of TMC is either reacted with MPD to form cross-linking bonds, or with H_2O to form free carboxylic acid. Theoretically, for a fully cross-linked PA the C/N and O/N ratios should be 6 and 1, respectively, while for a fully linear PA they should be 7.5 and 2, respectively [13]. Thus, the ratios of C/N and O/N should increase as the degree of cross-linking decreases [38]. Due to the presence of many oxygen atoms in HNT, O/N cannot be used to determine the degree of cross-linking. Therefore, only the C/N ratio is listed in Table 4.2. In the table, the C/N ratio of the TFC membrane is 6.8, indicating some cross-linking in the PA layer. The ratio remains unchanged when HNT-COOH is added. This is understandable since –COOH can react only with $–NH_2$ of MPD, prior to IP and affect the PA chain length but not cross-linking. When, however, one of HNT, HNT-NH_2 or G1 is added, the C/N ratio becomes nearly equal to or even slightly larger than 7.5, indicating the substantial decrease of cross-linking. This is because –OH or NH_2 of the NP reacts with –COOH

of TMC, which reduces the chances of cross-linking. This trend was also observed by Lind et al, when they used aluminosilicate zeolite Linde type A in their TFN membranes [37].

It should be noted that due to the complexity of the reactions and the number of C and N brought by functionalaized NP the analysis of XPS data is very complicated. In fact, all NP may react with more than one –COOH group, thus forming cross-linking. Regardless of the number of the –COOH groups reacted with NP, the C/N ratio should decrease substantially.

Table 4.2 Elemental composition of membranes obtained by the XPS analysis.

element	TFC	TFN-HNT	TFN-HNT-NH_2	TFN-HNT-G1	TFN-HNT-COOH
C (%)	72.97	65.85	66.1	67.29	57.86
O (%)	13.78	20.6	20.1	19.78	26.28
N (%)	10.74	9.08	8.71	8.97	8.54
Si (%)	0.21	2.59	2.44	2.14	4.56
Al (%)	0.04	1.63	1.3	1.24	2.54
C/N(-)	6.8	7.3	7.6	7.5	6.8

The FTIR spectra of the TFN membranes with embedded functionalized HNT are demonstrated in Figure 4.12. The characteristic peaks of the polysulfone substrate appear at 1486, 1503 and 1584 cm^{-1} [35]. The peak at 1541 cm^{-1} is attributed to the amide II of the control TFC membrane. Also, the peak at 1609 cm^{-1} corresponds to the aromatic amide [31]. The broad peak around 3330 cm^{-1} is linked to the N–H and O–H stretching. All peaks, which are associated with the aromatic =C–H stretching and the aliphatic C–H stretching, appear in the range of 3589-2851cm^{-1}. However, due to overlapping and breadth of the peaks, it is difficult to split them into individual peaks. Thus, the peak area in the range 3589-2851cm^{-1} represents the sum of the intensities of all the above mentioned bonds.

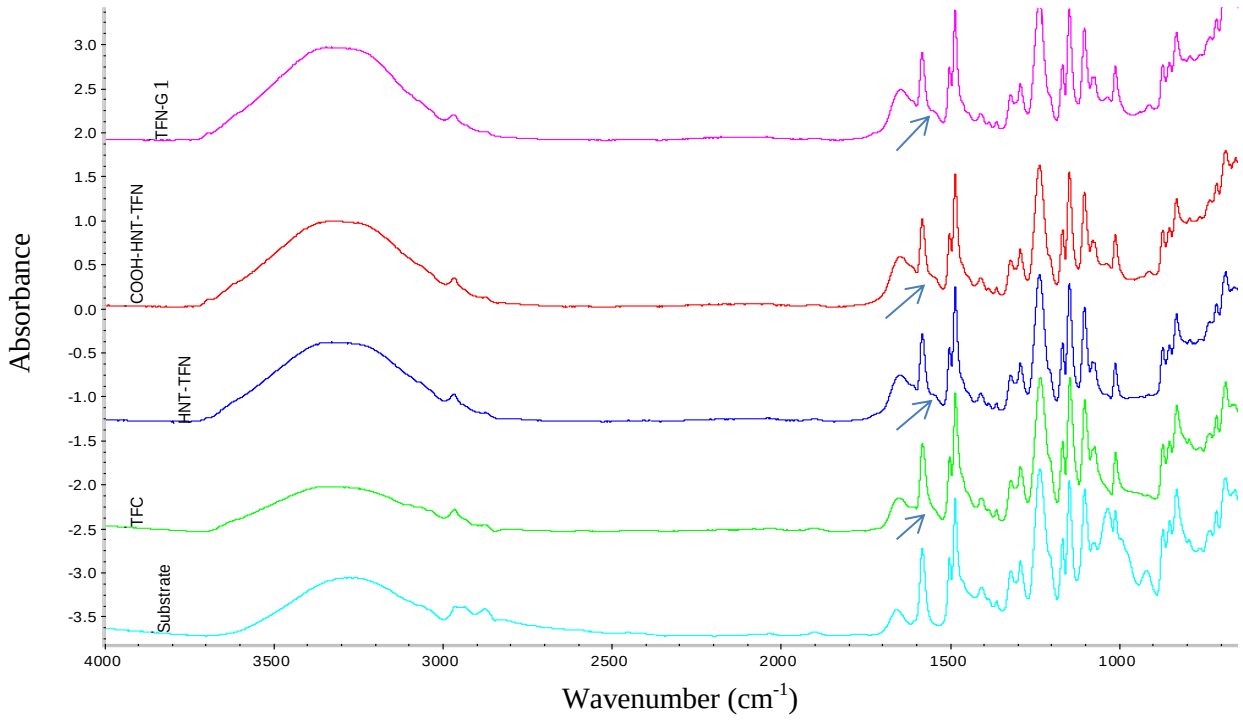

Figure 4.12 ATR-FTIR spectra for substrate, neat TFC, TFN-HNT, TFN-HNT-NH_2, TFN-HNT-G1, and TFN-HNT-COOH.

For further investigation of the ATR-FTIR spectra, the intensity of the peak at 1584 cm^{-1}, which belongs to the polysulfone group, was chosen as the internal standard [35]. Table 4.3 shows the normalized intensities of the peaks belonging to primary amine (1750-1620 cm^{-1}), secondary amide (1559-1520 cm^{-1}), aromatic amide (1620-1598 cm^{-1}) and amalgamation of various peaks in the range of 3802-2940cm^{-1}. The appeared amine and amide peaks for the commercial PS35 substrate membrane are probably due to the manufacturer's modifications for increased water flux. These results show that PA layer is formed in all TFC and TFN membranes. However, the PA for the characteristic peak for the TFC is lower compared to all TFN membranes. Particularly, the TFN membranes with amine-functionalized HNT, TFN-HNT-NH_2 and TFN-HNT-G1, had the highest amounts of the primary, secondary and aromatic amide, which indicates formation of more amide linkages in comparison with TFC membrane. This can be attributed to the reaction of functionalized HNT with the monomers or PA layer and also promotion of IP of PA.

Table 4.3 Peak area (PA) under 1750-1620 cm^{-1} (amide I), 1620-1598 cm^{-1} (Aromatic amide), 1559-1520 cm^{-1} (amide Π) and 3802-2940 cm^{-1} for substrate, TFC, TFC-HNT, TFN-HNT-NH2, TFN-HNT-G1, and TFN-HNT-COOH.

Membrane	Primary amide PA (1750-1620 cm^{-1})	Aromatic amide PA (1620-1598 cm^{-1})	Secondary amide PA (1559-1520 cm^{-1})	PA (3802-2940 cm^{-1})
Substrate	17.07	3.54	5.41	254.93
TFC	23.89	6.09	8.66	279.87
TFN-HNT	35. 74	8.75	10.33	423.76
TFN-HNT-NH_2	43.32	10.39	12.11	488.03
TFN-HNT-G1	52.49	12.97	15.28	587.55
TFN-HNT-COOH	38.22	9.59	11.61	460.35

Regarding the HNT leaching test, the results of tracing Al in the collected water after 48 h of the batch leaching tests are provided in Table 4.4. The presence of Al in the water sample of the TFC membrane is likely caused by noise, and shows the baseline for the magnitude of error. Therefore, the Al concentration in the TFC sample is considered as the baseline value. The smallest concentrations of Al were detected for the TFN-HNT-G1 and TFN-HNT–NH_2 membranes. As mentioned earlier (section 2.5), to our best of knowledge, there is no comprehensive standard method for testing the NP leaching from the TFN membranes.

The results of leaching test corroborate with the ATR-FTIR analysis regarding the interaction of the amine groups of NP with TMC. The lowest amount of leaching from the TFN-HNT-G1 and TFN-HNT-NH_2 membranes can be attributed to the covalent bonding with the TMC segment of PA. On the other hand, TFN-HNT-COOH exhibited the highest concentration of Al in the collected water sample. It is speculated that the reaction of HNT-COOH with MPD prior to IP, turns diamine to monoamine that can no longer act as a monomer for IP, and can readily be washed away. The highest Al concentration in the water sample was observed for TFN-HNT, which indicates that functionalization HNT reduces the NP leaching considerably.

Table 4.4 Concentrations of Al in the water sample after contacting with the membranes for 48 h

Membrane	Al (ppb)
TFC	2.58
TFN-HNT	51.10
TFN-HNT-NH_2	5.02
TFN-NHT-G1	2.92
TFN-HNT-COOH	13.53

4.6.3. Membrane performance

Water flux and salt rejection of the control TFC and TFN membranes with different surface-functionalized HNT are shown in Figure 4.13 (a and b). The averages of at least 4 coupons coming from two independently fabricated membranes are shown. The control TFC membrane had the water flux of 26.2 ± 2.5 L/m^2.h and NaCl rejection of 99.1% ± 0.1%. For all cases, incorporation of the HNT (with or without functionalization) increased the permeate flux. The ascending order of of the water flux is TFC < TFN-HNT < TFN-HNT-G1< TFN-HNT-NH_2 < TFN-HNT-COOH, which is precisely the reverse of the descending order of the contact angle (Figure 4.11). Therefore, it can be concluded that the flux increase is due to enhancement of surface hydrophilicity of the membranes.

Concerning the selectivity of the membranes, TFC, TFN-HNT, and TFN-HNT-COOH show the same NaCl rejections of 99.1% ± 0.1% indicating that incorporation of HNT does not deteriorate the quality of PA skin layer. Also, it shows that formation of defects caused by the NP agglomerates or by the gaps between the NP and PA matrix is insignificant. On the other hand, the salt rejection decline of the TFN-HNT-NH_2 and TFN-HNT-G1 can be attributed to the bonding of aliphatic chains by the reaction of the amine groups of NP with TMC, as illustrated in Figure 4.9.

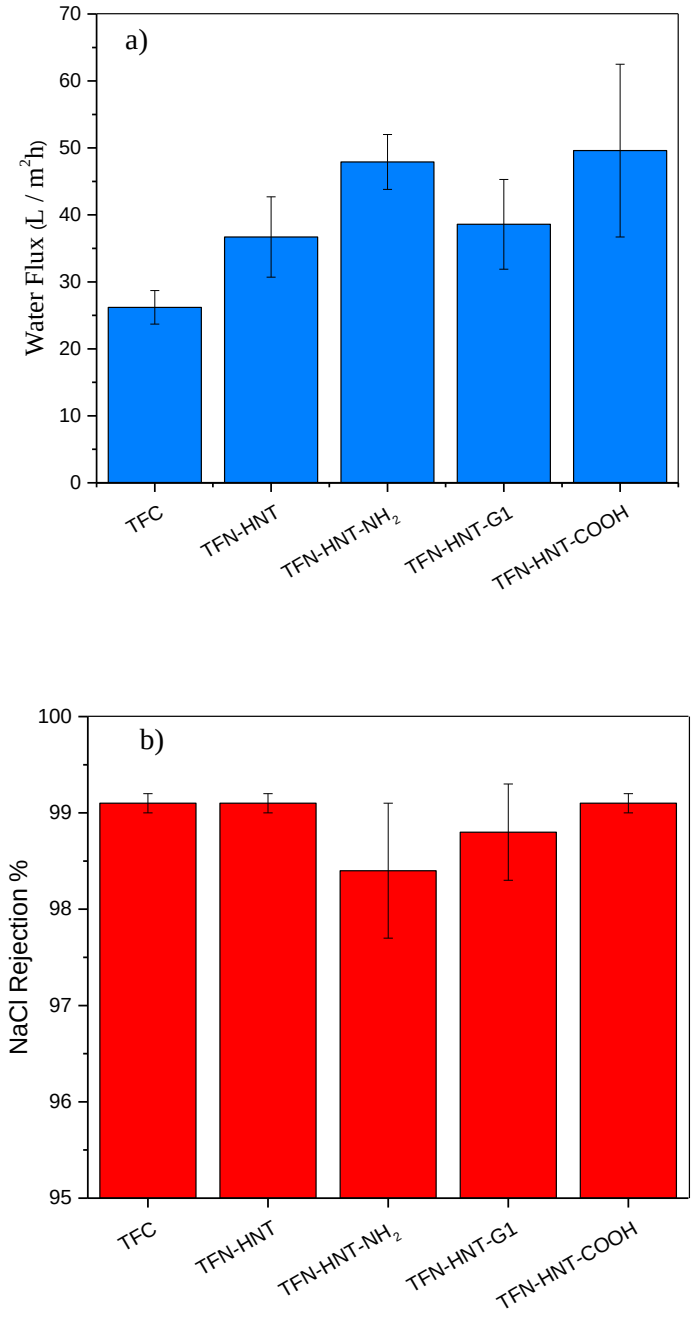

Figure 4.13 a) water flux and b) NaCl rejection of TFC and TFN membranes from desalination of synthetic brackish water by the RO system.

4.7. Conclusions

One of the major obstacles for the large scale use of TFN membranes is leaching out of the incorporated NP from the membrane into the downstream. This work is concerned with the incorporation of halloysite nanotubes (HNT), which are environmentally friendly and safe, and naturally grown nanoparticles. Also, we hypothesized that functionalization of the HNT can initiate more interactions and covalent bonds between the HNT and the monomers, and the PA layer. Thus, NP-PA compatibility would decrease leachability of the NP from the resulting TFN membranes.

TFN membranes were synthesized by in-situ IP of MPD with TMC and HNT. HNT were functionalized with amine, first generation of polyamidoamine (PAMAM) dendrimers, and carboxylicacid groups. Surface functionalization of HNT was confirmed by FITR, TGA and zeta potential analyses. Also, the morphology of HNT was characterized by SEM and TEM. The interactions of HNT with the monomers and the PA layer were qualitatively and quantitatively investigated by ATR-FTIR. The results showed that amine-functionalized HNT, HNT-NH_2 and HNT-G1, reacted with the TMC monomer, while the HNT-COOH reacted by the MPD monomers. Surface morphology of the membranes was characterized with SEM, and higher amount of "leaf-like" structures was observed in the TFN membranes with the amine functionalized HNT. Chemical properties of the membranes were investigated with XPS. It was found that the TFN-HNT-NH_2 and G1 membranes had lower extent of cross-linking. The membranes' top surface water contact angle measurements showed that wettability of the TFN was enhanced by adding the NP. By changing the functional group of the acid-washed HNT to the amine or carboxylic acid, the wettability of TFN membranes further increased. Higher inorganic content in TGA analysis for HNT-COOH can be credited to the higher hydrophilicity of the TFN-HNT-COOH comparing to the other samples.

In addition, membranes were examined in a batch leaching test using an incubator for 48 h, and it was found that HNT leaching from the TFN-HNT-NH_2 and TFN-HNT-G1 membranes were significantly less than from the TFN-HNT membrane. Separation characteristics of the membranes were studied by RO filtration tests with a synthetic brackish water. It was found that embedding HNT in the PA layer increased the membrane permeance in all cases without sacrificing the selectivity. The maximum water flux increase from 26.2 ± 2.5 L/m^2.hr to 49.6 ± 12.9 L/m^2.hr was observed for the membrane with HNT-COOH particles, with the corresponding salt rejection of

99.1 % ± 0.1 % which is similar to that of the control TFC membrane. The increase in the permeance and decrease in the HNT leaching were attributed to the increased membrane hydrophilicity and the formation of covalent bonds between the amine groups of HNT-NH_2 and HNT-G1 with acyl chloride functional groups of TMC monomers.

Our work shows that surface modification of nanoparticles with amine groups and the first generation of the amine terminated PAMAM dendrimers, not only improves membrane transport properties, but also increase the entanglement of nanoparticles within the PA layer.

Acknowledgement

Many thanks to Mr. Andre Francois for his assistance with the membrane testing as well as Dr. Siamak Lashkari, and QW Sea water desalination, China for their support.

4.8. References

[1] M. Elimelech, W.A. Phillip, The Future of Seawater Desalination: Energy, Technology, and the Environment, Science. 333 (2011) 712–717. doi:10.1126/science.1200488.

[2] R.W. Baker, Membrane Science and Technology, John Wiley & Sons, Ltd, 2012. http://onlinelibrary.wiley.com/doi/10.1002/9781118359686.ch1/summary (accessed April 9, 2017).

[3] W.J. Lau, S. Gray, T. Matsuura, D. Emadzadeh, J. Paul Chen, A.F. Ismail, A review on polyamide thin film nanocomposite (TFN) membranes: History, applications, challenges and approaches, Water Res. 80 (2015) 306–324. doi:10.1016/j.watres.2015.04.037.

[4] O.A. Sadik, N. Du, I. Yazgan, V. Okello, Chapter 6 - Nanostructured Membranes for Water Purification, in: A. Street, R. Sustich, J. Duncan, N. Savage (Eds.), Nanotechnol. Appl. Clean Water Second Ed., William Andrew Publishing, Oxford, 2014: pp. 95–108. doi:10.1016/B978-1-4557-3116-9.00006-8.

[5] M. Bhadra, S. Mitra, Chapter 7 - Advances in Nanostructured Membranes for Water Desalination, in: A. Street, R. Sustich, J. Duncan, N. Savage (Eds.), Nanotechnol. Appl. Clean Water Second Ed., William Andrew Publishing, Oxford, 2014: pp. 109–122. doi:10.1016/B978-1-4557-3116-9.00007-X.

[6] E.M.V. Hoek, M.T.M. Pendergast, A.K. Ghosh, Chapter 9 - Nanotechnology-Based Membranes for Water Purification, in: A. Street, R. Sustich, J. Duncan, N. Savage (Eds.), Nanotechnol. Appl. Clean Water Second Ed., William Andrew Publishing, Oxford, 2014: pp. 133–154. doi:10.1016/B978-1-4557-3116-9.00009-3.

[7] J. Duan, Y. Pan, F. Pacheco, E. Litwiller, Z. Lai, I. Pinnau, High-performance polyamide thin-film-nanocomposite reverse osmosis membranes containing hydrophobic zeolitic imidazolate framework-8, J. Membr. Sci. 476 (2015) 303–310. doi:10.1016/j.memsci.2014.11.038.

[8] H. Zhao, S. Qiu, L. Wu, L. Zhang, H. Chen, C. Gao, Improving the performance of polyamide reverse osmosis membrane by incorporation of modified multi-walled carbon nanotubes, J. Membr. Sci. 450 (2014) 249–256. doi:10.1016/j.memsci.2013.09.014.

[9] M. Safarpour, A. Khataee, V. Vatanpour, Thin film nanocomposite reverse osmosis membrane modified by reduced graphene oxide/TiO2 with improved desalination performance, J. Membr. Sci. 489 (2015) 43–54. doi:10.1016/j.memsci.2015.04.010.

[10] Y. Mansourpanah, Z. Jafari, Efficacy of different generations and concentrations of PAMAM–NH2 on the performance and structure of TFC membranes, React. Funct. Polym. 93 (2015) 178–189. doi:10.1016/j.reactfunctpolym.2015.04.010.

[11] B.-H. Jeong, E.M.V. Hoek, Y. Yan, A. Subramani, X. Huang, G. Hurwitz, A.K. Ghosh, A. Jawor, Interfacial polymerization of thin film nanocomposites: A new concept for reverse osmosis membranes, J. Membr. Sci. 294 (2007) 1–7. doi:10.1016/j.memsci.2007.02.025.

[12] J. Yin, Attachment of silver nanoparticles (AgNPs) onto thin-film composite (TFC) membranes through covalent bonding to reduce membrane biofouling, 441 (n.d.) 73–82.

[13] G.N.B. Baroña, J. Lim, M. Choi, B. Jung, Interfacial polymerization of polyamide-aluminosilicate SWNT nanocomposite membranes for reverse osmosis, Desalination. 325 (2013) 138–147. doi:10.1016/j.desal.2013.06.026.

[14] M. Ghanbari, D. Emadzadeh, W.J. Lau, S.O. Lai, T. Matsuura, A.F. Ismail, Synthesis and characterization of novel thin film nanocomposite (TFN) membranes embedded with halloysite nanotubes (HNTs) for water desalination, Desalination. 358 (2015) 33–41. doi:10.1016/j.desal.2014.11.035.

[15] H. Wu, Optimizing polyamide thin film composite membrane covalently bonded with modified mesoporous silica nanoparticles, J. Membr. Sci. 428 (2013) 341–348.

[16] D. Emadzadeh, W.J. Lau, M. Rahbari-Sisakht, H. Ilbeygi, D. Rana, T. Matsuura, A.F. Ismail, Synthesis, modification and optimization of titanate nanotubes-polyamide thin film nanocomposite (TFN) membrane for forward osmosis (FO) application, Chem. Eng. J. 281 (2015) 243–251. doi:10.1016/j.cej.2015.06.035.

[17] K.P. Lee, T.C. Arnot, D. Mattia, A review of reverse osmosis membrane materials for desalination—Development to date and future potential, J. Membr. Sci. 370 (2011) 1–22. doi:10.1016/j.memsci.2010.12.036.

[18] J.M. Gohil, P. Ray, A review on semi-aromatic polyamide TFC membranes prepared by interfacial polymerization: Potential for water treatment and desalination, Sep. Purif. Technol. 181 (2017) 159–182. doi:10.1016/j.seppur.2017.03.020.

[19] M.G. Buonomenna, Nano-enhanced reverse osmosis membranes, Desalination. 314 (2013) 73–88. doi:10.1016/j.desal.2013.01.006.

[20] L.Y. Ng, A.W. Mohammad, C.P. Leo, N. Hilal, Polymeric membranes incorporated with metal/metal oxide nanoparticles: A comprehensive review, Desalination. 308 (2013) 15–33. doi:10.1016/j.desal.2010.11.033.

[21] B. Rajaeian, A. Rahimpour, M.O. Tade, S. Liu, Fabrication and characterization of polyamide thin film nanocomposite (TFN) nanofiltration membrane impregnated with TiO2 nanoparticles, Desalination. 313 (2013) 176–188. doi:10.1016/j.desal.2012.12.012.

[22] Y.-L. Ji, W.-J. Qian, Y.-W. Yu, Q.-F. An, L.-F. Liu, Y. Zhou, C.-J. Gao, Recent developments in nanofiltration membranes based on nanomaterials, Chin. J. Chem. Eng. (n.d.). doi:10.1016/j.cjche.2017.04.014.

[23] G.-R. Xu, J.-N. Wang, C.-J. Li, Strategies for improving the performance of the polyamide thin film composite (PA-TFC) reverse osmosis (RO) membranes: Surface modifications and nanoparticles incorporations, Desalination. 328 (2013) 83–100. doi:10.1016/j.desal.2013.08.022.

[24] M. Zargar, Y. Hartanto, B. Jin, S. Dai, Polyethylenimine modified silica nanoparticles enhance interfacial interactions and desalination performance of thin film nanocomposite membranes, J. Membr. Sci. 541 (2017) 19–28. doi:10.1016/j.memsci.2017.06.085.

[25] Y. Joo, Y. Jeon, S.U. Lee, J.H. Sim, J. Ryu, S. Lee, H. Lee, D. Sohn, Aggregation and Stabilization of Carboxylic Acid Functionalized Halloysite Nanotubes (HNT-COOH), J. Phys. Chem. C. 116 (2012) 18230–18235. doi:10.1021/jp3038945.

[26] G. Cavallaro, D.I. Donato, G. Lazzara, S. Milioto, Films of Halloysite Nanotubes Sandwiched between Two Layers of Biopolymer: From the Morphology to the Dielectric, Thermal, Transparency, and Wettability Properties, J. Phys. Chem. C. 115 (2011) 20491–20498. doi:10.1021/jp207261r.

[27] M. Ghanbari, D. Emadzadeh, W.J. Lau, T. Matsuura, M. Davoody, A.F. Ismail, Super hydrophilic TiO2/HNT nanocomposites as a new approach for fabrication of high performance thin film nanocomposite membranes for FO application, Desalination. 371 (2015) 104–114. doi:10.1016/j.desal.2015.06.007.

[28] A. Moslehyani, M. Mobaraki, A.F. Ismail, T. Matsuura, S.A. Hashemifard, M.H.D. Othman, A. Mayahi, M. Rezaei DashtArzhandi, M. Soheilmoghaddam, E. Shamsaei, Effect of HNTs modification in nanocomposite membrane enhancement for bacterial removal by cross-flow ultrafiltration system, React. Funct. Polym. 95 (2015) 80–87. doi:10.1016/j.reactfunctpolym.2015.08.007.

[29] R. Esfand, D.A. Tomalia, Poly(amidoamine) (PAMAM) dendrimers: from biomimicry to drug delivery and biomedical applications, Drug Discov. Today. 6 (2001) 427–436. doi:10.1016/S1359-6446(01)01757-3.

[30] A. Sarkar, P.I. Carver, T. Zhang, A. Merrington, K.J. Bruza, J.L. Rousseau, S.E. Keinath, P.R. Dvornic, Dendrimer-based coatings for surface modification of polyamide reverse osmosis membranes, J. Membr. Sci. 349 (2010) 421–428. doi:10.1016/j.memsci.2009.12.005.

[31] J.Y. Sum, A.L. Ahmad, B.S. Ooi, Synthesis of thin film composite membrane using mixed dendritic poly(amidoamine) and void filling piperazine monomers, J. Membr. Sci. 466 (2014) 183–191. doi:10.1016/j.memsci.2014.04.040.

[32] F.S. Fard, S. Akbari, E. Pajootan, M. Arami, Enhanced acidic dye adsorption onto the dendrimer-based modified halloysite nanotubes, Desalination Water Treat. 57 (2016) 26222–26239. doi:10.1080/19443994.2016.1160437.

[33] J.C. Crittenden, R.R. Trussell, D.W. Hand, K.J. Howe, G. Tchobanoglous, Reverse Osmosis, in: MWHs Water Treat. Princ. Des. Third Ed., John Wiley & Sons, Inc., 2012: pp. 1335–1414. doi:10.1002/9781118131473.ch17.

[34] W. Jinhua, Z. Xiang, Z. Bing, Z. Yafei, Z. Rui, L. Jindun, C. Rongfeng, Rapid adsorption of Cr (VI) on modified halloysite nanotubes, Desalination. 259 (2010) 22–28. doi:10.1016/j.desal.2010.04.046.

[35] V. Freger, J. Gilron, S. Belfer, TFC polyamide membranes modified by grafting of hydrophilic polymers: an FT-IR/AFM/TEM study, J. Membr. Sci. 209 (2002) 283–292. doi:10.1016/S0376-7388(02)00356-3.

[36] S.-Y. Kwak, S.G. Jung, Y.S. Yoon, D.W. Ihm, Details of surface features in aromatic polyamide reverse osmosis membranes characterized by scanning electron and atomic force microscopy, J. Polym. Sci. Part B Polym. Phys. 37 (1999) 1429–1440. doi:10.1002/(SICI)1099-0488(19990701)37:13<1429::AID-POLB9>3.0.CO;2-B.

[37] M.L. Lind, D. Eumine Suk, T.-V. Nguyen, E.M.V. Hoek, Tailoring the Structure of Thin Film Nanocomposite Membranes to Achieve Seawater RO Membrane Performance, Environ. Sci. Technol. 44 (2010) 8230–8235. doi:10.1021/es101569p.

[38] W.J. Lau, A.F. Ismail, P.S. Goh, N. Hilal, B.S. Ooi, Characterization Methods of Thin Film Composite Nanofiltration Membranes, Sep. Purif. Rev. 44 (2015) 135–156. doi:10.1080/15422119.2014.882355.

Chapter 5

Conclusions and recommendations

Chapter 5-Conclusions and recommendations

Embedding nanoparticles into the polyamide matrix of Thin Film Nanocomposite (TFN) membranes is a new approach for fabrication of high-performance semipermeable Reverse Osmosis (RO) membranes. Leaching out of typically toxic inorganic nanoparticles into the downstream, agglomeration of nanoparticles in the polyamide matrix, and high production cost of the nanoparticles are the major challenges for large scale application of TFN membranes. In this thesis, these problems were addressed by incorporation of Cellulose Nanocrystals (CNC) and Halloysite NanoTubes (HNT) as inherently safe, low/no toxic, environmentally friendly, abundant, low-cost nanoparticles into the RO TFN membranes. Pristine CNC were utilized in Chapter 3 while in Chapter 4 functionalization of the HNT with carboxylic acid and amine groups as well as amine terminated poly(amidoamine) (PAMAM) dendrimers were investigated.

Membranes were fabricated via in situ interfacial polymerization of MPD with TMC and nanoparticles on top of PS35 ultrafiltration membrane. Physicochemical properties of CNC-TFN and HNT-TFN membranes were characterized with SEM, AFM, ATR-FTIR, XPS, XRD and contact angle measurements. The conclusions of this work regarding the separation characteristics of the membranes in the RO tests with brackish water are:

1- Incorporation of 0.1% (w/v) CNC in the TFN membranes almost doubled water flux from (28 to 63 $L/m^2.hr$) without sacrificing the selectivity of the membrane (97.8 %).
2- CNC loading 11% improved the antifouling capacity of the TFN membrane in comparison with the control TFC membrane.
3- For all cases, embedding functionalized HNT in the TFN membrane enhanced the permeance with no/low decrease in the selectivity. The ascending order of flux was TFC (26.2 $L/m^2.hr$) < TFN-HNT < TFN-HNT-G1 < TFN-HNT-NH_2 < TFN-HNT-COOH (49.6 $L/m^2.hr$), which is precisely the reverse of the descending order of the measured contact angle.
4- Leaching tests in a batch incubator revealed that functionalization of the HNT improved the interactions between the HNT and the thin polyamide matrix. TFN-HNT-NH_2 and TFN-HNT-G1 showed the lowest amount of leaching. These results corroborated the ATR-FTIR analyses regarding the formation of covalent bonds between the amine groups of nanoparticles with TMC.

This work may open new doors to a larger scale production of high-performance TFN membranes for various applications. Because of the improved performance of the CNC and functionalized HNT embedded TFN membranes, also, the safe and unique properties of CNC, HNT, and PAMAM dendrimers for fabrication of TFN membranes.

Based on the conclusions of this work and challenges faced during the course of this research and experiments, the following recommendations can be made.

1- Further research is required for better understanding the long-term performance, stability, and other applications of CNC-TFN membranes.

2- Surface properties of CNC can be tailored during its production; therefore, incorporation of functionalized CNC in TFN membranes is intriguing for various applications.

3- Investigation of novel methods of TFN membrane fabrication, such as “layer by layer” or “pre-seeding” approaches is recommended since CNC can have stable suspensions in water.

4- Additional work is required to optimize the use of the PAMAM dendrimers, with different generations, on the surface of the embedded nanoparticles in TFN membranes.

5- Investigating chlorine resistance of TFN membranes with amine terminated PAMAM dendrimers is an intriguing area to study.

6- Thorough investigations are required to develop and optimize an experiment for tracing the leached out NP of membranes in cross flow membrane filtration